Università degli Studi di Ferrara

DOTTORATO DI RICERCA IN
SCIENZE DELL'INGEGNERIA

CICLO XXVI

COORDINATORE Prof. TRILLO STEFANO

THE GRAIN REFINEMENT AND THE Ni/V CONTAMINATION IN THE A356 ALUMINIUM CASTING ALLOY: AN EXPERIMENTAL STUDY ON IMPACT AND TENSILE PROPERTIES

Settore Scientifico Disciplinare ING-IND/21

Dottorando

Dott. CASARI DANIELE

Tutore

Prof. GARAGNANI GIAN LUCA

Cotutore

Prof. MERLIN MATTIA

Anni 2011/2013

To my family

"Tho' much is taken, much abides; and tho'
We are not now that strength which in old days
Moved earth and heaven, that which we are, we are;
One equal temper of heroic hearts,
Made weak by time and fate, but strong in will
To strive, to seek, to find, and not to yield."

Alfred, Lord Tennyson

Preface

This doctoral thesis is the result of three years of study full-time, including courses and research at the University of Ferrara, Italy, from January 2011 to December 2013. Most of the experimental work was carried out at the Engineering Department (ENDIF) in Ferrara. Part of the experiments were conducted at the Norwegian University of Science and Technology in close cooperation with the Solidification/Casting Group during my stay in Trondheim from April to September 2013.

The work was partially founded by the "Bando Giovani Ricercatori - Fondi 5x1000 anno 2010 e Fondi Unicredit 2013 of the University of Ferrara". Additional financial support was given by Hydro Aluminium AS (Norway).

Professor Gian Luca Garagnani at the Engineering Department was the main supervisor. Assistant Professor Mattia Merlin was the co-supervisor. Professor Lars Arnberg hosted my stay at the Norwegian University of Science and Technology.

The main aim of my PhD work was to study the influence of grain refinement and Ni/V trace additions on the impact and tensile properties of the A356 aluminium casting alloy. The research was subdivided into separate projects and led to three publications, which represent the main part of this doctoral thesis. The manuscripts are:

A. D. Casari, M. Merlin and G.L. Garagnani, "A comparative study on the effects of three commercial Ti-B based grain refiners on the impact properties of A356 cast aluminium alloy," *Journal of Materials Science*, vol. 48(12), pp. 4365-4377, 2013.

B. D. Casari, T.H. Ludwig, L. Arnberg, M. Merlin and G.L. Garagnani, "The effect of Ni and V trace elements on the mechanical properties of A356 aluminium foundry alloy in as-cast and T6 heat treated conditions," **submitted to** *Materials Science and Engineering A*.

C. D. Casari, T.H. Ludwig, L. Arnberg, M. Merlin and G.L. Garagnani, "Impact behaviour of A356 foundry alloys in the presence of trace elements Ni and V," **submitted to** *Journal of Materials Engineering and Performance*.

The following list contains articles concerning research works and side activities on Al-Si casting alloys. These papers were written during the three years period but are not included in this thesis. The articles were either published or presented at conferences and seminars. In particular, publications n°4, 5, 6 are related to the grain refinement research project.

1. M. Merlin, D. Casari and G.L. Garagnani, "Influence of heat treatment and chemical composition on microstructure and mechanical properties, and hot tearing behaviour in aluminium alloy sand castings," *12^{th} International Summer School on Aluminium Alloys Technology*, Vicenza, Italy, 2011. (Poster presentation).

2. D. Casari, M. Merlin and G.L. Garagnani, "Influence of injection parameters on the final surface quality of Al-Si-Cu die cast components," *Proceedings of the 5^{th} International Conference High Tech Die Casting 2012*, 2012, Vicenza, Italy. Also published in *Metallurgical Science and Technology*, vol. 30-2, pp. 11-17, 2012.

3. D. Casari, "The lamination defect in HPDC aluminium components," *Annual Seminar of the NTNU Solidification/Casting Group*, Freiberg, Germany, 2013.

4. D. Casari, M. Merlin and G.L. Garagnani, "Effect of different types of refinements on A356 foundry aluminium alloy: thermal and microstructural analyses," *Metallurgical Science and Technology*, vol. 31-1, pp. 24-33, 2013.

5. D. Casari and C. Soffritti, "Valutazione comparativa dell'effetto di tre differenti tipologie di affinante sulle proprietà meccaniche e microstrutturali della lega di alluminio A356 da fonderia," *La Metallurgia Italiana*, vol. 4, pp. 31-40, 2013.

6. D. Casari, M. Merlin and G.L. Garagnani, "Fracture behaviour of grain refined A356 cast aluminium alloy: tensile and Charpy impact specimens," *Proceedings of the Convegno Nazionale IGF XXII*, pp. 314-321, Roma, Italy, 2013.

Theoretical and experimental investigations on the bending recovery performance of NiTi shape memory alloy strips were also performed during the doctoral studies, as a continuation of the M.S. degree. NiTi strips were characterised in terms of mechanical properties and shape setting parameters. Subsequently, a one-dimensional phenomenological constitutive equation was developed to model and estimate the theoretical evolution of the curvature of the strips during bending and subsequent shape recovery. Using the characterisation data as input parameters of the model, a good agreement between the theoretical curvature evolution and the experimental data was observed. The results were published in:

1. R. Rizzoni, M. Merlin and D.Casari, "Bending properties of heat-treated NiTi strips for actuation of smart reinforced beams," *Proceedings of the XX Congresso dell'Associazione Italiana di Meccanica Teorica e Applicata*, Bologna, Italy, 2011.

2. R. Rizzoni, M. Merlin and D.Casari, "Shape recovery behaviour of NiTi strips in bending: experiments and modeling," *Continuum Mechanics and Thermodynamics*, vol. 25, pp. 207-227, 2013.

Part of the research activities was also devoted to the supervision of the following B.S. and M.S. theses. Research and experiments were performed at the Engineering Department of the University of Ferrara.

1. Giulia Mazzacurati (2012), "Analisi degli effetti di diverse tipologie di affinante sulla microstruttura di leghe Al-Si-Mg da fonderia". Supervisors: M. Merlin, D. Casari.

2. Tommaso Stabellini (2012), "Studio degli effetti di tre tipologie di affinanti a base di TiB_2 sulle proprietà microstrutturali della lega di alluminio A356.0 da fonderia". Supervisors: M. Merlin, D. Casari.

3. Diego Cecchinato (2012), "L'analisi termica: generalità e applicabilità della tecnica allo studio della solidificazione di leghe di alluminio da fonderia". Supervisors: M. Merlin, D. Casari.

4. Andrea Formenti (2013), "Analisi microstrutturale di provini di trazione e resilienza in lega di alluminio A356 da fonderia trattata con diverse tipologie di affinante". Supervisors: M. Merlin, D. Casari.

5. Giacomo Vitali (2013), "Influenza del trattamento di affinazione sulle proprietà meccaniche e microstrutturali di getti in lega di alluminio A356: ricerca bibliografica ed indagine sperimentale". Supervisors: M. Merlin, D. Casari.

6. Emma Panini (2013), "Studio delle proprietà ad impatto e caratterizzazione microstrutturale di provini fullsize e subsize in lega di alluminio da fonderia A356". Supervisors: M. Merlin, D. Casari.

7. Federico Sacchi (2014), "Comportamento ad impatto di provini Charpy fullsize e subsize in lega di alluminio da fonderia A356 al variare della temperatura". Supervisors: M. Merlin, D. Casari.

Acknowledgements

The first of my appreciations goes to my supervisor, Prof. Gian Luca Garagnani, who encouraged me to undertake this three year experience. His guidance and support fostered the improvement of my academic and personal skills, and helped me face all issues linked to my research work, even the unexpected ones. I am also grateful to my co-supervisor, Prof. Mattia Merlin, for his continuous support from the early to the final stages of my PhD. Thanks for the stimulating discussions and for your willingness to proofread countless revisions of this manuscript, especially in the evenings and during the weekends.

It was a great pleasure to work with excellent researchers in the Metallurgy & Corrosion Group of the University of Ferrara. Prof. Fabrizio Zucchi, Prof. Cecilia Monticelli, Prof. Alessandro Frignani, Dr. Andrea Balbo, Dr. Federica Zanotto, Dr. Vincenzo Grassi, Dr. Ali Tahaei and Dr. Marco Abbottoni are gratefully acknowledged for the scientific discussions and for the assistance with the SEM, the Optical 3D Profiler and the preparation of the reagents.

Huge thanks go to Annalisa Fortini, Chiara Soffritti, Elettra Fabbri and Vincenzo Gabrielli for the constant support during my research activities and for the invaluable funny moments spent together. Working with you was a privilege.

I am also very thankful to all my colleagues at the Engineering Department, as well as to the administrative and technical staff, for creating a positive work environment and for all the help they have kindly provided to me.

I would like to express my sincere gratitude to Prof. Lars Arnberg and Prof. Marisa di Sabatino Lundberg, who hosted my stay at the Norwegian University of Science and Technology (NTNU) in Trondheim and gave an enormous contribution to my researches with their hints and ideas. Many thanks for giving me the opportunity of being part of the Solidification and Casting Group and participating in the Group Seminar in Freiberg. I also gratefully acknowledge Dr. Arne Nordmark and Dr. Kurt Sandaunet for helping during the casting trials and for sharing their expertise with me.

To the "Trondheim Crew", who transformed my experience abroad into one of the most engaging periods of my life: Arnaud Muller, Guilherme Gaspar, Enrico Riccardi, Benedikte Grimeland, Yvonne Grimeland, Sigbjørn Egge, Antoine Autruffe, Kai Erik Ekstrøm, Song Zhang, Torunn Ervik and the two aluminium guys, Thomas Hartmut Ludwig and Anil Chandra Ramesh Adamane. Special thanks go to Chiara Modanese, Jonida Abazaj and Emilio Catelli for the pleasant chats, the large and funny dinners, the ice creams n°25 and the future business plans.

To my friends, near and far, for the amazing moments we have shared, for listening, offering me advice and helping me overcome setbacks. We have grown up and we have changed, but the esteem I have for all of you has never been so high. Thanks for always making me feel at home just because of your presence, for your thoughts and well-wishes during all these years. Our debates, dinners, Trivial Pursuit nights, Skype calls, emails and travels are just parts of a bigger deal, for which I will never be able to thank you enough.

I owe my deepest gratitude to my family, especially my parents Cristina and Marco. None of this would have been possible without your love, patience and trust in me. Thanks for being there whenever I needed, for encouraging me in all my pursuits and inspiring me to follow my dreams and interests, knowing what I wanted before even I did.

A heartfelt thanks goes to my brother Paolo. You made me think positively even in the most stressful situations, always managing to get a smile out of me. I would like you to know that you are my source of inspiration, as a person and as a researcher. Thanks also for your constant IT support: without you, this thesis would not have become so beautiful, literally.

The Last and Uttermost thanks goes to my Cutie. I have Always been impressed by your ability to read into me, touching my innermost strings. No words can express how deeply grateful I am for your never-ending support, encouragement, patience and understanding, which go far beyond everyone else could give. Thank you from the deep.

Abstract

It is well-established that the static and dynamic properties of the A356 aluminium casting alloy (Al-7%Si-0.3%Mg) depend on several parameters, which in turn are related to (i) the casting process, i.e. melt treatments and solidification conditions, and (ii) the physical metallurgy of the alloy, i.e. chemical composition and heat treatment. However, despite the large amount of literature on this topic, few and inconclusive results concerning the influence of grain refinement on the mechanical properties of this widely used alloy have been provided so far. The presence of undesired impurity elements coming from the manufacturing process of primary aluminium has also recently arisen as a major issue for the final quality and structural performance of foundry alloy products. In particular, it has been reported that the elements Ni and V will progressively enter the chemical composition of future aluminium casting alloys, as currently there are no cost efficient methods for removal. Therefore, the aim of this doctoral thesis is to investigate the effect of grain refinement and Ni/V trace impurities on the impact and tensile properties of the A356 alloy. The main results of these separate research studies are summarized as follows:

- The influence of three commercial Ti-B based grain refiners in form of can (GR1), tab (GR2) and granular flux (GR3) on the impact properties of Sr-modified A356-T6 specimens obtained by permanent mould casting was studied by adding equal amounts of the products to the molten alloy. Even if the grain size could not be directly related to impact toughness, it was found that the grain refiners exert an indirect effect on impact properties through changes in the SDAS, whose slight increase allows fracture to propagate with a more severe low-energy transgranular mode, and modifications in the size and shape of β-Al_5(Fe,Mn)Si intermetallic compounds. These concurrent effects were taken into account by applying a multiple regression analysis technique, which was identified as a valid methodology to describe the variation of total absorbed energy.

- The tensile and impact properties of unmodified A356 alloys added with 600 ppm Ni or 1000 ppm V were assessed by analysing specimens obtained from sand and permanent mould casting in both as-cast and T6 heat treated conditions. It was observed that Ni and V markedly affect the *tensile properties* of sand cast samples in the as-cast condition, the former element by promoting the formation of harmful brittle Ni-rich

intermetallic compounds (Al_9FeNi and Al_3Ni), whereas the latter through a beneficial solid solution strengthening of the α-Al matrix, which allows the tensile specimens to bear higher stresses compared to the corresponding base alloy samples. Experimental results and SEM observations evidenced that either the application of T6 heat treatment or the high cooling rate linked to the permanent mould casting process can effectively counteract the detrimental influence of Ni. On the contrary, a V concentration of 1000 ppm generally exerted a positive effect on the tensile properties. This element had also a strong influence on the *impact properties* of A356 alloy. V-containing sand cast alloys absorbed slightly higher impact energies compared to the corresponding A356 base alloys, whereas a considerable decrease in the total absorbed energy was observed in the permanent mould cast alloys due to a loss of ductility linked to V in solid solution. Contrary to the tensile properties, it was found that the trace element Ni has a negligible effect on the impact toughness of the alloy.

Sommario

È noto che le proprietà statiche e dinamiche della lega di alluminio da fonderia A356 (Al-7%Si-0.3%Mg) sono funzione di diversi parametri, i quali dipendono (i) dal processo di colata, ovvero dal trattamento del metallo fuso e dalle condizioni di solidificazione, e (ii) dalla metallurgia fisica della lega, vale a dire dalla composizione chimica e dallo stato di trattamento termico. Nonostante tali aspetti siano stati ampiamente discussi in letteratura, pochi lavori hanno avuto come obiettivo lo studio dell'influenza dell'affinamento del grano sulle caratteristiche resistenziali della lega. I risultati presentati, inoltre, non hanno fornito un'indicazione definitiva sui reali benefici di questo trattamento, lasciando quindi spazio a futuri approfondimenti. Un'ulteriore tematica che negli ultimi anni ha suscitato crescenti preoccupazioni in ambito industriale consiste invece nel graduale incremento del contenuto di impurezze nei lingotti di alluminio primario. Le impurezze in tracce di Ni e V sono state poste sotto particolare osservazione soprattutto per quanto riguarda i possibili effetti sulle prestazioni meccaniche e sulla qualità finale dei getti, non essendo attualmente a disposizione tecniche efficaci ed economiche per la purificazione del metallo da questi elementi. Alla luce di tali considerazioni, lo scopo di questa tesi di dottorato è pertanto lo studio dell'effetto dell'affinamento del grano e degli elementi in tracce Ni e V sulle proprietà ad impatto e a trazione di questa importante lega da fonderia. I risultati principali di questi distinti progetti di ricerca sono riportati di seguito:

– Nella prima attività di ricerca è stata valutata l'influenza di tre affinanti commerciali a base di Ti-B, sotto forma di lattina (GR1), pastiglia (GR2) e flusso granulare (GR3), sulle proprietà ad impatto di leghe A356-T6 modificate allo Sr e colate in conchiglia. A tal fine, le leghe sono state trattate aggiungendo al metallo fuso identiche quantità in peso dei tre prodotti. Nonostante non sia stato possibile ricavare una correlazione diretta tra la dimensione del grano e la resistenza ad impatto del materiale, è stato osservato che tutti i prodotti affinanti realizzano comunque un effetto indiretto sulle proprietà ad impatto attraverso variazioni dello SDAS, il cui incremento permette alla frattura di propagare secondo modalità transgranulari a basso assorbimento di energia, e della dimensione e forma dei composti intermetallici β-Al_5(Fe,Mn)Si. L'utilizzo di tecniche di regressione multipla ha permesso di tenere conto di entrambi gli effetti e di descrivere con buona accuratezza la variazione dell'energia totale assorbita all'impatto.

– Oggetto del secondo progetto di ricerca è stato lo studio delle proprietà a trazione e ad impatto di campioni in lega A356 non modificata e colata sia in sabbia sia in conchiglia, a cui sono state aggiunte quantità dosate di Ni o V in modo da raggiungere rispettivamente un contenuto di 600 ppm di Ni o 1000 ppm di V. I campioni sono stati caratterizzati sia allo stato as-cast sia dopo trattamento termico T6. È stato osservato che Ni e V influenzano considerevolmente le *proprietà a trazione* dei campioni colati in sabbia e in condizione as-cast. Il primo elemento agisce incentivando la formazione di intermetallici fragili contenenti Ni (Al_9FeNi e Al_3Ni), i quali diminuiscono sia il carico di snervamento sia il carico di rottura della lega, mentre il V determina un effetto di rinforzo per soluzione solida all'interno della matrice di α-Al, consentendo ai provini di trazione di poter sopportare carichi più elevati prima del cedimento. I risultati delle prove sperimentali e le osservazioni al SEM hanno inoltre evidenziato che l'applicazione del trattamento termico T6 o la maggiore velocità di solidificazione ottenibile con la tecnica di colata in conchiglia possono contrastare efficacemente gli effetti negativi del Ni. Un generale miglioramento delle proprietà a trazione è stato invece riscontrato nelle leghe contenenti 1000 ppm di V. Questo elemento ha effetti rilevanti anche sulle *proprietà ad impatto*: le leghe colate in sabbia contenenti V assorbono maggiori energie all'impatto rispetto alle corripondenti leghe A356 di riferimento, mentre quelle colate in conchiglia manifestano una considerevole riduzione dell'energia totale assorbita a causa della perdità di duttilità della matrice dovuta al V in soluzione solida. Contrariamente alle proprietà a trazione, è stato osservato che il Ni ha un'influenza del tutto trascurabile sulla resistenza ad impatto della lega.

Contents

Part 2

Introduction

The objective of this thesis work is to develop new knowledge on the influence of grain refinement and Ni/V trace additions on the impact and tensile properties of the A356 aluminium casting alloy. To accomplish this, the following scheme has been adopted:

PART 1 is a literature survey intended to give the reader sufficient background on the theories of grain refinement and on the issue concerning the increasing of Ni and V concentrations in primary aluminium, as well as previously reported results on the influence of these parameters on the impact and tensile properties of the A356 aluminium casting alloy. The main features of this Al-Si-based alloy such as the effect of alloying and impurity elements, the microstructure and the heat treatment are also briefly discussed. Eventually, the summary and the main conclusions from the articles are reported in this part.

PART 2 contains the results of the work as a collection of three articles. The papers are presented in the form they were submitted for publication or printed. The manuscripts included in this section are:

A. D. Casari, M. Merlin and G.L. Garagnani, "A comparative study on the effects of three commercial Ti-B based grain refiners on the impact properties of A356 cast aluminium alloy," *Journal of Materials Science*, vol. 48(12), pp. 4365-4377, 2013.

B. D. Casari, T.H. Ludwig, L. Arnberg, M. Merlin and G.L. Garagnani, "The effect of Ni and V trace elements on the mechanical properties of A356 aluminium foundry alloy in as-cast and T6 heat treated conditions," **submitted to** *Materials Science and Engineering A*.

C. D. Casari, T.H. Ludwig, L. Arnberg, M. Merlin and G.L. Garagnani, "Impact behaviour of A356 foundry alloys in the presence of trace elements Ni and V," **submitted to** *Journal of Materials Engineering and Performance*.

Part 1

Chapter 1

Theoretical Background

1.1 Al-Si foundry alloys

Al alloys have become increasingly important over the past few decades as a result of their unique properties such as light weight, high strength and resistance to corrosion, which make them ideal materials for use in conventional and novel applications. The different alloys are designated as wrought and cast alloys and are classified into series based on the alloying elements and their typical range. The Al-Si alloys (3xx.x series, according to the cast alloy designation system of the Aluminum Association) form the mainstream of the industrially important engineering cast alloys. These alloys are widely used for automotive applications, including wheels, engine and gear parts due to their excellent castability, high strength to weight ratio and good corrosion and wear resistance [1–3].

The Al-Si system consists of a simple eutectic system with solid solution phases at both ends of the phase diagram, and fcc Al and diamond cubic Si (Figure 1.1) [3]. The maximum solubility of Si in Al is 1.5 at% at 577 °C and 0.05 at% at 300 °C, whereas the maximum solubility of Al in Si is 0.016 at% at 1190 °C and becomes negligible at lower temperatures. The only invariant reaction for the Al-Si system is a eutectic reaction (Liq. $\rightarrow$ Al(s) + Si(s)). The eutectic temperature is 577 °C at a composition of 12.2 at% Si. The solidification of hypoeutectic alloys starts by the formation of primary α-Al dendrites. Further cooling leads to the growth of this solid solution phase, which progressively rejects Si into the residual liquid until the eutectic temperature is reached. When the undercooling is large enough, the final eutectic reaction occurs. Unlike the previous alloys, the solidification of hypereutectic alloys starts by nucleation of polyhedral primary Si crystals and ends with the subsequent eutectic reaction.

The content of Si in commercial Al-Si alloys (which are not pure binary systems) varies from 4 to 22 wt%. The lower Si limit is related to the need to obtain a relatively narrow solidification gap and, as a consequence, a good castability, whereas the upper limit is set by the need to maintain a minimal amount of plasticity into the alloy. The expansion of Si crystals during solidification partially compensates for the contraction of Al, and thus

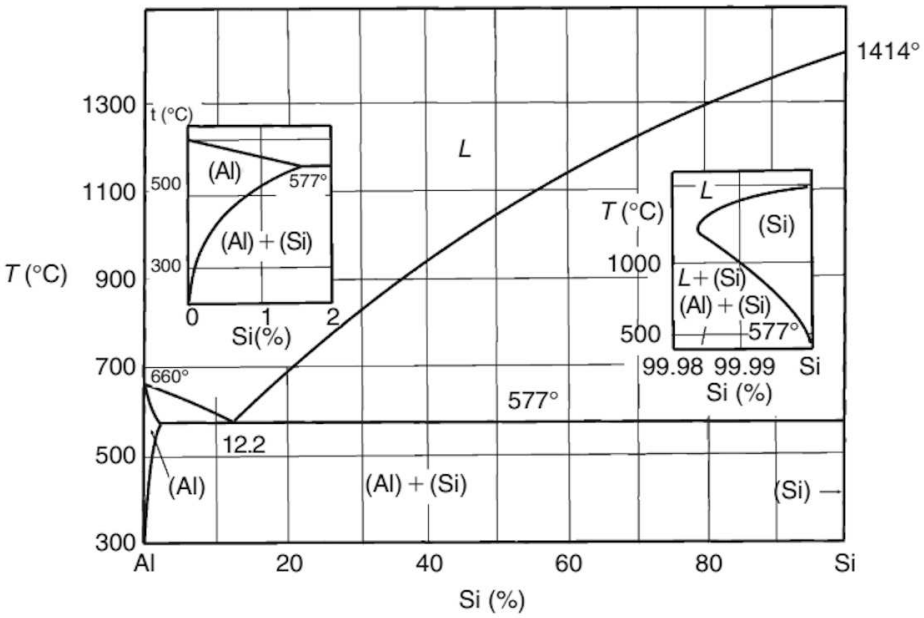

Figure 1.1 – *Al-Si phase diagram [3].*

diminishes the tendency of Al-Si alloys toward shrinkage and hot tearing. In the same way, Si reduces the thermal expansion coefficient. Moreover, Si improves the fluidity of Al-alloys owing to its high latent heat of fusion. Finally, Si constituent particles play an important role in controlling many of the Al-Si alloys' physical and mechanical properties [4]. In addition to the Al-Si eutectic phase, a number of intermetallic phases may form in commercial Al-Si alloys during solidification, depending on the chemical composition and cooling rate.

1.1.1 Grain refinement of hypoeutectic Al-Si alloys: nucleation and growth of the primary α-Al phase

Since hypoeutectic Al-Si alloys have a large volume fraction of primary α-Al dendrites in their microstructure, the formation of this phase is of great importance, as it will strongly influence the soundness and the mechanical properties of the castings. In general, castings with columnar or large grains have poor castability and mechanical properties. On the contrary, a fine and equiaxed grain structure generally improves mechanical and fatigue properties of castings and reduces hot-tearing susceptibility. Additionally, it provides a good castability, a better dispersion of secondary phases and microporosities, and an improvement in feeding during solidification.

The refinement of primary α-Al dendrites can be obtained by means of different techniques including (i) high cooling rates, (ii) heterogeneous nucleation, (iii) melt agitation and vibration during solidification and (iv) mould coating (a number of papers in [5]). Among all these methods, the grain refinement by heterogeneous nucleation (inoculation) has become the most popular and, as a result, a common industrial practice in the casting process. The addition of grain refiners, usually master alloys containing potent nucleant particles (see

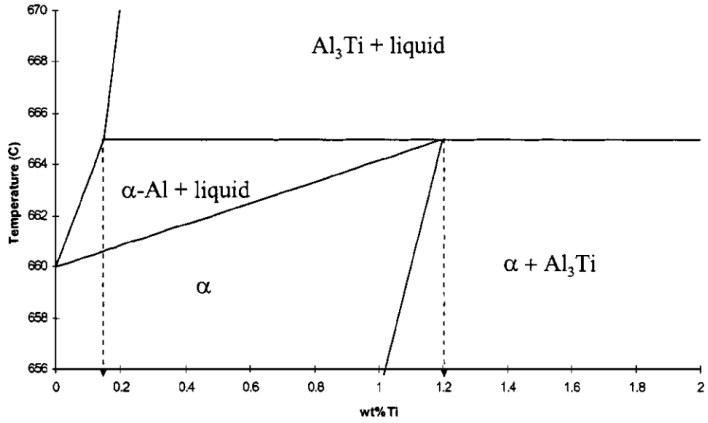

Figure 1.2 – *Al-rich end of the Al-Ti phase diagram. The peritectic concentration is 0.15 wt% [7].*

also Section 1.2.1.4), promotes the formation of a fine equiaxed macrostructure by deliberately suppressing the growth of columnar and twin columnar grains.

Many authors have investigated the fundamental aspects of grain refinement from both theoretical and industrial points of view. Several mechanisms for the nucleation of α-Al in Al-Ti-B-added alloys have been proposed and extensively reviewed [5–7]. While some authors have considered the importance of heterogeneous nucleating centres in obtaining a fine grain structure (*Nucleant Paradigm*) [8–11], others have focused on the influence of solute elements (*Solute Paradigm*) [12–14].

The first theories concerning the *Nucleant Paradigm* were postulated by Cibula in 1949 [8]. In particular, it was observed that the addition of Ti has a strong effect in nucleating the primary α-Al phase. The prior existence of Al_3Ti nuclei forming the primary phase via a peritectic reaction (Figure 1.2) was suggested as the fundamental reason for the increased nucleation of grains. In their study, Davies *et al.* [15] observed Al_3Ti particles at the centre of Al grains, thus demonstrating that they are active nuclei for primary α-Al phase. Their potency is probably due to the favourable orientation between the lattices of the two phases ($\approx$ 4% lattice disregistry at 298 K), the exact value depending on the planes considered [16, 17], and to several cristallographically equivalent planes capable of nucleating α-Al. According to the binary Al-Ti phase diagram, Al_3Ti is thermodynamically unstable in the liquid metal at a concentration below about 0.15 wt%. Typical dissolution times were observed to be less than a minute [18], thus leading to the fading of the grain refinement effect with time.

However, the results of several research works showed that the effect of Ti on the grain refinement of Al starts at concentrations even below 0.10 wt% (Figure 1.3) [19,20]. The effectiveness of Ti additions at these levels was proven by Schumacher and Greer [21, 22], who studied the nucleation event on an amorphous Al alloy, the $Al_{85}Y_8Ni_5Co_2$ (at%), inoculated with an Al-Ti-B master alloy and then quenched on a rapidly rotating, water-cooled copper wheel. Using TEM, they observed that Al_3Ti was present as absorbed layers on TiB_2 crystals, so that its existence was stabilised at Ti levels lower than that expected from the phase diagram. Additionally, Al_3Ti maintained its effectiveness in nucleating α-Al for longer periods,

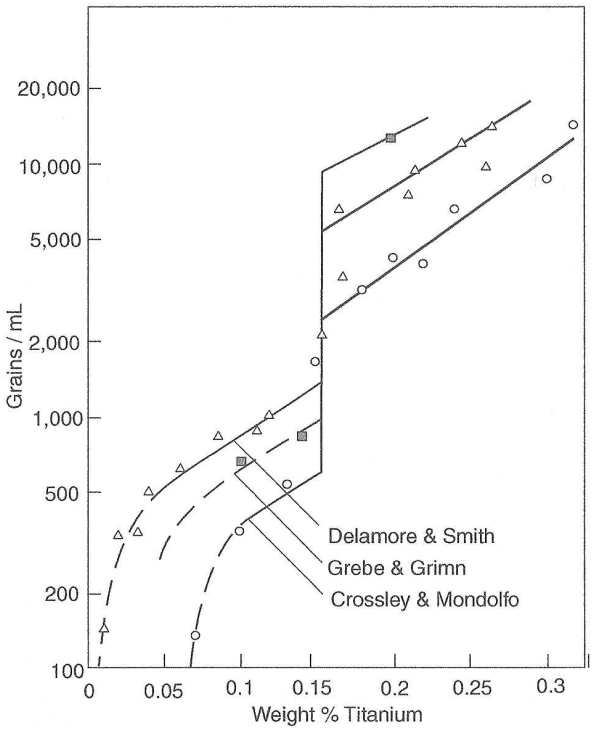

Figure 1.3 – *Increase in grain refinement with increasing Ti addition, particularly starting from the peritectic concentration [7].*

due to the near-insolubility of TiB_2 in the melt.

In some casting situations, boride particles are also responsible for the initiation of α-Al grains, which is consistent with the findings of several authors, who noticed TiB_2 particles at the centres of α-Al dendrites [23, 24]. As previously observed for Al_3Ti, this is due to the moderately low disregistry between specific TiB_2 and α-Al phase atomic planes ($\approx 5.9\%$ at 298 K). Similarly to TiB_2, AlB_2 are also active nuclei for α-Al grains. However, these particles are less stable than TiB_2, which increases the probability for B to be substituted by other alloying elements present into the melt [10]. Conversely, mixed $(Al,Ti)B_2$ boride particles appear to be more stable, since they have been observed even at long holding times within many dilute ternary alloys [16, 23, 24].

Hence, grain refinement can be promoted by borides or Al_3Ti, both of which are potent nuclei and provide very low grain-initiation undercoolings [18]. The grain refinement potency of Al_3Ti is higher but in its absence, i.e. in alloys containing less than 0.15 wt% Ti, borides become the nucleant phase. A small fraction of borides, however, provide an active nucleus for primary α-Al grains, whereas the excess particles are pushed by the growing grains and settle along the grain boundaries. It has been found that inactive particles have sub-micron size, while the active inoculants are larger [25]. According to Greer *et al.* [26], the number of grains is determined by a free-growth condition in which a grain grows from a refiner particle at an undercooling inversely proportional to the particle diameter. Larger particles can therefore support growth at a smaller undercooling. As the undercooling increases, more

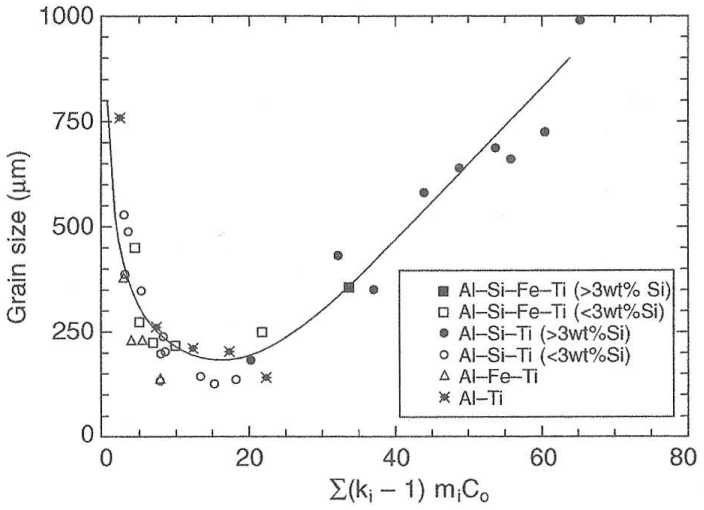

Figure 1.4 – *Effect of the growth restriction factor (GRF) on the grain size of various Al alloys [7].*

inoculants are activated. Nevertheless, when a certain nucleation rate is reached, the latent heat released from the grains exceeds the heat extracted from the system, so that the temperature increases and no more inoculants are activated. Since most of the inoculants are small, they remain inactive and are found at the grain boundaries.

Therefore, it appears that an optimum grain refining can be obtained when a surface is provided at, or just above, the liquidus temperature of the alloy. Effective grain refinement, however, also requires the suppression of grain growth, which is assumed to be controlled by segregating elements (*Solute Paradigm*). As a matter of fact, solute influences the dendrite growth by building up a constitutionally undercooled zone in front of the solid/liquid interface, which facilitates the nucleation of new grains [7,27]. The growth-restricting effect of solute elements can be quantified using the growth restriction factor GRF, which is defined as $mC_0(k-1)$, where m is the gradient of the liquidus, usually approximated to a straight line, C_0 is the concentration of the solute in the alloy, and k is the partition coefficient between the equilibrium concentrations in the solid and liquid at the growing interface. When a number of solutes are present into the melt, the GRFs are added under the hypothesis that no interaction between the solute phases occurs. Therefore, the GRF for an alloy with multiple solute elements is:

$$GRF = \sum mC_0(k-1) \tag{1.1}$$

The effect of GRF on the size of α-Al grains is shown in Figure 1.4. Initially, grain size decreases with increasing the total value of GRF (Figure 1.4). After a minimum ($\approx$ 150 - 200 μm), further increasing in GRF results in an increase in grain size. This growth is observed only for alloys with Si levels above 3 wt% and is probably related to a poisoning effect of Si towards Ti, as discussed below (see also Section 1.2.1.4) [28].

Therefore, according to the literature, both the addition of nucleant particles and the amount of segregating elements are fundamental in the grain refining process. After the beginning of

heterogeneous nucleation, the solute elements influence the grain refinement in two ways. First, they reduce the growth of the previous grains, thus increasing the duration of the nucleation phase. Then, their segregating ability leads to a constitutionally undercooled zone in front of the growing interface (constitutional undercooling-driven mechanism), hence activating the nucleation of new grains on other primary particles. This explains why, when TiB_2 particles are added to pure Al, no grain refinement is observed [9].
However, it must be noted that the grain size is strongly dependent on the type of alloying elements/impurities present, as reported in [29, 30] and in a number of papers in [5]. For the majority of solute elements, and particularly for Mg, Cu, Zn, an increase in solute content decreases the grain size and promotes an equiaxed microstructure. In contrast, certain elements, e.g. Cr, Zr, Li and Fe, and high levels of Si have an adverse effect on grain refinement. The mechanism of poisoning is not yet well understood but it is generally believed that these elements interact with the grain refining constituents either by altering the chemistry of inoculant particles (mainly Zr), rendering them incapable of acting as substrates for the formation of α-Al dendrites, or by leading to the formation of complex intermetallics that are unable to nucleate aluminium during solidification. Hence, as the presence of solute elements is not always beneficial to grain refinement, particular attention should be paid to the chemical composition of the alloy during the casting process, in order to avoid undesired detrimental effects on the grain refining response. This is especially true for the case of secondary alloys, which possess a higher total impurity content compared to primary alloys.

1.1.2 The issue of Ni and V trace elements

Aluminium producers that are currently focusing primarily on the control of dissolved hydrogen, Na content and inclusion removal, are now facing increasing Ni and V concentrations originating from the petroleum coke used for manufacturing of anodes for the Al electrolysis. In the upcoming years, the levels of Ni and V in the coke are expected to rise to 420 and 1080 ppm, respectively (Figure 1.5) [31]. Estimates show that approximately 50% of these elements partitions into the primary aluminium during the electrolytic reduction of alumina [32].
At this time, there is yet no cost efficient method available for removal of these elements. The existing non-commercial processes for production of ultra purity Al, e.g. three-layer electrolysis, zone refining and fractional crystallisation, can remove Ni and V but cannot be applied to everyday alloys due to their cost [33]. In a recent study, Rhamdhani *et al.* [34] reviewed the available commercial techniques for the removal of Ni impurity from the Al melt, concluding that, at present, none of them appears to be effective. Hence, the authors carried out experimental trials on various Al-Ni-X (X = P, B, Zr, Mg-Zr) systems in order to investigate the possible formation of Ni-containing phases in the Al melt. It was reported that Ni remains in the liquid until the later stages of solidification. Upon further cooling, Ni

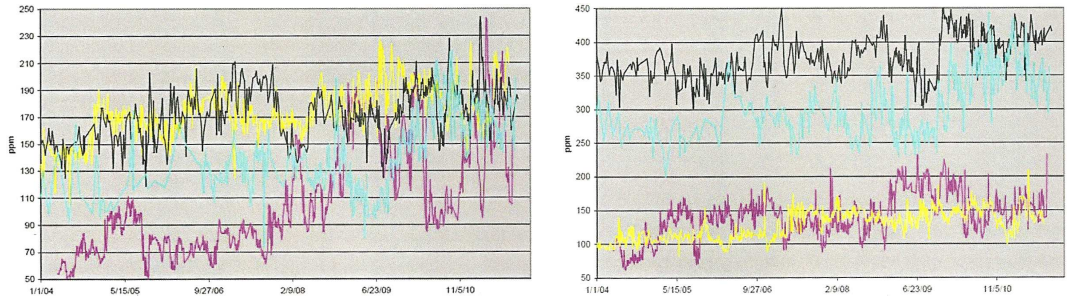

a) **b)**

Figure 1.5 – *Impurity fluctuations in anode grade calcined coke from one supplier given for a) Ni and b) V [31].*

precipitates as an Al-Ni intermetallic eutectic phase combined with any available Fe. Apart from the formation of a metastable Ni_3P phase, which re-dissolves in the melt upon new heating, none of the other added elements were observed to react with Ni, removing this element from the melt.

Conversely, V and other transition metal impurities can be eliminated from liquid Al via the addition of Al-B master alloys containing AlB_{12} or AlB_2 particles (boride treatment). In particular, V reacts with B to form stable vanadium borides (VB_2), which create a ring around the initial boron source [35]. These clusters of borides have higher densities compared to melt Al and settle at the bottom of the furnace. Since the presence of these rings inhibits further reaction between V and B, there is still a potential to improve the boride treatment by avoiding or disrupting the formation of the clusters. Further work is also required to comprehend the mechanism of borides' formation, in order to increase the efficiency and economy of the process.

At present, the response to the problem is essentially the monitoring of Ni and V levels during primary aluminium manufacturing and checking for any adverse effects [33, 36]. In the longer term, however, the increasing of Ni and V levels may significantly affect the final quality of the downstream products such as aluminium foundry alloys. It is thus of primary importance to establish whether Ni and V contaminations can have a beneficial or detrimental effect on the microstructural features, and consequently on mechanical, corrosion and manufacturing properties of Al-Si alloys, since they comprise 85 - 90% of the total aluminium cast parts produced.

1.2 The A356 alloy

Among Al-Si foundry alloys, the hypoeutectic A356 alloy (also designated as EN AB-42100, according to the EN 1676-2010 specification) is one of the most widely used in automotive and aerospace industries for critical structure applications because of its advantageous metallurgical and manufacturing characteristics such as good mechanical properties in the heat treated condition, corrosion resistance and excellent castability, which makes it easy to use

in the fabrication of complex machine parts through various casting processes with a low production cost.

1.2.1 Effect of element additions in A356 alloy

Table 1.1 shows the chemical composition of the A356 - EN AB-42100 foundry alloy. In addition to Si, other major alloying elements in this alloy are Mg, Fe and Mn, which are intentionally added in form of master alloys or are inevitably present as impurities from the primary Al production, scrap recycling or manufacturing processes. Further elements, e.g. Na, Sr, Sb, Ti and B, are also added on purpose during the casting process in order to produce specific effects or microstructural transformations. In accordance with the Aluminium Association designation system for cast alloys, a capital letter (*A, B, C*) before the digits indicates a variation in the chemical composition of the base 356 alloy with respect to the amount of Fe, which varies from 0.04 wt% (best primary metal, corresponding to the letter C) to 0.50 wt% (secondary metal), with typical primary levels in the 0.10 - 0.20 wt% range (letter A).

A356 - EN AB-42100	
Element	**Composition [wt%]**
Si	6.50 - 7.50
Mg	0.30 - 0.45
Fe	0.15
Cu	0.03
Mn	0.10
Zn	0.07
Ti	0.18
Others	0.03 (each) 0.10 (total)
Al	bal.

Table 1.1 – *Chemical composition of the A356 - EN AB-42100 foundry alloy in accordance with the EN 1676-2010 specification. No specific information about the maximal tolerable Cr, Ni, Pb and Sn concentrations is given.*

1.2.1.1 Effect of Mg

Mg is intentionally added into the A356 foundry alloy as a key alloying element in order to induce age hardening through the precipitation of fine Mg_2Si dispersoids into α-Al matrix, thus blocking dislocation movement and significantly improving the mechanical properties. Latest findings indicate the following precipitation sequence upon ageing: Supersaturated Solid Solution (SSSS) $\rightarrow$ independent clusters of Mg and Si, co-clusters of Si and Mg $\rightarrow$ Guinier-Preston (GP) zones $\rightarrow$ Si rich phase $\rightarrow \beta'' \rightarrow \beta' \rightarrow \beta$ [37]. GP zones are generally defined as agglomerates of atoms of the major solute elements that possess a diffuse, com-

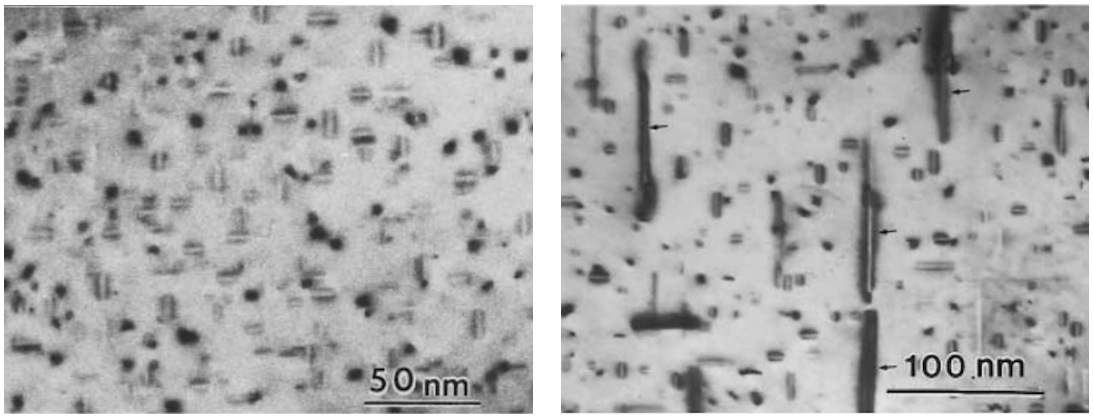

Figure 1.6 – *TEM micrographs of Mg-bearing precipitates obtained at different stages of artificial ageing: a) β'' needle-shaped dispersoids - 4h at 175 °C, b) β' rod-like precipitates - 20h at 200 °C [37].*

pletely or partially coherent boundary with the matrix. When Mg is added to the alloy in the above-mentioned composition range, GP zones are observed as fine plates having a thickness of one atomic layer ($\approx$ 2.5 nm) and a length of about 30 nm, which form randomly in the matrix and also heterogeneously on matrix dislocations [38–40]. They consists of alternating arrangement of the columns of Mg and Si atoms along the $\langle 100 \rangle_\alpha$ direction, with a chemical composition of Mg:Si = 1. Several GP zones aggregate with increasing ageing time to form needles and exhibit a complicated morphology. The β'' transition phase, whose chemical composition is Si:Al:Mg = 6:3:1, also shows a needle-like shape (Figure 1.6a). Calorimetric studies reveal that the formation of GP zones and β'' precipitates are parallel and competitive processes [41] and that the transition from GP zones to β'' proceeds without the dissolution of the former precipitates [37]. These two phases are easily sheared by dislocations due to their coherency with the matrix and small size. The presence of dispersoids homogenises the slip distribution in underaged alloys, so that local strain concentration at grain boundaries and consequent intergranular fracture are reduced. The next phase in the transformation sequence is the β' phase (Figure 1.6b), which has a lower Mg:Si ratio ($\approx$ 1.7) than the equilibrium phase β-Mg_2Si [42]. The β' precipitates are partially coherent with the matrix and also lie along the $\langle 100 \rangle_\alpha$ direction. However, they cannot be sheared by dislocations due to their rod-like morphology. Hence, the β' transition precipitates increase strength by Orowan looping (Figure 1.7). Further ageing leads to the final precipitation of the equilibrium phase β-Mg_2Si, which consists of non-coherent platelets that make little contribution to the strength of the alloy [2].

1.2.1.2 Effect of Fe and Mn

Fe is always present in a commercial A356 alloy. It is considered the main impurity element and perhaps the most detrimental to the mechanical properties of the alloy [44]. Fe enters the primary Al alloys through both the Bayer and Hall-Héroult processes, where it is present

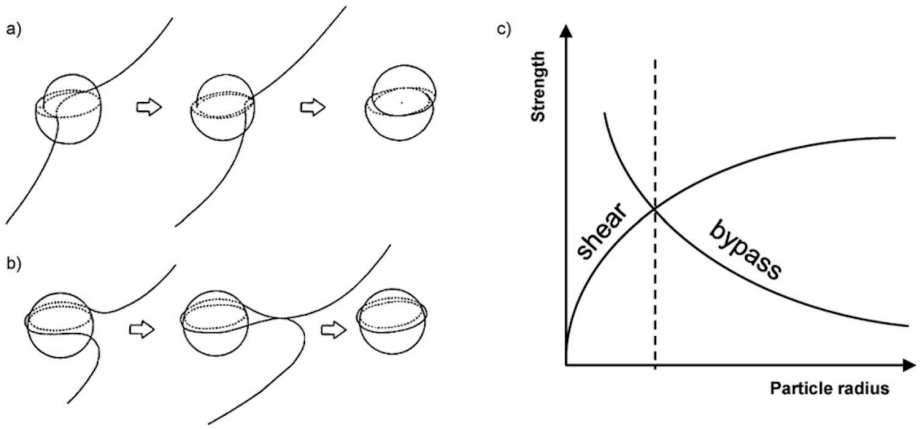

Figure 1.7 – *Precipitation hardening mechanisms: moving dislocations pass small and not too hard precipitates by a) shearing, whereas large and hard particles are usually bypassed by b) bowing (Orowan mechanism). c) shows the qualitative relationship between precipitate radius and strength of the particles to resist shearing or bypassing by dislocations [43].*

as Fe oxides in the ore and in the coke used for anodes, respectively. It is also accidentally added during melting and casting through the use of equipment that contains Fe, and via recycled scrap charges. Since there is no commercial method to efficiently reduce Fe levels, the presence of this element in final aluminium alloy parts is inevitable [45].

Although Fe is highly soluble in liquid aluminium and its alloys, it has very little solubility in the solid (max 0.05 wt%, 0.025 at%), and so it tends to combine with other elements to form intermetallic phase particles of various types. The most common Fe-rich phases in A356 foundry alloy are the β-Al_5FeSi phase with a needle or platelet morphology (Figure 1.8a) and the α-Al_8Fe_2Si with a "Chinese-script"shape (Figure 1.8b). High Mg contents promote the formation of the π-$Al_8Mg_3FeSi_6$ quaternary phase with a "Chinese-script"morphology (Figure 1.8c,d). The precipitation of specific intermetallic phases depends on the Fe content, the cooling rate, the presence of other elements soluble in the Fe-rich phases and the thermal history of the melt.

The mechanical properties are negatively affected by these Fe-bearing intermetallics, whose influence is defined not only by their morphology, but also by their size and distribution. As reviewed in detail by Mbuya *et al.* in [44], the most harmful effect on mechanical properties is exerted by the β-Al_5FeSi needle-shaped particles. Their elongated morphology impedes the movement of dislocations more efficiently compared to the other Fe-rich phases. As a consequence, the dislocation pile-ups on the β-Fe particles cause severe stress concentrations, thus leading to the crack of both these brittle intermetallic compounds [46] and/or the interface between β-Al_5FeSi phases and the Al matrix [47]. The other intermetallic phases are less detrimental for mechanical properties due to their more favorable morphologies.

Mn is commonly added to control the deleterious effects of Fe through the formation of the α-$Al_{15}(Fe,Mn)_3Si_2$ intermetallic compounds [48–50], which possess a less detrimental "Chinese-script"morphology compared to β-Al_5FeSi needles. However, the overall amount

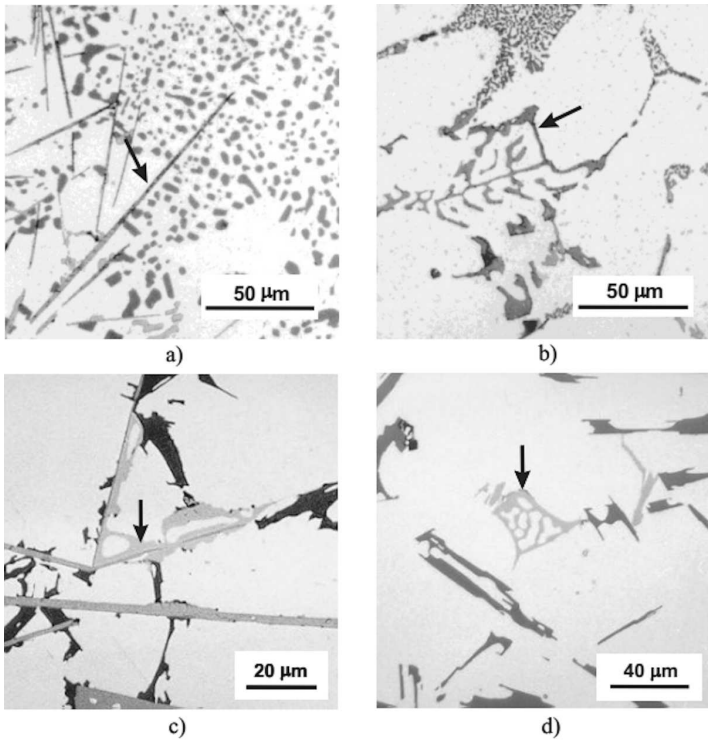

Figure 1.8 – *Micrographs of the most common Fe-bearing intermetallic compounds detected in A356 alloy: a) β-Al_5FeSi platelets, b) α-Al_8Fe_2Si with a "Chinese-script"morphology, c) π-$Al_8Mg_3FeSi_6$ growing from the β-phase, d) "Chinese-script"shaped π-phase [45].*

of Mn + Fe should not exceed 1 - 1.5 wt% (depending on Si concentration) in order to avoid the formation of colonies of large α-$Al_{15}(Fe,Mn)_3Si_2$ primary crystals (sludge) that have a detrimental effect on the mechanical properties of the alloys [3, 44].

1.2.1.3 Effect of Na, Sr and Sb

Na, Sr and Sb are added as impurity elements to molten Al in order to modify the as-cast structure of eutectic Si particles from a coarse acicular or flake morphology, which causes the casting to exhibit poor ductility, to a fine fibrous structure (Figure 1.9), thus resulting in a substantial improvement of mechanical properties.
Even though several theories have been put forward in the last decades in order to explain how eutectic Si modification occurs, the exact mechanism by which the modifier element changes the morphology of Si is still under debate. A comprehensive literature review including proposed modification mechanisms, interaction of defects and non-destructive assessment by thermal analysis has been recently presented by Hegde and Prabhu [51].
As for the practical aspects of modification melt treatment, Sr and Sb are generally added as master alloys and ingots, whereas the addition of Al-Na-based master alloys is not convenient due to the very low solubility of Na in solid Al ($\approx$ 0.002 at% [3]). Therefore, elemental Na vacuum-packed in aluminium cans is commonly used, as well as Na-containing fluxes or salts. Na or Sr are usually added at levels in the range of 0.01 - 0.02 wt% [52–54]. Although

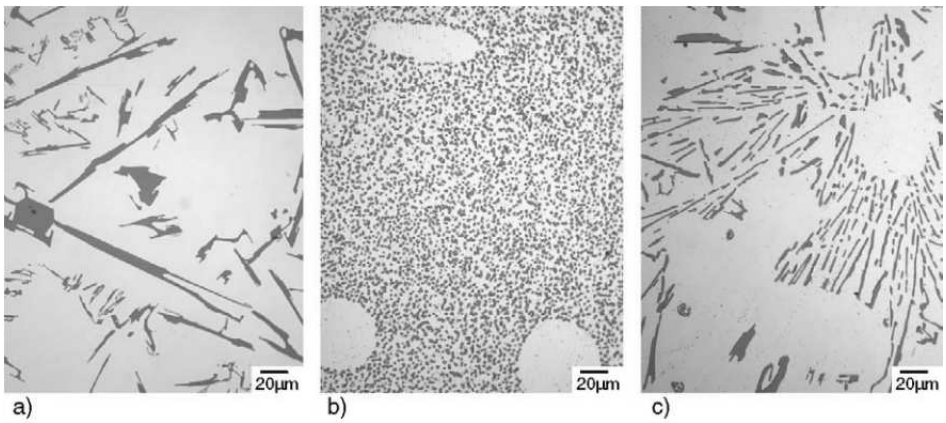

Figure 1.9 – *Eutectic Si morphology in a) unmodified, b) Sr-modified (300 ppm Sr) and c) Sb-modified (2400 ppm Sb) hypoeutectic Al-Si alloys [58].*

less Na is required to achieve the same optimum level of eutectic modification compared to Sr (100 ppm Na vs. 200 ppm Sr) [55], Na-modified alloys are observed to have an increased propensity to microporosity formation compared to Sr-modified alloys [56]. Additionally, Na fades faster than Sr due to its high vapor pressure at melt temperatures, so that a short holding time is required between modification treatment and casting [57]. In contrast, Sr is an effective modifier with much longer retention times than Na (up to 10 h) owing to its low oxidation sensitivity. Further significant advantages of Sr are its good recovery (90% of Sr addition vs. 20 - 30% of Na) and the possibility to accurately control the amount of addition. Optimum mechanical properties are obtained in the range 50 - 150 ppm. A decline in properties above this level is generally due to both the increase in the amount and size of porosity and the formation of the Al_4SrSi_2 intermetallic compound (usually above 300 ppm) [52, 57]. In contrast to the previous modifying elements, additions of Sb up to a few thousand ppm merely refine the coarse Si flakes to fine closely spaced Si platelets and results in partial modification [58].

1.2.1.4 Effect of Ti and B

Ti and B are commonly added in form of Al-Ti, Al-Ti-B and Al-B master alloys to molten Al in order to produce an equiaxed grain structure in the castings through heterogeneous nucleation, i.e. the formation of α-Al dendrites is promoted by potent Al_3Ti, TiB_2 and AlB_2 nucleant particles dispersed into the melt (see also Section 1.1.1). Master alloys are usually added in form of rods, waffles and ingots. Further grain refinement methods involve the reaction of molten Al with tabs of halide salts (K_2TiF_6 and KBF_4). Novel techniques include the addition of a granulated flux during the stirring of the melt or powder injection into the molten Al [59, 60].

In Al-Ti master alloys, the Ti content usually falls in the range 6 - 10 wt%, whereas ternary Al-Ti-B master alloy can have either Ti or B in excess of the TiB_2 stoichiometry (Ti:B = 2.22). The Al-5Ti-1B is one the most used and offers a remarkable performance in the continuous and

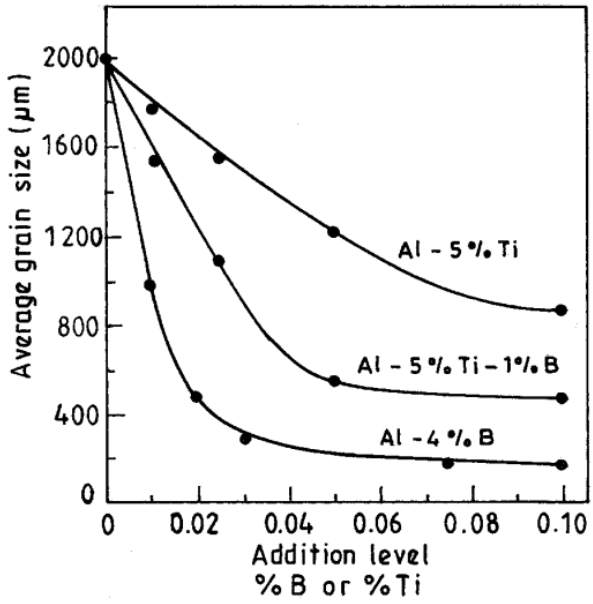

Figure 1.10 – *Grain refinement of A356 alloy with Al-5Ti, Al-5Ti-1B and Al-4B master alloys [5].*

semi-continuous casting of wrought alloys, but fails to meet the expectations, as well as the Al-Ti master alloys, in the case of Al-Si alloys with a Si content larger than 3 wt%, due to the reaction between Si and Ti to form Ti-Si phases at the expense of Al_3Ti particles [11, 28, 61]. Therefore, some new master alloys, such as Al-3Ti-3B, Al-1Ti-3B and Al-3B/Al-4B have been developed and reported to provide better grain refinement performances than the Al-5Ti-1B, since a higher amount of stable and potent nucleant particles, i.e. $(Al,Ti)B_2$, is introduced (Figure 1.10) [28, 62]. Additionally, Al-3B and Al-1Ti-3B master alloys have been found to be more efficient grain refiners even at long holding times. As a result, the mechanism of fading of the grain refiners, i.e. the developing of a coarse grain structure in the castings due to either dissolution or settling/floating (or both) of nucleating particles during long holding [5], is not observed [62].

As previously discussed, in addition to high levels of Si, some alloying/impurity elements such as Cr, Zr, Li and Fe can produce a detrimental effect on the grain refining efficiency of Al-Ti-B master alloys, resulting in much coarser α-Al grains compared to the primary grains obtained in their absence [5, 29, 30]. A mutual poisoning effect between Sr and B is also noticed in Al-Si casting alloys when the contents of Sr and B exceed certain limits, namely 0.040 wt% Sr and 0.028 wt% B [63]. Conversely, the addition of Mg to Al-Si alloys, e.g. the A356 alloy, improves the grain refining response and helps in overcoming the poisoning effect of Si by reducing the surface tension and improving the wettability of the melt with the heterogeneous nucleating sites [64, 65]. In their research on a number of alloys having compositions in the range 7 - 20 wt% Si and 0 - 0.8 wt% Mg, Kori *et al.* [65] showed that there exists an optimum level of Mg to be effective, which depends on the Si content of the alloy and the addition level of the grain refiner.

Therefore, in industrial practice, it is suggested to avoid large additions of soluble Ti to

Al-Si alloys with high Si levels, such as the A356 alloy, thus refining with the B-richer Al-Ti-B master alloys. The recommended addition is 10 - 20 ppm of B, with low dissolved Ti levels to improve grain refining efficiency and to avoid sludge [66]. More specifically, good grain refinement with grain sizes below 200 μm after 120 min holding can be achieved with addition levels of 0.022 wt% B, 0.025 wt% B, and 0.035 wt% Ti respectively with Al-1Ti-3B, Al-3B, and Al-5Ti-1B master alloys [62]. In most cases, however, further additions of Ti as a growth restriction element are generally not required, as commercial primary and secondary Al-Si casting alloys contain very high residual amounts of Ti (> 0.15 wt%) resulting from repeated recycling and generous specifications.

1.2.2 Microstructure

The microstructure of the A356 alloy in the as-cast condition generally consists of primary α-Al dendrites, a dispersion of eutectic Si particles and various intermetallic compounds such as Mg_2Si, β-Al_5FeSi and π-$Al_8Mg_3FeSi_6$ (Figure 1.11). The solidification behaviour of the unmodified A356 alloy is well documented in literature [46, 67] and depends on Mg and Mn contents [68], Mg:Fe ratio [69] and cooling rate. The typical solidification sequence noted for this alloy is:

- *T = 883 K (610 °C)* - Start of solidification and formation of α-Al dendrites
- *T = 841 K (568 °C)* - Start of main eutectic reaction: Liq. $\rightarrow$ Al + Si + Al_5FeSi
- *T = 830 K (557 °C)* - Precipitation of Mg_2Si: Liq. $\rightarrow$ Al + Si + Mg_2Si
- *T = 823 K (550 °C)* - Precipitation of complex eutectic: Liq. $\rightarrow$ Al + Si + Mg_2Si + $Al_8Mg_3FeSi_6$
- *T = 816 K (543 °C)* - Solidus

The α-Al dendrites contains some dissolved Si and Mg, which are distributed with a concentration profile from the centre to the edge of the dendrite arms due to segregation effects. The morphology of primary α-Al grains can be categorised as equiaxed or columnar, the latter developing in the absence of inoculant particles. The Al-Si eutectic can occur in two main forms: an unmodified form in which Si precipitates as coarse needle-like particles, and a chemical (Na, Sr and Sb additions) or thermal (high cooling rates) modified form in which the Si phase grows as bundles of fine fibers or platelets. The Mg_2Si phase of the ternary eutectic typically grows with a fine "Chinese-script"morphology. As previously observed, the β-Al_5FeSi phase precipitates as randomly distributed platelets, whereas the π-$Al_8Mg_3FeSi_6$ phase occurs in "Chinese-script"and blocky morphologies, both of which sometimes grow directly upon acicular β-Fe intermetallics.

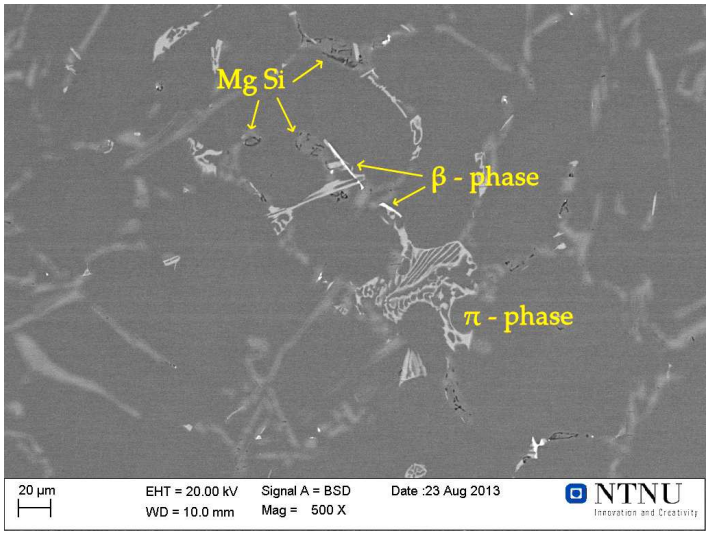

Figure 1.11 – *BSE-SEM micrograph of the as-cast A356 foundry alloy. Aluminium dendrites are in dark grey, whereas Si particles in the interdendritic regions appear in light grey. Intermetallic phases with typical morphologies are also detected and labeled.*

1.2.3 Heat treatment

Various heat treatment cycles can be applied to Al-Si alloys depending on the casting process, the alloy composition and the desired mechanical properties. A typical heat treatment applied to sand and permanent mould cast A356 alloys is the T6 heat treatment, which consists of three stages [43]:

- *Solution treatment* at a high temperature, generally close to the eutectic temperature of the alloy, in order to (i) dissolve the intermetallic particles precipitated during solidification, (ii) obtain a high and homogeneous concentration of the alloying elements in solid solution, and (iii) spheroidise the eutectic Si particles.
- *Quenching*, usually to room temperature, to attain a supersaturated solid solution of solute atoms and vacancies.
- *Age hardening*, either at room temperature (natural ageing) or at an elevated temperature (artificial ageing), to cause the precipitation of strengthening Mg_2Si particles from the supersaturated solid solution.

The possible range of *solution heat treatment* temperatures for the A356 alloy is 475 - 566 °C. In practice, temperature is generally kept below 555 °C in order to avoid incipient melting of the ternary eutectic, with typical solution treatment temperatures around 540 °C. The solution heat treatment gradually dissolves the Mg_2Si and π-$Al_8Mg_3FeSi_6$ phases. The dissolution of the former intermetallic compound is usually completed after 2 - 4 min [43], whereas the latter undergoes necking and is partially replaced by β-Al_5FeSi phase through the progressive dissolution of its Mg and Si into the α-Al matrix. This transformation is both a time-

and composition-dependent reaction, and appears to approach near-saturation within 30 min, hence allowing maximum predicted Mg levels into the matrix to be reached [70,71]. Fe-bearing phases formed during solidification are much harder to dissolve. While β-Al_5FeSi intermetallics fragment and undergo dissolution after a long time at a high temperature, the α-$Al_{15}(Fe,Mn)_3Si_2$ phase is almost unaffected by solution heat treatment. The morphology of eutectic Si particles is also altered by solution heat treatment [72]. A process involving fragmentation, spheroidisation and coarsening takes place and leads to better ductility in both modified and unmodified alloys. The time needed for spheroidisation strongly depends on the solution treatment temperature and on the morphology and size of the eutectic Si particles in the as-cast condition. In particular, fibrous Sr-modified structures are easier to fragment and spheroidise, so that solution treatment time can be decreased.
The *quenching* stage causes the equilibrium solid solution chemistry obtained at the chosen high solution temperature to be retained as a supersaturated solution at room temperature. Faster quenching rates retain a higher vacancy concentration, enabling higher mobility of the Mg and Si atoms in the primary α-Al phase during ageing. However, the drawback with quick cooling is that thermal stresses are induced in the castings. Conversely, slow cooling rates reduce residual stresses and distortions in the components, but also lead to the heterogeneous precipitation of particles at grain boundaries or dislocation, which thus results in a reduction of supersaturation of solute, in a subsequent lower volume fraction of β'' precipitates, and consequently in a lower yield strength after ageing [43,73,74].
The high level of supersaturation and the high vacancy concentration after quenching cause the *age-hardening* to rapidly take place also at room temperature in A356 foundry alloy [75]. However, the formation of metastable precipitates that are either coherent or semi-coherent with the matrix (see also Section 1.2.1.1) is enhanced by artificial ageing, which is usually performed at temperatures in the range of 150 - 210 °C [43,76]. As a direct consequence, the peak hardness in an artificially aged A356 alloy results 30 HV higher than the peak hardness of an equivalent alloy aged at room temperature (Figure 1.12a). Additionally, when an elevated temperature is used, ageing time can be reduced: the time to peak hardness decreases from 10 h to only 20 min when temperature is increased from 170 °C to 210 °C. However, if temperature is increased above 210 °C, a decrease in strength is observed (Figure 1.12b). This effect is related to a change in hardening precipitates. According to Eskin [77], the β' phase precipitates at temperatures above 200 °C, substituting the β'' phase and thus giving a lower contribution to strength.

1.3 Tensile and impact properties of A356 alloy

The tensile and impact properties of the A356 casting alloy (Table 1.2) are governed by various factors, namely (i) those coming from the casting process itself and (ii) those that are influenced by the physical metallurgy of the alloy. Most castings fabricated by the conventional casting processes inevitably contain *casting defects* such as porosities, shrinkage

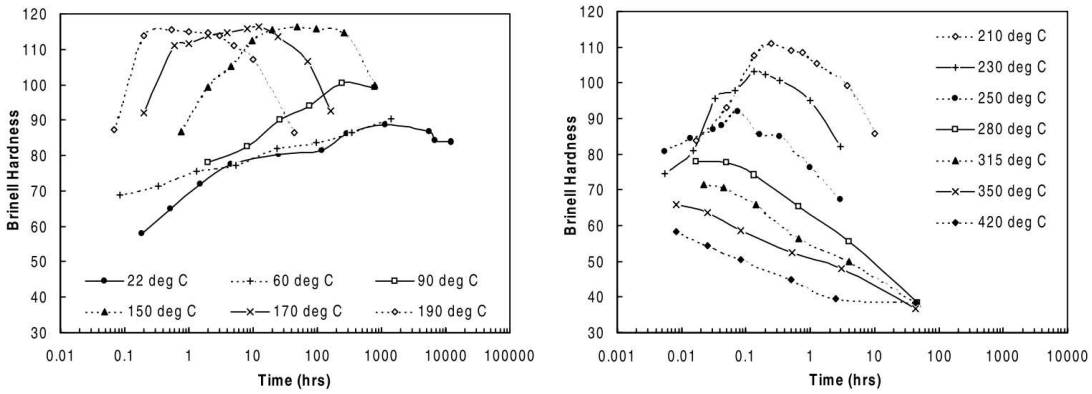

Figure 1.12 – *Artificial ageing curves for A356 foundry alloy in the ranges a) 22 - 190 °C and b) 210 - 420 °C [76].*

		Tension			
Casting Technique	**Temper**	**UTS [MPa]**	**YS [MPa]**	**A%**	**CIE [J]**
Sand Casting	T6	230	190	2	2.3 - 7.3
Permanent Mould Casting	T6	290	210	4	2.3 - 20.3

Table 1.2 – *Tensile and impact properties of the A356 - EN AC-42100 casting alloy in the T6 heat treated condition. Tensile data refer to the minimum tensile properties required for separately cast test pieces in accordance with the EN 1706-2010 specification. Charpy impact energy (CIE) ranges are taken from [109,111] for Sr-modified alloys. A detailed overview of the physical and mechanical properties of the alloy (except for impact properties) is given in [4].*

cavities, oxide bifilms and inclusions. Since these defects are almost always at least one order of magnitude larger than the microstructural constituents, they play a major role in the deterioration of the performance of the alloy, being elements of discontinuity and acting as stress concentrators (Figure 1.13a) [1,78–85].

However, tighter controls currently applied during the manufacture of the castings as well as the advancements of the casting processes have resulted in a reduction of size and amount of these structural defects. Therefore, the *microstructural constituents* arise as the main features influencing the mechanical properties of A356 foundry alloy. In particular, an accurate investigation of the physical metallurgy background of this alloy indicates that the chemical composition, solidification rate and heat treatment are the key parameters to alter both the tensile and impact properties (Figure 1.13b) [39,43,44,47,52,71,72,86–111].

According to the literature [89–91], the microstructural features that mainly control the mechanical properties of a pore-free A356 casting alloy are the secondary dendrite arm spacing (SDAS), eutectic Si particles and intermetallic phases. The fracture process generally consists of three stages: (i) particle fracture caused by plastic deformation in the α-Al matrix, (ii) microcrack formation and growth and (iii) linkage of microcracks [90]. The eutectic Si particles and brittle intermetallics crack because of the high stress concentrations originated by dislocations piling-up at the interfaces between these particles and α-Al matrix [91]. Once

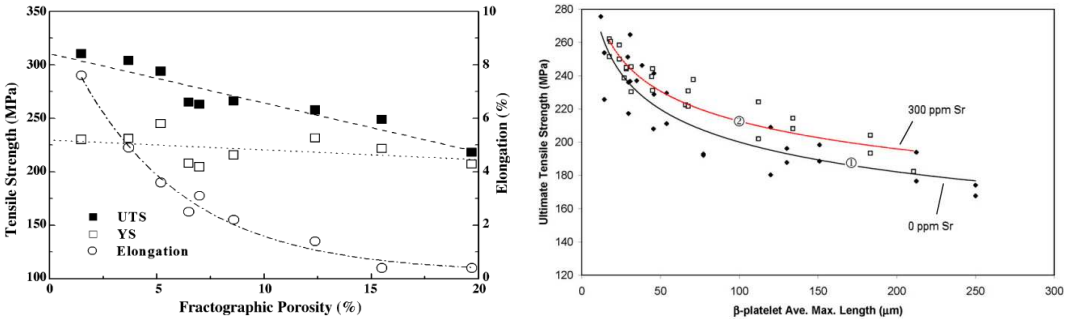

Figure 1.13 – *Mechanical properties of A356 foundry alloy: a) influence of casting defects (tensile properties as a function of fractographic porosity); b) influence of microstructural constituents (UTS as a function of β-Al_5FeSi intermetallics' size and Sr content) [82, 96].*

a particle cracks, a microvoid is formed and tends to grow. This particle cracking process continues until a critical volume fraction of cracked particles is reached. Eventually, the alloy fails because of a rapid linking process among microcracks, which is favoured by coarse microstructural constituents and by the clustering of eutectic Si particles and intermetallic phases among the secondary arms of α-Al dendrites (also called dendrite cells). In particular, when SDAS is large (> 50 μm), a strong interaction occurs during deformation between the slip bands generated in the secondary dendrite arms and the dense array of Si particles in the surrounding interdendritic regions. The microcrack linking process then takes place more easily along the cell boundaries, thus leading to a low-energy transgranular fracture mode. Conversely, in the fine microstructures, the smaller SDAS (< 30 μm) and Si particles make dendrite cell boundaries more discontinuous. Therefore fracture propagates throughout the grain boundaries, which offer an alternative continuous path. This transition from transgranular to intergranular fracture mode is usually accompanied by an increase in the ductility of the alloy [90]. It is also worth noting that an increase in particles' size increases their probability of fracture due to the presence of a larger amount of defects, which generally cause the particles to have a lower fracture stress [89, 112]. Additionally, when casting defects are also present, the crack nucleates at lower strain in response to the local stress concentration resulting from the existence of these detrimental internal discontinuities.

1.3.1 Influence of chemical grain refiners

Despite the significant amount of literature dealing with the theories of grain refinement and the effectiveness of various grain refiners' compositions in decreasing the grain size (see Sections 1.1.1 and 1.2.1.4), a small number of articles focused on the influence of this melt treatment on the tensile and impact properties of the A356 casting alloy. Only in the recent years there has been an increasing amount of literature on this topic, which comprises also research studies on the Mg-free Al-7Si alloy. As discussed in more detail below, while some authors have reported a considerable increase in mechanical properties, others have

given evidence that grain refinement alone exerts only minor beneficial effects, its influence being generally low compared to the modification of eutectic Si particles or the concurrent application of both melt treatments. Therefore, at present, there is still some controversy on the performance improvement provided by grain refining. More experiments are thus required in order to fill the lack of knowledge on this subject.

In their studies, Kori *et al.* [62, 113] investigated the effect of different Al-Ti-B-based master alloys on the tensile properties of as-cast Al-7Si and Al-7SiMg alloys poured into cylindrical graphite moulds. Grain refiners were added either alone or in combination with a Sr-containing modifier. Even if grain refiners alone increased the tensile properties to a some extent, it was found that both the additions are needed to obtain significant improvements in the performances of the alloys. In particular, Al-1Ti-3B and Sr in the addition levels of 1.0 wt% and 0.02 wt% gave the highest increase in the yield strength and percentage elongation, to the extent of above 18% and 88% in case of Al-7Si alloy, and 10% and 60% in case of Al-7SiMg alloy. Tensile properties of as-cast A356 foundry alloy with individual or combined addition of Ti, B and Sr were also studied by Mallapur *et al.* [114], who noticed that the joint addition of 0.65% Al-3Ti, 0.60% Al-3B and 0.20% Al-10Sr master alloys results in the maximum improvement of tensile properties as compared to the individual addition of grain refiner and modifier (Figure 1.14). A similar trend was also observed by the same authors in graphite mould cast, forged and then T6 heat treated A356 alloy samples, thus confirming the beneficial effect of a combined addition of grain refiners and modifier [115]. In all the cases, the improvement in tensile properties was credited to the change from columnar to equiaxed grains, which provided a more homogeneous microstructure, and to the concurrent modification in shape and size of eutectic Si particles due to the addition of Sr. When added alone, however, the grain refiner was found to be slightly less effective than the modifier in increasing the tensile properties of the alloys [62,113–115], thus proving once again the great contribution of eutectic phase modification to final performances of Al-7Si alloys. The same findings were reported by Basavakumar *et al.* [116], who also extended the analysis to the impact properties.

In another study, Chen *et al.* [117] quantitatively analysed the grain refining response of an Al-7SiMg foundry alloy to inoculation via the Al-3B master alloy. After the melt treatment, the alloy was poured into a preheated graphite mould, and the samples were tested in the as-cast condition. Significant grain refinement and improvement in tensile properties were obtained due to the addition of the grain refiner, which increased yield strength (YS), ultimate tensile strength (UTS) and percentage elongation by $\approx$ 15 MPa, 40 MPa and 1.5%, respectively. A recent study by Birol [118] involved the employment of two standard grain refiners, Al-5Ti-1B and Al-3B, to investigate the potential of B additions to grain refine the A356 alloy and increase its mechanical properties. Tensile samples were obtained by permanent mould casting and then tested in both as-cast and T6 heat treated conditions. Although no comparison between refined and unrefined samples was provided by the author, it was reported that the two groups of grain refined as-cast samples exhibit very similar yield and

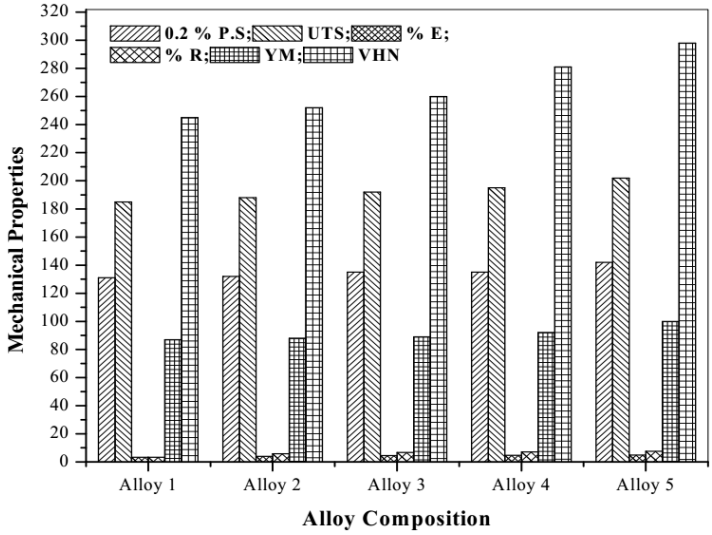

Figure 1.14 – *Mechanical properties of A356 alloy before and after the addition of grain refiner and/or modifier. Alloy 1: A356, Alloy 2: A356 + 0.65% Al-3Ti, Alloy 3: A356 + 0.60% Al-3B, Alloy 4: A356 + 0.20% Al-10Sr, Alloy 5: A356 + 0.65% Al-3Ti + 0.60% Al-3B + 0.20% Al-10Sr [5].*

ultimate tensile strength values, thus evidencing that the secondary dendrite arm spacing (SDAS), rather than the grain size, controlled the tensile performances of the castings. Conversely, the alloy refined with the Al-3B master alloy showed significantly superior tensile properties after T6 heat treatment, with higher strength and percentage elongation values compared to the one refined with the Al-5Ti-1B master alloy (YS: 238$\pm$8 vs. 205$\pm$1 MPa, UTS: 284$\pm$8 vs. 228$\pm$8 MPa, and A%: 3$\pm$0.7 vs. 1$\pm$0.5). Additional research studies were performed by Aguirre-De la Torre *et. al* [119] on the mechanical properties of T6 heat treated A356 automotive wheels produced by low-pressure die casting. It was found that the addition of Al-5Ti-B master alloy up to 0.13 wt% causes also a decrease in SDAS, thus resulting in a higher elongation to fracture average value. However, further additions of the grain refiner exerted a detrimental effect on elongation, whose decrease was credited to the reduced sliding between grains related to the precipitation of strengthening particles in the larger grain boundary region. The same tendency was also observed for the impact energy. Finally, since neither YS nor UTS were significantly altered by Al-5Ti-1B additions, the strengthening provided by grain refinement was reported to be negligible compared to T6 heat treatment.

In their comparative study on the effect of grain refiners on the tensile and impact properties of A356 cast alloy, Samuel *et al.* [120] tested as-cast and T6 heat treated samples added with various concentrations of different master alloys, such as Al-10Ti, Al-4B, Al-5Ti-1B, Al-2.5Ti-2.5B and Al-1.7Ti-1.4B. Combined additions of Sr (in the levels of 30 and 200 ppm) and grain refiners were also considered in order to clarify the effect of Sr-B interaction. No significant variations were noticed in the yield strength of the as-cast alloy, regardless of the amount of Sr or grain refiner additions. Conversely, T6 heat treated grain refined samples showed higher yield strengths compared to the unrefined alloy at both low and high Sr levels, with a

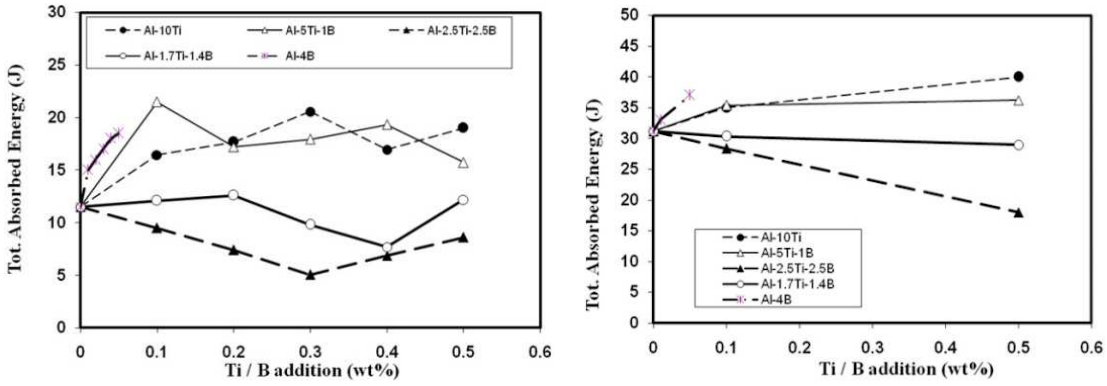

Figure 1.15 – *Variation of total absorbed energy as a function of Ti or B content in a) as-cast and b) T6 heat treated A356.2 alloy, modified with 30 ppm Sr. It is observed that increasing the B:Ti ratio in the Al-Ti-B master alloys from 1:5 to 1:1 results in significant reduction in the achieved toughness compared to the unrefined alloy, probably due to Sr-B interaction. In particular, the Al-2.5Ti-2.5B master alloy shows the greatest decrease upon increasing Ti content [120].*

rising trend discernible for all grain refiner additions in the 200 ppm Sr-modified alloy. The addition of either Al-2.5Ti-2.5B or Al-1.7Ti-1.4B master alloys caused a moderate decrease in both percentage elongation and ultimate tensile strength of the as-cast 200 ppm Sr-modified alloy due to Sr-B interaction. In particular, the increase in the content of B beyond 0.1 wt% changed the shape and size of the eutectic Si particles, thus negatively affecting both the tensile parameters. T6 heat treatment did not lead to any improvement in the percentage elongation of the grain refined alloys, whereas the ultimate tensile strength showed higher values after the addition of lower amounts of the master alloys, in the range 0.02 - 0.04 wt% Ti. The impact toughness was found to be more sensitive than tensile properties to the microstructural variations associated with Sr addition. Combinations of Ti and B improved the impact strength of as-cast samples, but only in the fully modified state and using the right type of master alloy and the suitable addition level. The addition of master alloys with a B:Ti ratio close to 1:1 always resulted in a significant reduction in toughness, probably due to the Sr-B interaction (Figure 1.15). T6 heat treated alloys showed higher impact properties than the as-cast ones, irrespective of the type of grain refiner used [120, 121].

1.3.2 Influence of Ni and V alloying and trace elements

There are few data available in the literature about the influence of Ni and/or V on the tensile and impact properties of Al-Si alloys. A number of studies have recently dealt with the potential of Ni as an alloying element for Al alloys [122, 123]. Ni concentrations around 1 wt% have been found to exert a positive influence on the high temperature strength and on the thermal stability of Al-Si-based alloys. This increase has been credited to the presence of Al_3Ni and Al_9FeNi intermetallics forming a rigid, interconnected, long-range 3D structure that preserves its contiguity and ability to bear loads even when the matrix softens. How-

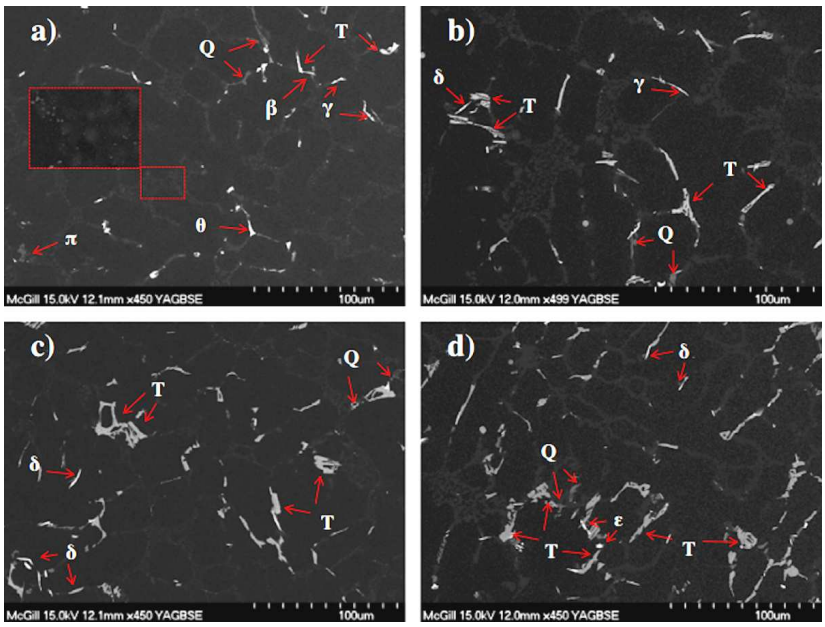

Figure 1.16 – *Ni-Cu-bearing intermetallics detected in the microstructure of the as-cast Al-7Si-0.5Cu-0.35Mg-0.1Fe with a) 0.1 Ni, b) 0.3 Ni, c) 0.6 Ni and d) 1.0 Ni. The chemical composition of the Q intermetallic phase is $Al_5Mg_8Cu_2Si_6$ [126].*

ever, a decrease of strength, elongation and hardness compared to Ni-lean alloys has been observed when the Al_3Ni phase precipitates and agglomerates in the interdendritic regions without creating this interconnected hybrid reinforcement [124].

In combination with Cu, Ni is generally added to many engine piston alloys in concentrations varying from 0.5 to 3 wt% [125–127]. Depending on Ni and Cu contents, different Ni-Cu-bearing phases may form, namely ϵ-Al_3Ni, δ-Al_3CuNi, γ-Al_7Cu_4Ni, T-Al_9FeNi (Figure 1.16). These intermetallics are thermally stable and lead to high strength at elevated temperature, even if at the expense of ductility. Therefore, a high temperature heat treatment is usually performed on these Al-Si alloys in order to increase the ductility.

As for V, it has been reported that the peritectic formation of the Al_3V intermetallic compound upon cooling possesses some grain refinement potential of Al alloys [128], which may exert a beneficial effect on both static and dynamic properties. In particular, it has been recently observed that the addition of V in levels from 0.15 to 1.00 wt% is an effective approach to introduce active heterogeneous nucleant particles ($Al_{10}V$) through in-situ formation in the melt, thus promoting the grain refinement of the alloy [129]. However, the effect of V on grain size appears to be lower than for conventional grain refiners. A recent study on the effects of low levels of V (600 and 2000 ppm) on the phase selection of Fe-rich intermetallic particles in a high purity Al-7Si foundry alloy has reported that V stabilises the α-Al_8Fe_2Si phase in a way similar to, but less effective than, the effect of Mn [130]. Hence, a decrease in the amount of acicular β-Al_5FeSi intermetallic compounds might positevely affect the mechanical properties. Additionally, V is also added in combination with Zr (or Ti) to Al-Si alloys in order to stabilise the mechanical properties at both room and elevated

temperatures through the formation of Al_3X trialuminide phases during the ageing stage of heat treatment [131–133]. These uniformly distributed nano-sized precipitates, which possess crystal structures similar to the FCC structure of the Al matrix, appear to be very effective in the blockage of dislocations movement, leading to an increased yield strength at the expense of the dislocation storage capacity [131]. Furthermore, they are more thermally stable than Cu- and Mg-based precipitates and therefore contribute more likely to the strength retention at elevated temperatures [132, 133].

Even though it is known that Ni and V contaminations may represent a major issue for the purity of primary aluminium and consequently for the structural performances of Al-Si alloys (see Section 1.1.2), literature concerning the influence of these elements on the tensile and impact properties is scarce. Only recently Grandfield *et al.* [32] have presented preliminary results of combined Ni and V additions of 300 ppm each to A356 foundry alloy. It has been observed that the joint addition of these elements has only a moderate influence on the tensile properties, causing a slight reduction in strength but no change in ductility in the T6 heat treated condition. However, it was impossible to distinguish between the effects of Ni and V. Further research works are therefore required in order to determine (i) how Ni or V trace additions affect the mechanical properties of Al-Si alloys and (ii) which amount of these trace elements can be tolerated without compromising the structural integrity of the alloy.

References

[1] J. Campbell, *Complete Casting Handbook*. Butterworth-Heinemann (2011).

[2] G. E. Totten and D. S. MacKenzie, *Handbook of Aluminum - Vol.1 Physical Metallurgy and Processes*. Marcel Dekker (2003).

[3] V. S. Zolotorevsky, N. A. Belov, and M. V. Glazoff, *Casting Aluminum Alloys*. Elsevier (2007).

[4] J. G. Kaufman and E. L. Rooy, *Aluminum Alloy Castings: Properties, Processes and Applications*. ASM International (2004).

[5] B. S. Murty, S. A. Kori, and M. Chakraborty, "Grain refinement of aluminium and its alloys by heterogeneous nucleation and alloying," *Int. Mater. Rev.*, vol. 47, pp. 3–29, 2002.

[6] D. G. McCartney, "Grain refining of aluminium and its alloys using inoculants," *Int. Mater. Rev.*, vol. 34, pp. 247–260, 1989.

[7] M. Easton and D. StJohn, "Grain Refinement of Aluminum Alloys: Part I. The Nucleant and Solute Paradigms-A Review of the Literature," *Metall. Mater. Trans. A*, vol. 30, pp. 1613–1623, 1999.

[8] A. Cibula, "The Mechanism of Grain Refinement of Sand Castings in Aluminium Alloys," *J. Inst. Met.*, vol. 76, pp. 321–360, 1949.

[9] P. S. Mohanty and J. E. Gruzleski, "Mechanism of grain refinement in aluminium," *Acta Metall. Mater.*, vol. 43, pp. 2001–2012, 1995.

[10] G. P. Jones and J. Pearson, "Factors affecting the grain refinement of aluminium using titanium and boron additives," *Metall. Trans. B*, vol. 7, pp. 223–234, 1976.

[11] G. K. Sigworth, "The Grain Refining of Aluminum and Phase Relationships in the Al-Ti-B System," *Metall. Trans. A*, vol. 15, pp. 277–282, 1984.

[12] M. Johnsson, "The influence of composition on equiaxed crystal-growth mechanisms and grain-size in Al-alloys," *Z. Metallkd*, vol. 87, pp. 216–220, 1996.

[13] P. A. Tøndel, "Grain refinement of hypoeutectic Al-Si foundry alloys," Ph.D. dissertation, University of Trondheim, 1994.

[14] J. A. Spittle and S. Sadli, "Effect of alloy variables on grain-refinement of binary aluminum-alloys with Al-Ti-B," *Mater. Sci. Technol.*, vol. 11, pp. 533–537, 1995.

[15] I. G. Davies, J. M. Dennis, and A. Hellawell, "The nucleation of aluminum grains in alloys of aluminum with titanium and boron," *Metall. Trans.*, vol. 1, pp. 275–280, 1970.

[16] L. Arnberg, L. Bäckerüd, and H. Klang, "Intermetallic particles in Al-Ti-B-type master alloys for grain refinement of aluminium," *Met. Technol.*, vol. 9, pp. 7–13, 1982.

[17] P. Schumacher, A. L. Greer, J. Worth, P. V. Evans, M. A. Kearns, P. Fisher, and A. H. Green, "New studies of nucleation mechanisms in aluminium alloys: implications for grain refinement practice," *Mater. Sci. Technol.*, vol. 14, pp. 394–404, 1998.

[18] M. Johnsson, L. Bäckerüd, and G. K. Sigworth, "Study of the Mechanism of Grain Refinement of Aluminum after Additions of Ti- and B-Containing Master Alloys," *Metall. Mater. Trans. A*, vol. 24, pp. 481–491, 1993.

[19] F. A. Crossley and L. F. Mondolfo, "Mechanism of Grain Refinement in Aluminum Alloys," *J. Metals*, vol. 191, pp. 1143–1148, 1951.

[20] G. W. Delamore and R. W. Smith, "The mechanisms of grain refinement in dilute aluminum alloys," *Metall. Trans.*, vol. 2, pp. 1733–1738, 1971.

[21] P. Schumacher and A. L. Greer, "Devitrification of the stable Al-Rich amorphous alloy $Al_{85}Y_8Ni_5Co_2$," *Key Eng. Mat.*, vol. 81–83, pp. 631–636, 1993.

[22] ——, "Enhanced Heterogeneous Nucleation of Alpha-Al in Amorphous Aluminum-Alloys," *Mater. Sci. Eng. A*, vol. 182, pp. 1335–1339, 1994.

[23] A. J. Cornish, "The Influence of Boron on the Mechanism of Grain Refinement in Dilute Aluminium-Titanium Alloys," *Met. Sci.*, vol. 9, pp. 477–484, 1975.

[24] M. Johnsson and L. Bäckerüd, "Nucleants in grain refined aluminum after addition of Ti- and B- containing master alloys," *Z. Metallkd*, vol. 83, pp. 774–780, 1992.

[25] T. E. Quested and A. L. Greer, "The effect of the size distribution of inoculant particles on as-cast grain size in aluminium alloys," *Acta Mater.*, vol. 52, pp. 3859–3868, 2004.

[26] A. L. Greer, A. M. Bunn, A. Tronche, P. V. Evans, and D. J. Bristow, "Modelling of inoculation of metallic melts: application to grain refinement of aluminium by Al-Ti-B," *Acta Mater.*, vol. 48, pp. 2823–2835, 2000.

[27] M. Easton and D. StJohn, "Grain Refinement of Aluminum Alloys: Part II. Confirmation of, and a Mechanism for, the Solute Paradigm," *Metall. Mater. Trans. A*, vol. 30, pp. 1625–1633, 1999.

[28] T. E. Quested, A. Dinsdale, and A. L. Greer, "Thermodynamic evidence for a poisoning mechanism in the Al-Si-Ti system," *Mater. Sci. Technol.*, vol. 22, pp. 1126–1134, 2006.

[29] M. N. Binney, D. H. StJohn, A. K. Dahle, J. A. Taylor, E. C. Burhop, and P. S. Cooper, "Grain refinement of secondary aluminium-silicon casting alloys," in *LIGHT METALS 2003*, P. N. Crepeau, Ed. TMS, 2003, pp. 917–922.

[30] A. K. Dahle and L. Arnberg, "On the assumption of an additive effect of solute elements in dendrite growth," *Mater. Sci. Eng. A*, vol. 225, pp. 38–46, 1997.

[31] G. Jha, F. Cannova, and B. Sadler, "Increasing Coke Impurities - Is this Really a Problem for Metal Quality?" in *LIGHT METALS 2012*, C. E. Suarez, Ed. TMS, 2012, pp. 1303–1306.

[32] J. Grandfield, L. Sweet, C. Davidson, J. Mitchell, A. Beer, S. Zhu, X. Chen, and M. Easton, "An initial assessment of the effects of increased Ni and V content in A356 and AA6063 alloys," in *LIGHT METALS 2013*, B. Sadler, Ed. TMS, 2013, pp. 39–44.

[33] M. A. Rhamdhani, J. F. Grandfield, A. Khaliq, and G. Brooks, "Management of impurities in Cast House with particular reference to Ni and V," in *LIGHT METALS 2013*, B. Sadler, Ed. TMS, 2013, pp. 33–38.

[34] M. A. Rhamdhani, M. A. Dewan, J. Mitchell, C. J. Davidson, G. A. Brooks, M. Easton, and J. F. Grandfield, "Study of Ni-Impurity Removal from Al Melt," in *LIGHT METALS 2012*, C. E. Suarez, Ed. TMS, 2012, pp. 1091–1097.

[35] A. Khaliq, M. A. Rhamdhani, J. B. Mitchell, C. J. Davidson, G. A. Brooks, and J. F. Grandfield, "Analysis of Transition Metal (V,Zr) Borides Formation in Al Melt," in *Proceedings of EMC 2011 - Volume 3*. EMC 2011, 2011, pp. 825–838.

[36] J. Grandfield and J. A. Taylor, "The Impact of Rising Ni and V Impurity Levels in Smelter Grade Aluminium and Potential Control Strategies," *Mater. Sci. Forum*, vol. 630, pp. 129–136, 2010.

[37] G. A. Edwards, K. Stiller, G. L. Dunlop, and M. J. Cooper, "The Precipitation Sequence in Al-Mg-Si Alloy," *Acta Mater.*, vol. 46, pp. 3893–3904, 1998.

[38] K. Matsuda, H. Gamada, K. Fujii, Y. Uetani, T. Sato, A. Kamio, and S. Ikeno, "High Resolution Electron Microscopy on the Structure of Guinier Preston Zones in an Al-1.6 Mass Pct Mg_2Si alloy," *Metall. Mater. Trans. A*, vol. 29, pp. 1161–1168, 1998.

[39] D. W. Pashley, J. W. Rhodes, and A. Sendorek, "Delayed Ageing in Aluminium-Magnesium-Silicon Alloys: Effect on Structure and Mechanical Properties," *J. Inst. Metals*, vol. 94, pp. 41–49, 1966.

[40] M. H. Jacobs, "The Structure of the Metastable Precipitates Formed during Ageing of an Al-Mg-Si Alloy," *Phil. Mag.*, vol. 26, pp. 1–13, 1972.

[41] I. Dutta and S. M. Allen, "A Calorimetric Study of Precipitation in Commercial Aluminium Alloy 6061," *J. Mater. Sci. Let.*, vol. 10, pp. 323–326, 1991.

[42] S. J. Andersen, H. W. Zandbergen, J. Jansen, C. Træholt, U. Tundal, and O. Reiso, "The crystal structure of the β'' phase in Al-Mg-Si alloys," *Acta Mater.*, vol. 46, pp. 3283–3298, 1998.

[43] E. Sjölander and S. Seifeddine, "The heat treatment of Al-Si-Cu-Mg casting alloys," *J. Mater. Process. Tech.*, vol. 210, pp. 1249–1259, 2010.

[44] T. O. Mbuya, B. O. Odera, and S. P. Ng'ang'a, "Influence of iron on castability and properties of aluminium silicon alloys: literature review," *Int. J. Cast. Metal. Res.*, vol. 16, pp. 451–465, 2003.

[45] J. A. Taylor, "Iron-containing intermetallic phases in Al-Si based casting alloys," *Procedia Materials Science*, vol. 1, pp. 19–39, 2012.

[46] L. Bäckerüd, G. Chai, and J. Tammninen, *Solidification Characteristics of Aluminium Alloys - Vol. 2: Foundry Alloys*. AFS, Des Plaines, IL, USA (1990).

[47] O. Vorren, J. E. Evensen, and T. B. Pedersen, "Microstructure and Mechanical Properties of AlSi(Mg) Casting Alloys," *AFS Trans.*, vol. 92, pp. 459–466, 1984.

[48] A. Couture, "Iron in Aluminum Casting Alloys - A Literature Survey," *AFS Int. Cast. Met. J.*, vol. 6, pp. 9–17, 1981.

[49] H. Y. Kim, T. Y. Park, S. W. Han, and H. M. Lee, "Effects of Mn on the crystal structure of α-Al(Mn,Fe)Si particles in A356 alloys," *J. Cryst. Growth*, vol. 291, pp. 207–211, 2006.

[50] H. Y. Kim, S. W. Han, and H. M. Lee, "The influence of Mn and Cr on the tensile properties of A356-0.20Fe alloy," *Mater. Lett.*, vol. 60, pp. 1880–1883, 2006.

[51] S. Hegde and K. N. Prabhu, "Modification of eutectic silicon in Al-Si alloys," *J. Mater. Sci.*, vol. 43, pp. 3009–3027, 2008.

[52] B. Closset and J. E. Gruzleski, "Structure and properties of hypoeutectic Al-Si-Mg alloys modified with pure strontium," *Metall. Mater. Trans. A*, vol. 12, pp. 945–951, 1982.

[53] M. M. Haque, "Effects of strontium on the structure and properties of aluminium-silicon alloys," *J. Mater. Process. Tech*, vol. 55, pp. 193–198, 1995.

[54] T. N. Ware, A. K. Dahle, S. Charles, and M. J. Couper, "Effect of Sr, Na, Ca & P on the Castability of Foundry Alloy A356.2," in *Proceedings of the 2nd International Aluminium Casting Technology Symposium*. ASM International, 2002.

[55] F. Paray and J. E. Gruzleski, "Factors to Consider in Modification," *AFS Trans.*, vol. 102, pp. 833–842, 1994.

[56] R. Fuoco, H. Goldenstein, and J. E. Gruzleski, "Evaluation of effect of modification-induced eutectic undercooling on microporosity formation in 356 al alloy," *AFS Trans.*, vol. 102, pp. 297–306, 1994.

[57] L. Lu, K. Nogita, and A. K. Dahle, "Combining Sr and Na additions in hypoeutectic Al-Si foundry alloys," *Mater. Sci. Eng. A*, vol. 399, pp. 244–253, 2005.

[58] A. K. Dahle, K. Nogita, S. D. McDonald, C. Dinnis, and L. Lu, "Eutectic modification and microstructure development in Al-Si Alloys," *Mater. Sci. Eng. A*, vol. 413–414, pp. 243–248, 2005.

[59] C. Limmaneevichitr and W. Eidhed, "Novel technique for grain refinement in aluminium casting by Al-Ti-B powder injection," *Mater. Sci. Eng. A*, vol. 355, pp. 174–179, 2003.

[60] B. T. Sofyan, D. J. Kharistal, L. Trijati, K. Purba, and R. E. Susanto, "Grain refinement of AA333 aluminium cast alloy by Al-Ti granulated flux," *Mater. Design*, vol. 31, pp. 536–543, 2010.

[61] D. Qiu, J. A. Taylor, M. X. Zhang, and P. M. Kelly, "A mechanism for the poisoning effect of silicon on the grain refinement of Al-Si alloys," *Acta Mater.*, vol. 55, pp. 1447–1456, 2007.

[62] S. A. Kori, B. S. Murty, and M. Chakraborty, "Development of an efficient grain refiner for Al-7Si alloy and its modification with strontium," *Mater. Sci. Eng. A*, vol. 283, pp. 94–104, 2000.

[63] H. Liao and G. Sun, "Mutual poisoning effect between Sr and B in Al-Si casting alloys," *Scripta Mater.*, vol. 48, pp. 1035–1039, 2003.

[64] M. E. J. Birch and P. Fisher, "Grain refining of commercial aluminium alloys with titanium boron aluminium." Proceedings of the Conference on Aluminium Technology 86, The Institute of Metals, London, 1986.

[65] S. A. Kori, B. S. Murty, and M. Chakraborty, "Influence of silicon and magnesium on grain refinement in aluminium alloys," *Mater. Sci. Technol.*, vol. 15, pp. 986–992, 1999.

[66] G. K. Sigworth, M. A. Easton, J. Barresi, and T. A. Kuhn, "Grain Refining of Al-Si Casting Alloys," in *LIGHT METALS 2007 - Volume 3: Cast Shop Technology*, M. Sørlie, Ed. TMS, 2007, pp. 691–696.

[67] L. Arnberg and L. Bäckerüd, *Solidification Characteristics of Aluminium Alloys - Vol. 3: Dendrite Coherency*. AFS, Des Plaines, IL, USA (1996).

[68] R. I. Mackay and J. Gruzleski, "Quantification of magnesium in 356 alloy via thermal analysis," *Int. J. Cast Met. Res.*, vol. 10, pp. 255–266, 1998.

[69] ——, "Quantification of iron in aluminium-silicon foundry alloys via thermal analysis," *Int. J. Cast Met. Res.*, vol. 10, pp. 131–146, 1997.

[70] J. A. Taylor, D. H. StJohn, L. H. Zheng, G. A. Edwards, J. Barresi, and M. J. Couper, "Solution Treatment Effects in Al-Si-Mg Casting Alloys: Part I. Intermetallic Phases," *Alum. Trans.*, vol. 4–5, pp. 95–110, 2001.

[71] J. A. Taylor, D. H. StJohn, J. Barresi, and M. J. Couper, "Influence of Mg Content on th Microstructure and Solid Solution Chemistry of Al-7%Si-Mg Casting Alloys During Solution Treatment," *Mater. Sci. Forum*, vol. 331–337, pp. 277–282, 2000.

[72] D. Apelian, S. Shivkumar, and G. Sigworth, "Fundamental aspects of heat treatment of cast Al-Si-Mg alloys," *AFS Trans.*, vol. 97, pp. 727–742, 1989.

[73] J. T. Staley, "Quench factor analysis of aluminum alloys," *Mater. Sci. Technol.*, vol. 3, pp. 923–935, 1987.

[74] C. E. Bates, "Quench optimization for aluminum alloys," *AFS Trans.*, vol. 101, pp. 1045–1054, 1994.

[75] S. Shivkumar, C. Keller, and D. Apelian, "Aging behavior in cast Al-Si-Mg alloys," *AFS Trans.*, vol. 98, pp. 905–911, 1990.

[76] P. A. Rometsch and G. B. Schaffer, "An age hardening model for Al-7Si-Mg casting alloys," *Mater. Sci. Eng. A*, vol. 325, pp. 424–434, 2002.

[77] D. G. Eskin, "Decomposition of supersaturated solid solutions in Al-Cu-Mg-Si alloys," *J. Mater. Sci.*, vol. 38, pp. 279–290, 2003.

[78] A. Herrera and V. Kondic, "The effect of porosity on tensile properties of two al-si alloys," in *Proc. Int. Conf. on Solidification and Cast Metals*. The Metals Society, Sheffield, UK, 1977, pp. 460–465.

[79] M. K. Surappa, E. W. Blank, and J. C. Jaquet, "Effect of Macro-Porosity on the Strength and Ductility of Cast Al-7Si-0.3Mg Alloy," *Scr. Metall. Mater.*, vol. 20, pp. 1281–1286, 1986.

[80] C. H. Cáceres, "On the effect of macroporosity on the tensile properties of the Al-7%Si-0.4%Mg casting alloy," *Scr. Metall. Mater.*, vol. 32, pp. 1851–1856, 1995.

[81] A. M. Gokhale and G. R. Patel, "Origins of variability in the fracture-related mechanical properties of a tilt-pour-permanent-mold cast Al-alloy," *Scr. Mater.*, vol. 52, pp. 237–241, 2005.

[82] C. D. Lee, "Effects of microporosity on tensile properties of A356 aluminum alloy," *Mater. Sci. Eng. A*, vol. 464, pp. 249–254, 2007.

[83] C. H. Cáceres and B. I. Selling, "Casting defects and the tensile properties of an Al-Si-Mg alloy," *Mater. Sci. Eng. A*, vol. 220, pp. 109–116, 1996.

[84] M. Merlin, G. Timelli, F. Bonollo, and G. L. Garagnani, "Impact behaviour of A356 alloy for low-pressure die casting automotive wheels," *J. Mater. Process. Tech.*, vol. 209, pp. 1060–1073, 2009.

[85] C. D. Lee, "Variability in the impact properties of A356 aluminum alloy on microporosity variation," *Mater. Sci. Eng. A*, vol. 565, pp. 187–195, 2013.

[86] K. T. Kashyap, S. Murali, K. S. Raman, and K. S. S. Murty, "Casting and heat treatment variables of Al-7Si-Mg alloy," *Mater. Sci. Technol.*, vol. 9, pp. 189–203, 1993.

[87] R. E. Spear and G. R. Gardner, "Dendrite Cell Size," *AFS Trans.*, vol. 71, pp. 209–215, 1963.

[88] C. H. Cáceres, C. J. Davidson, and J. R. Griffiths, "The deformation and fracture behaviour of an Al-Si-Mg casting alloy," *Mater. Sci. Eng. A*, vol. 197, pp. 171–179, 1995.

[89] Q. G. Wang and C. H. Cáceres, "The fracture mode in Al-Si-Mg casting alloys," *Mater. Sci. Eng. A*, vol. 241, pp. 72–82, 1998.

[90] Q. G. Wang, "Microstructural Effects on the Tensile and Fracture Behavior of Aluminum Casting Alloys A356/357," *Metall. Mater. Trans. A*, vol. 34, pp. 2887–2899, 2003.

[91] C. H. Cáceres and J. R. Griffiths, "Damage by the cracking of Silicon particles in an Al-7Si-0.3Mg casting alloy," *Acta Mater.*, vol. 44, pp. 25–33, 1996.

[92] Q. G. Wang, C. H. Cáceres, and J. R. Griffiths, "Damage by Eutectic Particle Cracking in Aluminum Casting Alloys A356/357," *Metall. Mater. Trans. A*, vol. 34, pp. 2901–2911, 2003.

[93] C. H. Cáceres, C. J. Davidson, J. R. Griffiths, and Q. G. Wang, "The Effect of Mg on the Microstructure and Mechanical Behavior of Al-Si-Mg Casting Alloys," *Metall. Mater. Trans. A*, vol. 30, pp. 2611–2618, 1999.

[94] S. A. Kori, M. S. Prabhudev, and T. M. Chandrashekharaiah, "Studies on the microstructure and mechanical properties of A356 alloy with minor additions of copper and magnesium," *Trans. Indian I. Metals*, vol. 62, pp. 353–356, 2009.

[95] Q. G. Wang, P. E. Jones, and M. Osborne, "Effect of iron on the microstructure and mechanical properties of an Al-7%Si-0.4%Mg casting alloy," *SAE Trans.*, vol. 112, pp. 396–303, 2003.

[96] Z. Ma, A. M. Samuel, F. H. Samuel, H. W. Doty, and S. Valtierra, "A study of tensile properties in Al-Si-Cu and Al-Si-Mg alloys: Effect of β-iron intermetallics and porosity," *Mater. Sci. Eng. A*, vol. 490, pp. 36–51, 2008.

[97] A. M. A. Mohamed, F. H. Samuel, A. M. Samuel, H. W. Doty, and S. Valtierra, "Influence of Tin Addition on the Microstructure and Mechanical Properties of Al-Si-Cu-Mg and Al-Si-Mg Casting Alloys," *Metall. Mater. Trans. A*, vol. 39, pp. 490–501, 2008.

[98] S. S. S. Kumari, R. M. Pillai, K. Nogita, A. K. Dahle, and B. C. Pai, "Influence of Calcium on the Microstructure and Properties of an Al-7Si-0.3Mg-xFe Alloy," *Metall. Mater. Trans. A*, vol. 37, pp. 2581–2587, 2006.

[99] S. S. S. Kumari, R. M. Pillai, and B. C. Pai, "A study on the structural, age hardening and mechanical characteristics of Mn and Ca added Al-7Si-0.3Mg-0.6Fe alloy," *J. Alloy Compd.*, vol. 453, pp. 167–173, 2008.

[100] S. G. Shabestari and F. Shahri, "Influence of modification, solidification conditions and heat treatment on the microstructure and mechanical properties of A356 aluminum alloy," *J. Mater. Sci.*, vol. 39, pp. 2023–2032, 2004.

[101] S. Murali, K. S. Raman, and K. S. S. Murthy, "Effect of Trace Additions (Be, Cr, Mn and Co) on the Mechanical Properties and Fracture Toughness of Fe-Containing Al-7Si-0.3Mg Alloy," *Cast Metals*, vol. 6, pp. 189–198, 1994.

[102] M. Ravi, U. T. S. Pillai, B. C. Pai, A. D. Damodaran, and E. S. Dwarakadasa, "The effect of mischmetal addition on the structure and mechanical properties of a cast Al-7Si-0.3Mg alloy containing excess iron (up to 0.6 Pct)," *Metall. Mater. Trans. A*, vol. 33, pp. 391–400, 2002.

[103] L. Y. Zhang, Y. H. Jiang, Z. Ma, S. F. Shan, Y. Z. Jia, C. Z. Fan, and W. K. Wang, "Effect of cooling rate on solidified microstructure and mechanical properties of aluminium-A356 alloy," *J. Mater. Process. Tech.*, vol. 207, pp. 107–111, 2008.

[104] J. H. Peng, X. L. Tang, J. T. He, and D. Y. Xu, "Effect of heat treatment on microstructure and tensile properties of A356 alloys," *T. Nonferr. Metal. Soc.*, vol. 21, pp. 1950–1956, 2011.

[105] D. L. Zhang, L. H. Zheng, and D. H. S. John, "Effect of a short solution treatment time on microstructure and mechanical properties of modified Al-7wt.%Si-0.3wt.%Mg alloy," *J. Light Met.*, vol. 2, pp. 27–36, 2002.

[106] O. Elsebaie, A. M. Samuel, F. H. Samuel, and H. W. Doty, "The effects of mischmetal, cooling rate and heat treatment on the hardness of A319.1, A356.2 and A413.1 Al-Si casting alloys," *Mater. Sci. Eng. A*, vol. 486, pp. 241–252, 2008.

[107] S. Murali, K. S. Raman, and K. S. S. Murthy, "Effect of magnesium, iron (impurity) and solidification rates on the fracture toughness of Al-7Si-0.3Mg casting alloy," *Mater. Sci. Eng. A*, vol. 151, pp. 1–10, 1992.

[108] F. Paray, B. Kulunk, and J. E. Gruzleski, "Impact properties of Al-Si foundry alloys," *Int. J. Cast Metals Res.*, vol. 13, pp. 17–37, 2000.

[109] S. Shivkumar, L. Wang, and C. Keller, "Impact properties of A356-T6 Alloys," *J. Mater. Eng. Perform.*, vol. 3, pp. 83–90, 1994.

[110] Z. Ma, A. M. Samuel, F. H. Samuel, H. W. Doty, and S. Valtierra, "Effect of Fe Content and Cooling Rate on the Impact Toughness of Cast 319 and 356 Aluminum Alloys," *AFS Trans.*, vol. 3, pp. 255–265, 2003.

[111] O. Elsebaie, A. M. Samuel, and F. H. Samuel, "Effects of Sr-modification, iron-based intermetallics and aging treatment on the impact toughness of 356 Al-Si-Mg alloy," *J. Mater. Sci.*, vol. 46, pp. 3027–3045, 2011.

[112] W. H. Hunt, J. R. Brockenbrough, and P. E. Magnusen, "An Al-Si-Mg composite model system: Microstructural effects on deformation and damage evolution," *Scr. Metall. Mater.*, vol. 25, pp. 15–20, 1991.

[113] S. A. Kori, B. S. Murty, and M. Chakraborty, "Development of an efficient grain refiner for Al-7Si alloy," *Mater. Sci. Eng. A*, vol. 280, pp. 58–61, 2000.

[114] D. G. Mallapur, S. A. Kori, and K. R. Udupa, "Influence of Ti, B and Sr on the microstructure and mechanical properties of A356 alloy," *J. Mater. Sci.*, vol. 46, pp. 1622–1627, 2011.

[115] D. G. Mallapur, K. R. Udupa, and S. A. Kori, "Studies on the influence of grain refining and modification on microstructure and mechanical properties of forged A356 alloy," *Mater. Sci. Eng. A*, vol. 528, pp. 4747–4752, 2011.

[116] K. G. Basavakumar, P. G. Mukunda, and M. Chakraborty, "Influence of grain refinement and modification on microstructure and mechanical properties of Al-7Si and Al-7Si-2.5Cu cast alloys," *Mater. Charact.*, vol. 59, pp. 283–289, 2008.

[117] Z. Chen, T. Wang, L. Gao, H. Fu, and T. Li, "Grain refinement and tensile properties improvement of aluminum foundry alloys by inoculation with Al-B master alloy," *Mater. Sci. Eng. A*, vol. 553, pp. 32–36, 2012.

[118] Y. Birol, "Impact of grain size on mechanical properties of AlSi7Mg0.3 alloy," *Mater. Sci. Eng. A*, vol. 559, pp. 394–400, 2013.

[119] E. Aguirre-De la Torre and U. Afeltra and C. D. Gómez-Esparza and J. Camarillo-Cisneros and R. Pérez-Bustamante and R. Martínez-Sánchez, "Grain Refiner Effect on the Microstructure and Mechanical Properties of the A356 Automotive Wheels," *J. Mater. Eng. Perform.*, vol. 23, pp. 581–587, 2014.

[120] E. Samuel, B. Golbahar, A. M. Samuel, H. W. Doty, S. Valtierra, and F. H. Samuel, "Effect of grain refiner on the tensile and impact properties of Al-Si-Mg cast alloys," *Mater. Design*, vol. 56, pp. 468–479, 2014.

[121] A. M. Samuel, H. W. Doty, S. Valtierra, and F. H. Samuel, "Effect of grain refining and Sr-modification interactions on the impact toughness of Al-Si-Mg cast alloys," *Mater. Design*, vol. 56, pp. 264–273, 2014.

[122] F. Stadler, H. Antrekowitsch, W. Fragner, H. Kaufmann, and P. J. Uggowitzer, "The effect of Ni on the high-temperature strength of Al-Si cast alloys," *Mater. Sci. Forum*, vol. 690, pp. 274–277, 2011.

[123] Z. Asghar, G. Requena, and F. Kubel, "The role of Ni and Fe aluminides on the elevated temperature strength of an AlSi12 alloy," *Mater. Sci. Eng. A*, vol. 527, pp. 5691–5698, 2010.

[124] J. A. García-Hinojosa, C. R. González, G. M. González, and Y. Houbaert, "Structure and properties of Al-7Si-Ni and Al-7Si-Cu cast alloys nonmodified and modified with Sr," *J. Mater. Process. Tech.*, vol. 143–144, pp. 306–310, 2003.

[125] L. Heusler, F. J. Feikus, and M. O. Otte, "Alloy and Casting Process Optimization for Engine Block Application," *AFS Trans.*, vol. 109, pp. 215–223, 2001.

[126] A. R. Farkoosh, M. Javidani, M. H. D. Larouche, and M. Pekguleryuz, "Phase formation in as-solidified and heat-treated Al-Si-Cu-Mg-Ni alloys: Thermodynamic assessment and experimental investigation for alloy design," *J. Alloy Compd.*, vol. 551, pp. 596–606, 2013.

[127] Y. Yang, K. Yu, Y. Li, D. Zhao, and X. Liu, "Evolution of nickel-rich phases in Al-Si-Cu-Ni-Mg piston alloys with different Cu additions," *Mater. Design*, vol. 33, pp. 220–225, 2012.

[128] L. F. Mondolfo, *Aluminum Alloys: structure and properties*. Butterworths, London (1976).

[129] F. Wang, Z. Liu, D. Qiu, J. A. Taylor, M. A. Easton, and M. Zhang, "Revisiting the role of peritectics in grain refinement of Al alloys," *Acta Mater.*, vol. 61, pp. 360–370, 2013.

[130] E. S. Daehlen, "The Effect of Vanadium on AlFeSi - Intermetallic Phases in a Hypoeutectic Al-Si Foundry Alloy," Master's thesis, Chemical Engineering and Biotechnology - NTNU, 2013.

[131] H. A. Elhadari, H. A. Patel, D. L. Chen, and W. Kasprzak, "Tensile and fatigue properties of a cast aluminum alloy with Ti, Zr and V additions," *Mater. Sci. Eng. A*, vol. 528, pp. 8128–8138, 2011.

[132] W. Kasprzak, D. Emadi, M. Sahoo, and M. Aniolek, "Development of Aluminium Alloys for High Temperature Applications in Diesel Engines," *Mater. Sci. Forum*, vol. 618–619, pp. 595–600, 2009.

[133] W. Kasprzak, B. S. Amirkhiz, and M. Niewczas, "Structure and Properties of Cast Al-Si based Alloy with Zr-V-Ti Additions and its Evaluation of High Temperature Performance," *J. Alloy Compd.*, 2013. [Online]. Available: {http://dx.doi.org/10.1016/j.jallcom.2013.11.209}

Chapter 2

Main Contributions and Impact of the Research

2.1 Overview of the Articles

Article A

Article A presents a comparative study on the impact properties of a permanent mould cast Sr-modified A356-T6 alloy added with equal amounts of commercial Ti-B based grain refiners in form of can (GR1), tab (GR2) and granular flux (GR3). The mould and pouring temperatures were kept constant throughout the casting trials in order to avoid any influence of the cooling rate on the microstructure. The results of impact tests and microstructural analyses showed that the grain size has no direct influence on impact properties. However, all the products were observed to cause some further changes in the overall microstructure of the alloys. In particular, contrary to common expectations, the addition of grain refiners strongly affected the secondary dendrite arm spacing (SDAS), leading to a general increase of this microstructural feature. This produced a shift from a mixed transgranular-intergranular fracture mode to a more severe transgranular mode, i.e. fracture propagated more easily following a low-energy path through the dendrites rather than along the more irregular grain boundary region. Fracture propagation was also promoted by the presence of brittle β-Al_5(Fe,Mn)Si intermetallic compounds, whose size was reported to increase with the addition of all the grain refiners. The complementary effects of bad grain refinement (due to the insufficient stirring of the melt), large SDAS and increased β-platelets average maximum length produced a significant reduction in the impact properties of the alloys refined with GR1 and GR2. Conversely, the granular flux produced a more homogeneous microstructure, thus leading to impact energy values closer to those of the Reference alloy. A multiple regression model based on SDAS and β-platelets size was found to reliably describe the variation of total absorbed energy Wt. The high correlation coefficient (R^2 = 0.897) confirmed the validity of the approach.

Article B

Article B deals with the tensile properties of sand cast and permanent mould cast unmodified A356 alloys contaminated with 600 ppm Ni or 1000 ppm V. Such properties were investigated in both as-cast and T6 heat treated conditions. Fracture profiles and surfaces of the tensile specimens were observed with SEM-EDS and EPMA to document the microstructural features involved in the failure process of the alloys. It was found that Ni and V exert a strong effect on both the yield strength ($Rp_{0.2}$) and ultimate tensile strength (UTS) of the sand cast A356 alloy in as-cast condition. In particular, Ni reduced $Rp_{0.2}$ and UTS by 87% and 37%, respectively. According to the approach based on the calculation of the relative fracture strain of stiff secondary particles (eutectic Si and intermetallic compounds) embedded into a softer matrix (primary α-Al phase), this decrease was attributed to early fracture of brittle polygonal and flake-like Ni-rich intermetallics, namely Al_3Ni and Al_9FeNi, which were largely observed on the fracture surfaces of tensile specimens. Additionally, these phases were often detected close to either eutectic Si particles or π-$Al_8FeMg_3Si_6$ intermetallics. Therefore, it was inferred that large decohesion areas were created since the early stage of tensile deformation due also to further intercrystalline cracks in these brittle phases. In contrast, a solid solution strengthening effect produced by V was credited for the increase of $Rp_{0.2}$ and UTS by 42% and 25%, respectively. T6 heat treatment was found to improve the tensile properties of all the sand cast alloys. For the case of Ni-containing alloy, Ni-rich intermetallics underwent spheroidisation, thus reducing their detrimental effect on tensile properties. The cooling rate was identified as the main parameter influencing the tensile properties of permanent mould cast alloys in both as-cast and T6 conditions: the finer microstructure neutralised both the detrimental effects of Ni-rich intermetallics or the improvement related to V solid solution strengthening. It was concluded that the application of T6 heat treatment can effectively counteract the detrimental effects induced by Ni-bearing intermetallics in case of Ni contamination up to 600 ppm, particularly for low cooling rate casting methods. In contrast, the addition of 1000 ppm V was determined to be always beneficial for the tensile properties of the A356 alloy.

Article C

The aim of Article C was to study the effect of Ni/V trace element additions (600 ppm Ni, 1000 ppm V) on the impact properties of sand cast and permanent mould cast unmodified A356 alloys in as-cast and T6 heat treated conditions, thus complementing the findings of Article B. Samples were tested using an instrumented Charpy pendulum. The measurement of relevant impact data (maximum load, energy at maximum load, propagation energy and total absorbed energy), as well as the SEM-EDS observations of both fracture profiles and surfaces, gave important information on the impact behaviour of the alloys. The energies at maximum load *Wm* and the propagation energies *Wp* were reported to change depending on the chemical composition (V solid solution strengthening), solidification conditions (SDAS

and eutectic Si particles size) and heat treatment (precipitation of coherent Mg_2Si particles), thus varying the total absorbed energies *Wt* correspondingly. All the investigated alloys showed low total absorbed energy average values (*Wt* < 2 J). These results were attributed to a Si-driven quasi-cleavage transgranular fracture mode, whose features remained even after the solutionising stage of the T6 heat treatment. Slightly higher impact energies were reported for the permanent mould cast alloys compared to sand cast specimens owing to the finer microstructure, which led to local intergranular contributions to fracture. On the other hand, an overall reduction of the propagation energies was observed after the application of T6 heat treatment because of Mg_2Si dispersoids, which hardened the α-Al matrix at the expense of ductility. While the addition of Ni had a negligible influence on the impact properties of A356 alloy, the trace element V exerted a significant effect. In the sand cast alloys, V solid solution strengthening increased the energy at maximum load with minor detrimental effects on the propagation energy, which was found to be controlled by the coarse microstructure and, after T6 heat treatment, also by the precipitation of coherent Mg_2Si particles. However, as V had a prevalent effect, V-containing sand cast alloys showed showed slightly higher total absorbed energies compared to the corresponding A356 base alloys. Conversely, for the case of permanent mould cast alloys, the beneficial effect of a finer microstructure on the energy at maximum load did not counterbalance the considerable loss of ductility, i.e. propagation energy, caused by V in solid solution. As a result, a significant decrease of total absorbed energy was observed.

2.2 Industrial Implications

The main conclusions of the research projects have been discussed in detail above. However, some of the results reported in this manuscript will also have an important industrial impact, providing useful indications to the manufacturers of A356 cast components.

Grain Refinement

- For the case of compact one-piece grain refiners added to a Sr-modified A356 alloy, the duration of the melt stirring stage should be prolonged compared to the common procedure, e.g. in the range of 15 - 20 min, to limit the amount of nucleant particles' agglomerations, as they have a detrimental effect not only on the grain refinement effectiveness, but also on other microstructural features and, as a direct consequence, on the impact properties.

- The use of granular fluxes is particularly recommended due to the smaller size of nucleants and their uniform dispersion into the melt, which lead to a more homogeneous microstructure and a slightly higher impact toughness.

- The practice of further grain refining primary or secondary high-Si aluminium alloys

containing high Ti levels ($\geq$ 0.15 wt%) is strongly discouraged, as the prior Ti concentration appears to be adequate enough to obtain a pronounced grain refining response, as well as fairly good impact properties.

Ni/V Contamination

- Ni concentrations up to 600 ppm can be tolerated into unmodified A356 cast parts without impairing their tensile properties, providing that a T6 heat treatment is applied. This is particularly suggested for low cooling rate casting methods, such as sand casting, whereas the presence of Ni can always be accepted if high cooling rate techniques (e.g. permanent mould casting) are employed.
- Similar precautions are not needed for V levels up to 1000 ppm, as V generally exerts a beneficial effect on the tensile properties.
- Since V in solid solution tends to reduce the ductility of the alloy, its presence in the chemical composition should be carefully checked in order to meet the specific service requirements in terms of impact toughness.
- For the same reason, the application of a T6 heat treatment should be performed with great care in an unmodified A356 alloy. An increase in the duration of the solutionising step (e.g. up to 12 h) is recommended, as the beneficial effect related to the fragmentation and spheroidisation of eutectic Si crystals can counteract the ductility reduction associated with the precipitation of Mg_2Si particles. In case a shorter solution time is specifically required by the customer, a suitable heat treatment should be developed in order to find the better compromise between tensile and impact properties.

It is evident that the modification of the eutectic phase would strongly increase the mechanical properties of A356 alloy. Additionally, modification might be a suitable way to neutralise the detrimental effect of Ni trace additions on the tensile properties, as the fine fibrous structure of eutectic Si particles would be less prone to propagate the fracture after the early rupture of Ni-rich intermetallics. On the contrary, V solid solution strengthening of α-Al matrix might still affect both the tensile and impact properties to a some extent even after modification. Further investigations on a modified A356 alloy are thus recommended, as they would clearly establish whether the maximum tolerable concentration for Ni and V listed in current alloy specification charts, e.g. EN 1676-2010, can be permanently increased without any deterioration of the mechanical properties.

Part 2

Article A

A comparative study on the effects of three commercial Ti-B based grain refiners on the impact properties of A356 cast aluminium alloy

Authors: D. Casari[1], M. Merlin[1] and G. L. Garagnani[1]
Published in: Journal of Materials Science, 2013, 48(12), pp 4365-4377

Abstract

The effect of three commercial Ti-B based grain refiners on the impact properties of the A356 cast aluminium alloy was assessed. The impact tests were performed by means of an instrumented Charpy pendulum. During impact testing, the maximum load (*Fmax*) and the total impact energy (*Wt*), as well as its complementary contributions, the energy at maximum load (*Wm*) and the crack propagation energy (*Wp*), were measured. Impact properties were studied as a function of size and shape of the main microstructural features, which were analysed by means of optical microscopy (OM) and scanning electron microscopy (SEM). The results show that the influence of grain refinement on microstructure involves beneficial and detrimental concurrent effects which strongly affect impact properties. The total impact energy decreases with the addition of all the grain refiners due to a shift from a mixed transgranular-intergranular fracture mode to a more severe transgranular mode. Crack initiation and propagation occur mainly through the fracture of Fe-intermetallics and brittle Si particles, and the mechanism of void coalescence. No direct correlation between grain size and impact properties is found. Moreover, the aspect ratio of eutectic Si particles does not change with grain refinement, implying that there are no mutual poisoning effects between

[1]Engineering Department - ENDIF, University of Ferrara, Via Saragat 1, I-44122 Ferrara, Italy

Sr and B. Total impact energy is found to depend on both SDAS and β-platelets size. The concurrent effects of SDAS and β-platelets average maximum length on total impact energy can be taken into account using the multiple regression analysis technique.

A.1 Introduction

With respects to the total production volume, the Al-Si alloys represent the 90% of the aluminium based alloys used in the automotive industry. This is mainly due to their high strength/weight ratio, high impact toughness, excellent castability, low thermal expansion coefficient and good corrosion resistance. Among these alloys, the A356 (Al-Si-Mg) is one of the most used to produce a wide selection of automotive cast components, such as rims, engine and gear parts.

The production of aluminium alloy sound castings requires a close control of many parameters. One of the most important parameters is the grain size. A fine and equiaxial grain structure generally improves mechanical and fatigue properties of castings and reduces hot-tearing susceptibility. Additionally, it provides a good castability, a better dispersion of secondary phases and microporosities, and an improvement in feeding during solidification.

Many authors have investigated the fundamental mechanisms of grain refinement from both theoretical [1–4] and industrial [5–9] points of view. While some authors have considered the importance of heterogeneous nucleating centres in obtaining a fine grain structure ("nucleant paradigm") [10–14], others have focused on the influence of solute elements ("solute paradigm") [15–17]. According to the most recent models, both the addition of nucleant particles (TiB_2, AlB_2, $(Ti,Al)B_2$, $TiAl_3$, TiC) and the amount of segregating elements are fundamental in the grain refinement process. After the beginning of heterogeneous nucleation, the solute elements influence grain refinement in two ways. First they reduce the growth of the previous grains, thus increasing the last of nucleation phase. Then, their segregating ability leads to a constitutionally undercooled zone in front of the growing interface (constitutional undercooling-driven mechanism) [16], hence activating the nucleation of new grains on other primary particles [4, 18, 19].

The most widely used grain refiners are Al-Ti, Al-B, Ti-B, Al-Ti-B or Al-Ti-C based, in form of cans, bars, tabs, waffles and ingots. Novel techniques for grain refinement also include the addition of a granulated flux during the stirring of the melt, or powder injection into the molten aluminium [7, 20].

The Charpy impact test is a very useful and straightforward experimental method that can be used to assess the effect of microstructure, casting defects and process parameters on the impact properties of aluminium alloys. Murali *et al.* [21] investigated the influence of Mg and Fe on the impact toughness of the AlSi7Mg0.3 alloy; they proved that an increase of both elements in a specific range leads to a decrease of the total absorbed energy. Ma *et al.* [22] also studied the effect of Fe content, showing that the detrimental effect in the A356.2 alloy is significant when β-platelet lengths lie within the range of 10 - 50 μm. Shivkumar *et*

al. [23] showed that the Sr modification and the increase of cooling rate improve the impact properties of the A356 alloy, while Zhang *et al.* [24] reported that the T6 heat treatment is beneficial to ductility, yield stress and toughness. Merlin *et al.* [25] applied instrumented Charpy impact test in measuring the total absorbed energy of sub-size specimens. They stated that casting defects nearby the V-notch have a strong detrimental effect on impact toughness, becoming dominant compared to microstructure. Therefore, although authors have investigated the effect of many parameters on impact properties of the A356 foundry alloy, literature about the influence of different kind of grain refiners on the impact properties of this widely used alloy is poor [26].
The aim of the present work is to study the influence of three commercial Ti-B based grain refiners on microstructure and impact properties of A356 aluminium alloy. Microstructural features have been correlated to experimental findings in terms of absorbed energy, maximum load, crack nucleation and propagation energy. Furthermore, fractographic analyses have been performed to investigate the predominant fracture mechanisms and the microstructural components involved in the crack process. Finally, a multiple regression analysis technique has been applied to take into account the concurrent effects of microstructural parameters on crack initiation and propagation, and consequently on impact properties.

A.2 Experimental Procedure

A commercial A356 aluminium alloy was used in this study. Its chemical composition is given in Table A.1.

Si	**Fe**	**Cu**	**Mn**	**Mg**	**Cr**	**Zn**	**Ni**
6.900	0.124	0.0075	0.0071	0.339	< 0.01	0.0128	< 0.003
Ti	**B**	**Ca**	**Pb**	**Sr**	**Na**	**Li**	**Al**
0.136	< 0.0005	< 0.001	< 0.0012	0.0094	< 0.0017	0.0008	bal.

Table A.1 – *Chemical composition (wt%) of the A356 aluminium alloy used in this study.*

The melt alloy [1] was modified using several bars of Al-10%Sr master alloy in order to reach 200 ppm of Sr, and then degassed for 10 min by means of argon inert gas. After that, the melt was stirred and grain refined by the addition of three commercial Ti-B based grain refiners in form of can, tab and granulated flux, which were named respectively GR1, GR2 and GR3. The grain refiners quantities were fixed in one can, one tab and 300 g of powder, in order to compare the effects of the two one-piece grain refiners to a proportional amount of granular flux. Despite this solution, it is evident that an equal weight of grain refiner does not correspond to an equal grain refinement effect; this is due to the different chemical composition of the commercial grain refiners considered in this study.

[1] N.B. the holding furnace had a 700 kg molten aluminium capacity

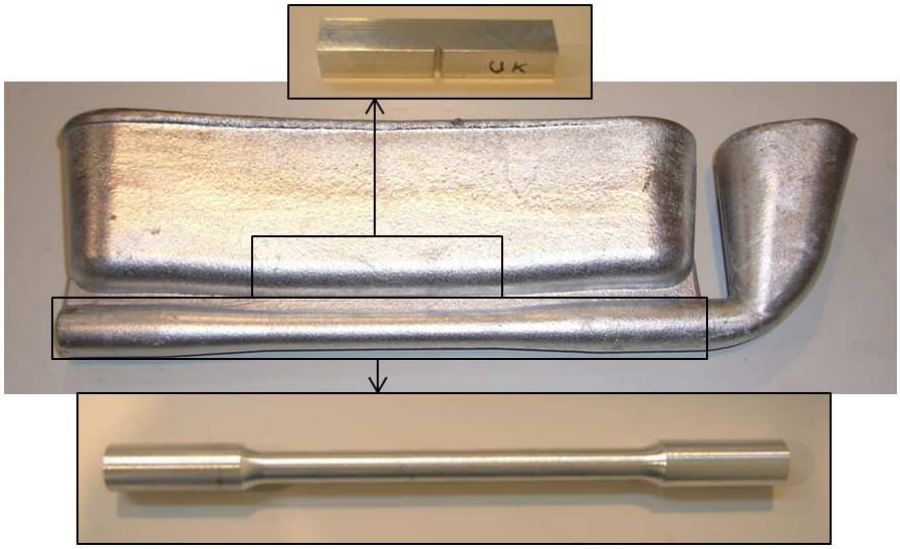

Figure A.1 – *Casting design used in the experiments. The black boxes show the areas where the Charpy and tensile specimens were drawn.*

Molten alloy was subsequently poured into a steel mould, and cooled at a constant cooling rate. A number of 20 castings was obtained (Figure A.1), n°5 for each experimental condition (Reference, GR1, GR2 and GR3). The sprue was oversized in order to get both tensile specimens and Charpy impact samples with a low amount of casting defects. Charpy impact specimens were drawn by means of machining from the middle of the sprue. Only one specimen was drawn from each casting. The specimen dimensions were typical full size Charpy V notch 10x10x55 mm, according to the UNI EN ISO 148-1 specification. The same number of tensile specimens was drawn from the castings; these specimens were then tested and the results were collected in a complementary work. All the Charpy specimens were subjected to the same T6 heat treatment including heating up to 520 °C for 4 h, quenching in a solution of water and glycol (25 °C) and ageing at 160 °C for 6 h.

The impact tests were performed on a CEAST instrumented Charpy pendulum, specifically designed for testing light alloy specimens, according to the ASTM E-23 specification. During impact testing the total impact energy (*Wt*), calculated as the integral of load-displacement curve, and the maximum load (*Fmax*) were measured, as well as the energy at maximum load (*Wm*) and the crack propagation energy (*Wp*), i.e. the energy absorbed from the maximum load to the end of the test, which is considered when the load comes to the 2% of its peak. The energy absorption was also evaluated through the measurement of the pendulum's angle of rise (*Cv*).

The fracture surfaces of the Charpy specimens after the impact test were observed and analysed by scanning electron microscopy (SEM) and by energy dispersive X-ray spectroscopy (EDS). Metallographic samples were cut out perpendicularly to the fracture surface, then embedded in phenolic resin and finally prepared via standard grinding and polishing procedures. The samples were electrolytically etched with Barker's reagent (5 wt% HBF4 in

water solution) and anodized for 75 s at 20 V to reveal the grain structure. Microstructural analyses were performed by optical microscopy (OM) using polarised light. An image analyser program and the line intercept method were used to determine the average grain size (according to the ASTM E-112 specification). The measurements of other significant microstructural features, such as SDAS, eutectic silicon particles aspect ratio and β-Al_5(Fe,Mn)Si platelets length were also performed. Important information, concerning fracture path and microstructure components involved in crack process, was obtained observing the fracture profile.

A.3 Results

A.3.1 Impact Toughness

The effect of grain refiners on the impact properties of A356 alloy was studied by testing refined (GR1, GR2 and GR3) and not refined (Reference) samples. The average impact properties and their standard deviations are given in Table A.2. Figure A.2 shows the mean recorded results for the different experimental conditions in terms of variation of load and energy with time.

	Fmax [N]	**Cv [J]**	**Wt [J]**	**Wm [J]**	**Wp [J]**
Reference	6699 ± 330	4.48 ± 0.93	4.82 ± 1.08	2.07 ± 0.58	2.75 ± 0.57
GR1	6226 ± 493	3.24 ± 0.93	3.30 ± 1.06	1.53 ± 0.40	1.80 ± 0.68
GR2	6178 ± 292	3.29 ± 0.50	3.41 ± 0.54	1.64 ± 0.38	1.77 ± 0.20
GR3	6536 ± 439	3.75 ± 0.76	3.97 ± 0.91	1.84 ± 0.48	2.13 ± 0.52

Table A.2 – *Energy absorption evaluated through the measurement of the pendulum's angle of rise (Cv) and as the integral of load-displacement curve (Wt). Wm and Wp represent the energy at maximum load and the crack propagation energy, respectively.*

It is observed that the addition of grain refiners to the melt leads to a decrease in terms of maximum load (*Fmax*) and total absorbed energy (*Cv* and *Wt*). However, because of its lowest deviation from the total absorbed energy of the Reference, the powder (GR3) appears to have a less detrimental effect than GR1 and GR2. Total absorbed energy Wt was also split into the two main complementary contributions, *Wm* and *Wp*, which were measured as previously described and reported as a percentage of the total impact energy in Figure A.3. It is possible to observe that the contribution of propagation energy (*Wp*) to total absorbed energy is higher than *Wm* for all the experimental conditions. Note also that the Reference has the highest contribution of *Wp* to total absorbed energy, whereas the alloys refined with GR1 and GR2 show the lowest mean values of this parameter.

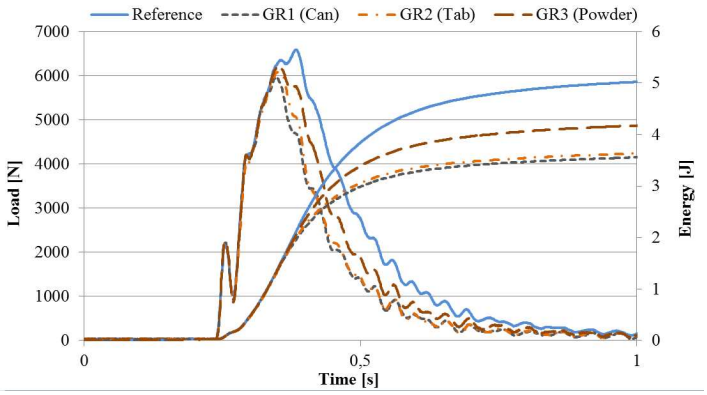

Figure A.2 – *Load-time and Energy-time mean curves for the different experimental conditions.*

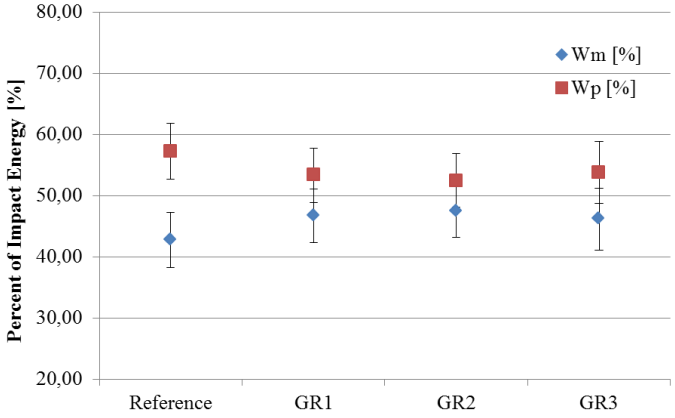

Figure A.3 – *Percentage of absorbed energy during crack nucleation and propagation for the different experimental conditions. Standard deviations are reported as error bars.*

A.3.2 Microstructural Analyses

Microstructures of some samples are shown in Figure A.4. The microstructure consists of a primary α-Al solid phase, and an Al-Si eutectic mixture. The addition of grain refiners to the molten alloy leads to a massive heterogeneous nucleation during cooling. Therefore, the α-Al primary phase morphology evolves from fully columnar (dendritic) to equiaxed. The morphology of the eutectic Si particles is fibrous, as a result of the addition of Sr to the melt. Intermetallic Fe-based compounds, such as α-$Al_{15}(Fe,Mn)_3Si_2$, β-$Al_5(Fe,Mn)Si$ and π-$Al_9FeMg_3Si_6$, were also observed. The morphology of β-$Al_5(Fe,Mn)Si$ intermetallic compounds is acicular and occasionally polygonal, whereas α-$Al_{15}(Fe,Mn)_3Si_2$ and π-$Al_9FeMg_3Si_6$ intermetallics have the typical "Chinese-script"shape.

Measurements of microstructural features are collected in Table A.3. As far as SDAS is concerned, more than 750 measurements were performed for each experimental condition in order to achieve statistically meaningful results. The comparison reveals that the addition of grain refiners leads to an increase in SDAS average values. The addition of GR1 (can) and GR2 (tab) causes the largest increases of SDAS average values, which are 8 - 9 μm higher than for the Reference. Conversely, GR3 (powder) has only a slight effect on SDAS, which

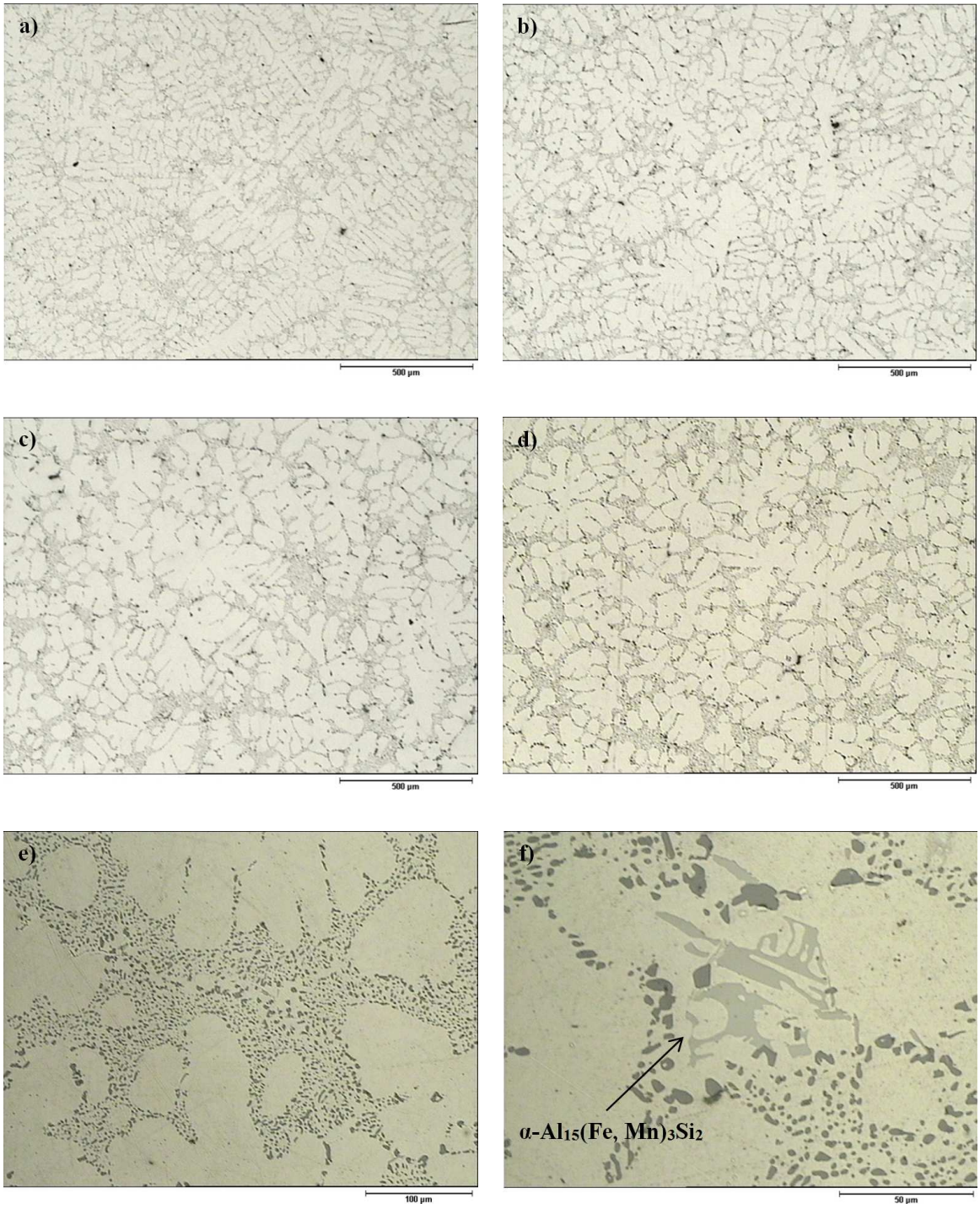

Figure A.4 – *Microstructure of A356: a) Reference, b) refined with GR1, c) refined with GR2, d) refined with GR3, e) fibrous shaped eutectic Si particles, f) magnification of a "Chinese-script"-shaped α-$Al_{15}(Fe,Mn)_3Si_2$ intermetallic.*

	SDAS [μm]	**Grain Size [μm]**	**Aspect Ratio (Si)**	**β-Al_5(Fe,Mn)Si Ave. Max. Length [μm]**
Reference	34.3 ± 8.9	453.1 ± 18.4	1.75 ± 0.74	19.17 ± 9.14
GR1	43.9 ± 10.0	341.9 ± 34.8	1.73 ± 0.71	34.58 ± 12.31
GR2	42.2 ± 9.7	372.1 ± 12.9	1.68 ± 0.67	25.45 ± 3.46
GR3	36.6 ± 8.4	276.3 ± 37.6	1.75 ± 0.75	26.40 ± 12.35

Table A.3 – *Average values and standard deviations of the measured microstructural features for each analysed condition.*

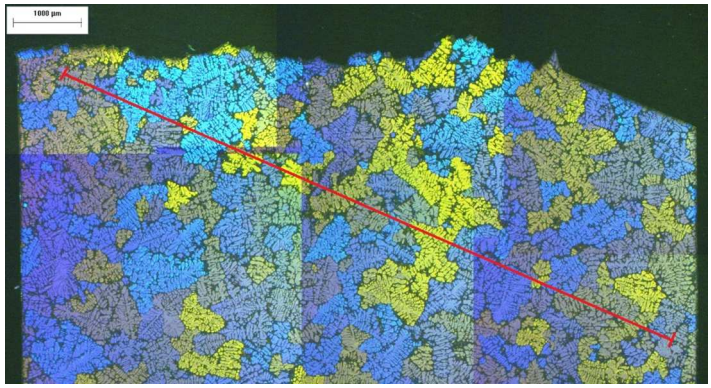

Figure A.5 – *Grain size measurement performed on one of the Reference samples. The red bar is 10000 μm length.*

remains comparable to the Reference. This can be explained as follows. It is well-known that SDAS is mainly affected by solidification time and cooling rate [27, 28]. However, it has been proved that excessive amounts of grain refiners can decrease the grain refinement efficiency due to the coincidence and agglomeration of nucleants and the interaction of their energy domains [29]. Moreover, the B/Ti mass ratio has to be accurately controlled in order to have effective nuclei for the primary α-Al phase [30]. In this case, it is supposed that the combined effects of low grain refinement potency and insufficient stirring of the melt have produced areas with different grade of refining. Therefore, while some zones of the castings were deeply affected by grain refiners, other areas were less (or not) refined because of the presence of these agglomeration of nucleants. As a consequence, grain refined alloys have higher mean values of SDAS than the Reference. Furthermore, the spread of SDAS values is probably linked to the assessment of SDAS on the whole specimens, considering refined and not refined areas.

Average grain size measurements were carried out according to the ASTM E-112 specification. As can be seen, the addition of grain refiners to the melt alloy produces a decrease in grain size and converts large dendrites to fine and equiaxed grains (Figure A.5 and Figure A.6). The best results in terms of grain refinement efficiency were obtained with the granular flux (GR3); GR1 and GR2 had similar but lower effects on grain size.

Since the morphology of eutectic silicon particles and β-Al_5(Fe,Mn)Si intermetallics strong-

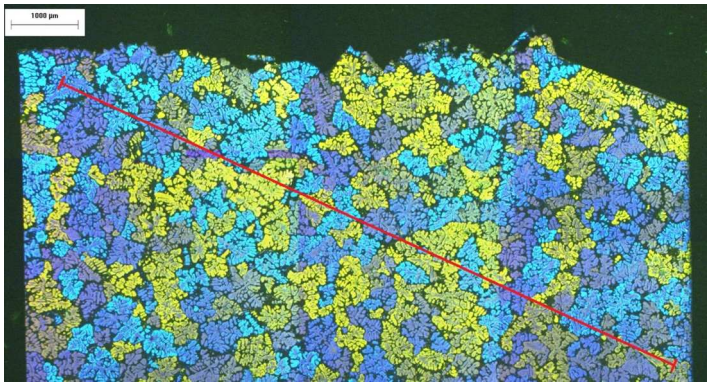

Figure A.6 – *Grain size measurement performed on one of the GR1 samples. The red bar is 10000 μm length.*

ly affects the mechanical properties of Al-Si alloys [22, 31, 32], some geometrical parameters of these two important microstructural features were measured and quantified. As may be seen from Table A.3 and Figure A.4e, the Si particles are present in a fibrous form with an average aspect ratio which lies within the range 1.68 - 1.75. This implies that the addition of grain refiners has not poisoning effects on the effectiveness of Sr addition as a modifier. Additionally, as already stated in [22], the length of β-Al_5(Fe,Mn)Si intermetallics is considered to be a suitable parameter to represent the effects of β-platelet size on the impact energy of the studied alloys. Therefore, in this work the lengths of the three longest β-platelets were recorded for each specimen and their average values were collected for all the experimental conditions. Data reveal that the average maximum length of the β-platelets increases in the refined conditions with respect to the Reference. Notwithstanding, microstructural analysis reveals that the addition of the grain refiners generally leads to a more homogeneous distribution of intermetallic compounds. Therefore, the addition of grain refiners realises opposite effects on the A356 cast alloy, concurrently increasing the secondary dendrite arm spacing and the average maximum length of β-platelets, and reducing the average grain size.

A.3.3 Fractographic Observations

Both the Reference and the refined alloys show a mixed transgranular-intergranular fracture mode [33, 34]. As can be seen in Figure A.7a and Figure A.7b, the fracture profile follows a preferential path through the eutectic phase, and in many cases it separates a secondary dendrite arm from the following one. The more ductile α-Al primary phase is not involved in the fracture process. Some authors [34,35] pointed out that fracture development involves the cracking of Si particles and acicular β-Al_5(Fe,Mn)Si intermetallics due to the formation of internal stresses in the particles by plastic deformation (Figures A.7c-A.7e). Once the particle cracks, a microvoid is formed and tends to grow. This particle cracking process continues until a critical volume fraction of cracked particles is reached. Eventually, the alloy fails because of a rapid linking process among microcracks. When SDAS is large, this

linkage is transgranular, whereas in small SDAS structures it becomes intergranular. It is observed that these phenomena lead not only to the propagation of the main fracture, but also to the formation of secondary cracks parallel to the main one (Figure A.7f) and normal to the tensile stress induced by the presence of the V-notch, in agreement with the analytical solution proposed by Berto *et al.* [36].
The SEM analysis of the fracture surfaces confirms the mixed transgranular-intergranular fracture mode (Figure A.8a and Figure A.8b). The fracture surface is mainly ductile; the edges of the deformed and fractured micronecks in both transgranular and intergranular eutectic regions can be easily distinguished. As previously observed, this is due to the specific damage process of the A356 alloy, which starts with the cracking of Si and β-Al_5(Fe,Mn)Si particles due to high local plastic strain (Figure A.8c and Figure A.8d). The presence of secondary phases was revealed on the fracture surfaces of all the samples in the interdendritic paths of fracture or emerging from the microvoids. The analysis with the EDS microprobe indicates the nature of the precipitates as brittle β-Al_5(Fe,Mn)Si platelets and "Chinese-script"-shaped α-$Al_{15}(Fe,Mn)_3Si_2$ and π-$Al_9FeMg_3Si_6$ intermetallic compounds (Figures A.9a - A.9b).

A.4 Discussion

As can be observed from data collected in Table A.2 and Table A.3, the Reference alloy, which has the lowest mean value of SDAS with respect to the grain refined alloys, realises the highest average values of *Fmax* and *Wt*. Figure A.10 shows the influence of this parameter on maximum load and total absorbed energy for all the tested specimens; as can be seen, as the SDAS increases, *Fmax* and *Wt* decrease with a nearly linear dependence.
This tendency, also observed in [37, 38], can be justified as follows. It is known from literature [35] that Al-Si-Mg alloys modified with Sr show a decrease in ductility when their dendritic cell size, which can be assumed a microstructural feature comparable to SDAS, is in the range from 40 μm to 80 μm. This is due to a transition in the fracture mode, which is transgranular for larger cell sizes and intergranular for finer cell sizes (i.e. for large and small SDAS respectively). In fact, when the cell size is large, eutectic Si particles precipitate not only at the grain boundaries, but also between the secondary arms. Eutectic Si particles and the interface eutectic Si/α-Al are more fragile than the α-Al matrix itself. When fracture starts, the eutectic between the secondary dendrite arms provides an easier path for its propagation with respect to the more irregular grain boundary zone, which would require a larger energy amount [34]. Thus, although grain refiners broaden the grain boundary region, their benefits in terms of impact properties are small because of the opposite effects linked to the increase of SDAS cell size and to the availability of many slip systems in aluminium alloys.
The direct consequence of this fracture behaviour is the decrease in the propagation energy contribution (*Wp*) to total impact energy for the alloys refined with GR1 and GR2 (Figure

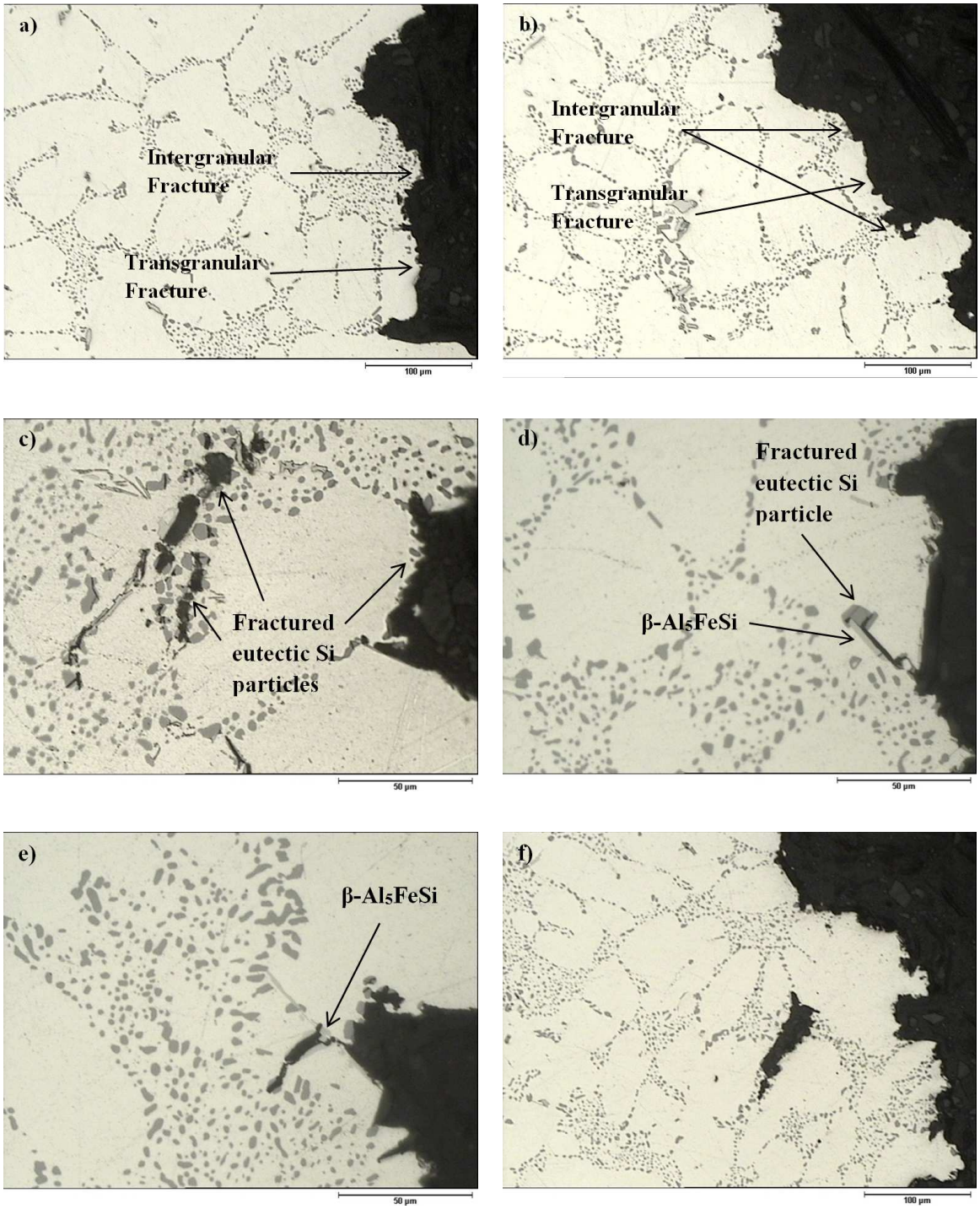

Figure A.7 – *Optical micrographs of fracture profiles: a) Mixed transgranular-intergranular fracture on GR2 refined alloy; b) Mixed transgranular-intergranular fracture on GR3 refined alloy; c,d,e) Acicular β-Al_5(Fe,Mn)Si intermetallics and fractured eutectic Si particles along and near the fracture profile; f) Formation of secondary cracks parallel to the main one.*

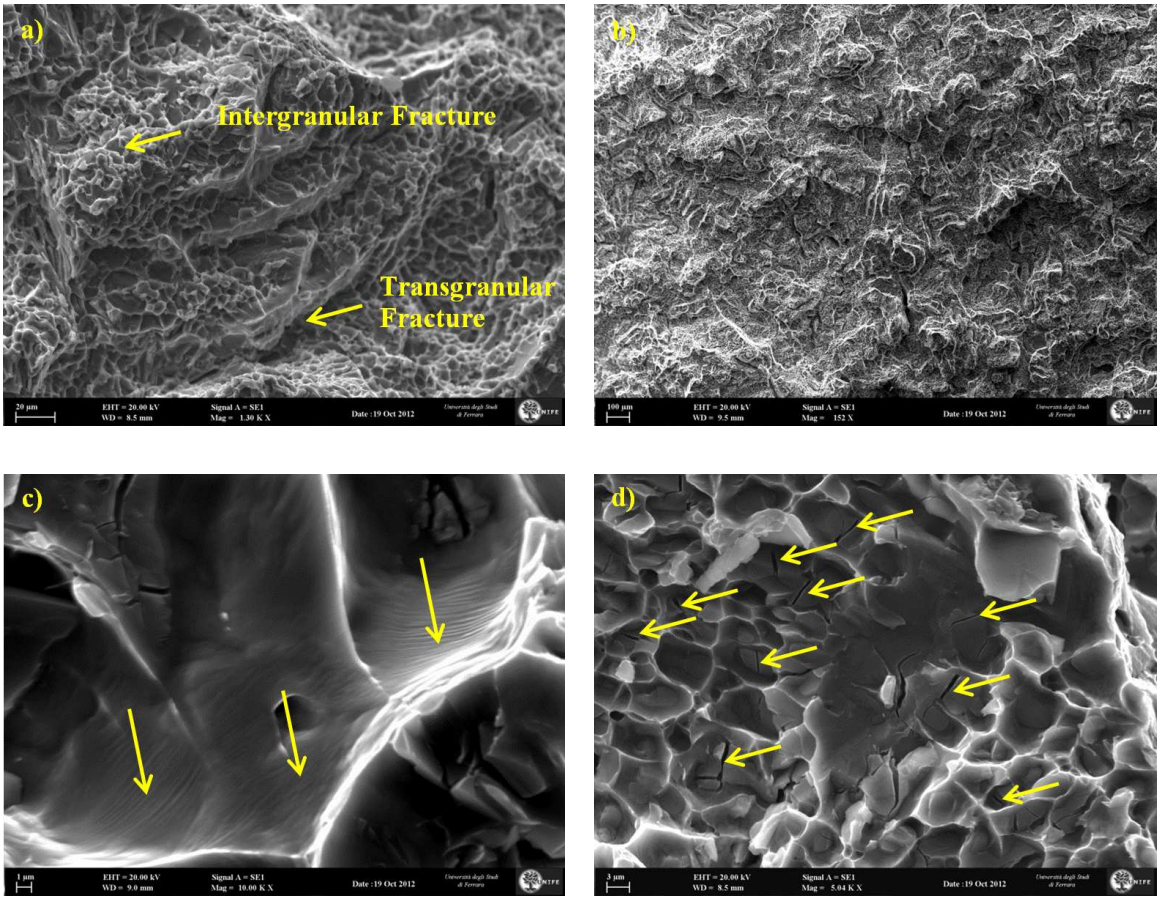

Figure A.8 – *SEM fractographs: a) mixed transgranular-intergranular fracture mode on GR3 refined alloy at high magnification; b) mixed transgranular-intergranular fracture mode on GR1 refined alloy at low magnification; c) shear bands generated in the matrix at the tip of the microvoids; d) cracked eutectic Si particles.*

A.4). This can be due to the complementary effects of bad refinement and large dendrite cell size (i.e. transgranular fracture). As it is described below, this behaviour also depends on the increase in Fe-based intermetallics size caused by the addition of grain refiners. Conversely, GR3 shows an energy propagation value nearer to that of the Reference, probably because of its better grain refinement potency. Consequently, despite its higher SDAS, the presence of smaller and more globular grains in the GR3 alloy leads to a fracture propagation which is not mainly transgranular, but continuously shifts from transgranular to intergranular, thus absorbing a larger amount of energy.

Figure A.11 and Figure A.12 present the two contributions to total impact energy as a function of SDAS. Li *et al.* [38] found a linear inverse correlation between SDAS and impact energy, i.e. a coarser microstructure corresponds to a lower impact energy. As can be seen, both *Wm* and *Wp* are found to decrease with an increase in the SDAS value.

As regards to *Wm*, the GR3 refined alloy shows a trend similar to the Reference, whereas GR1 and GR2 seem to have higher Wm values at the same SDAS size, and correspondingly

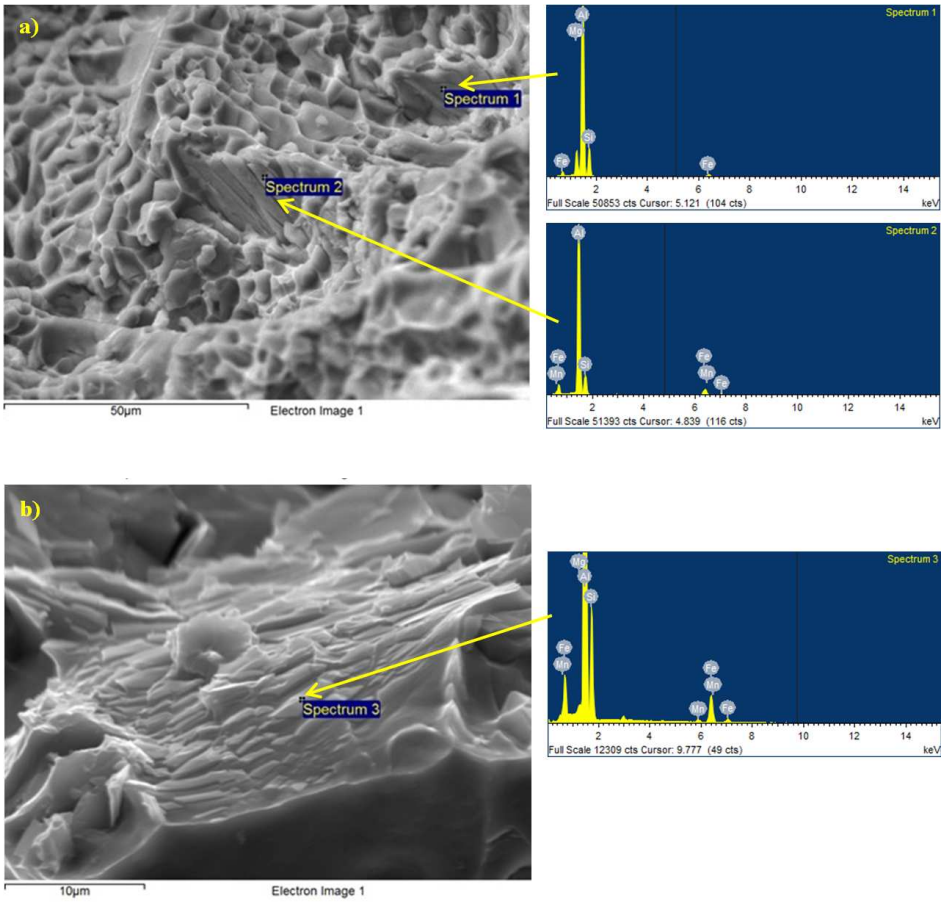

Figure A.9 – *SEM micrographs of the intermetallic compounds observed on the fracture surface of the samples: a) π-$Al_9FeMg_3Si_6$ (spectrum 1) and β-$Al_5(Fe,Mn)Si$ (spectrum 2); b) "Chinese-script"π-$Al_9FeMg_3Si_6$ and α-$Al_{15}(Fe,Mn)_3Si_2$ (spectrum 3).*

the same energy at maximum load despite a higher SDAS. Hence, GR1 and GR2 seem to have a better effect on Wm with respect to GR3. Unluckily this effect is only virtual, because of the tendency for these grain refiners to increase SDAS mean values, that is to promote transgranular fracture.

Concerning *Wp*, GR1 shows the highest detrimental effect due to the increase in SDAS size, thus leading to the lowest mean value of total absorbed energy Wt (see also Table A.2). Conversely, GR2 has a lesser decrease of *Wp* with the increase of SDAS values. Despite GR3 correlation coefficient ($R^2 \approx 0{,}7$), GR3 trend is similar to that of the Reference; this probably indicates that the powder can realise a double positive effect, which consists of a good grain refinement without overly increasing the SDAS size, and a fracture behaviour similar to the Reference, capable of absorbing a higher amount of energy.

Figure A.13 and Figure A.14 show the influence of grain size on the two contributions to total absorbed energy. As can be seen, *Wm* and *Wp* values are spread, so that no correlation between grain size and impact properties is found. This is in agreement to the fact that al-

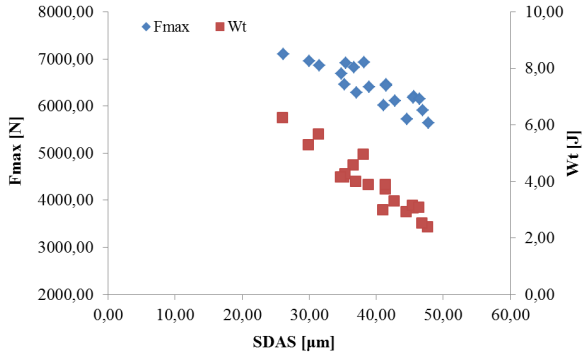

Figure A.10 – *Maximum load and total absorbed energy as a function of SDAS for all the tested specimens.*

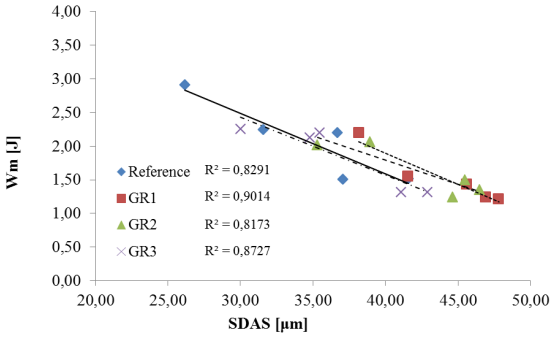

Figure A.11 – *Energy at maximum load of the studied alloys as a function of SDAS.*

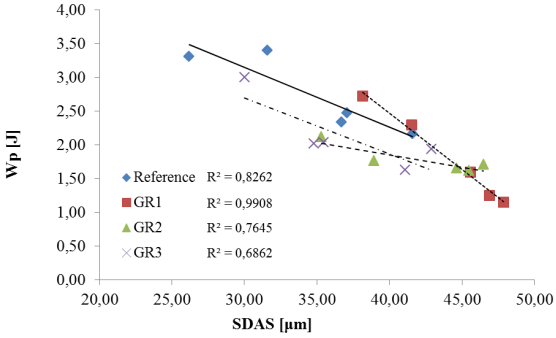

Figure A.12 – *Propagation energy of the studied alloys as a function of SDAS.*

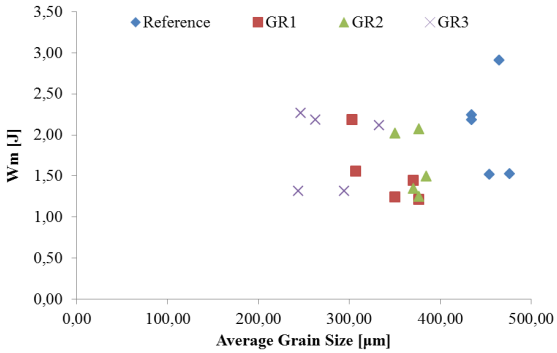

Figure A.13 – *Energy at maximum load of the studied alloys as a function of average grain size.*

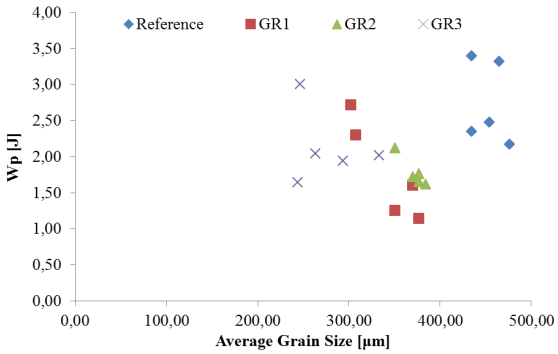

Figure A.14 – *Propagation energy of the studied alloys as a function of average grain size.*

though grain refinement of aluminium alloys is useful, its effects are generally over-rated in terms of mechanical properties, becoming important only when the grain size is strongly reduced [27]. The mere grain refinement seems not to be so influent on mechanical properties unless grain refiners and Sr modifiers are both added to the melt alloy [23,24,26,38–41].

Conversely, the effect of β-platelets size on impact properties seems to be more certain, as already stated in literature [21,22,32]. Ma *et al.* found that β-iron intermetallics strongly deteriorate impact properties of the A356.2 alloy, following a power correlation between impact energy and β-platelet length/area. Figure A.15 and Figure A.16 show the energy at maxi-

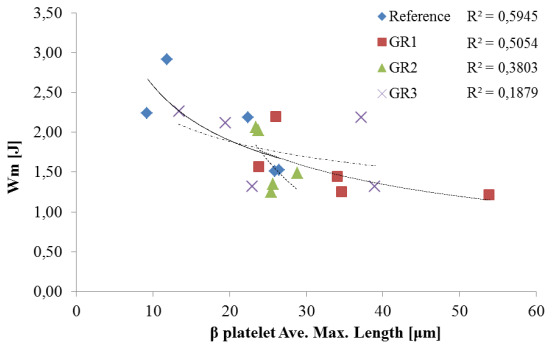

Figure A.15 – *Energy at maximum load of the studied alloys as a function of β-platelet average maximum length.*

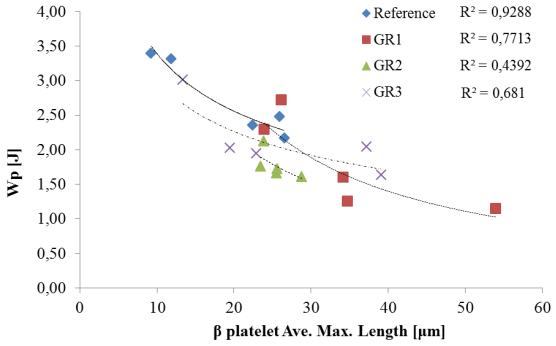

Figure A.16 – *Propagation energy of the studied alloys as a function of β-platelet average maximum length.*

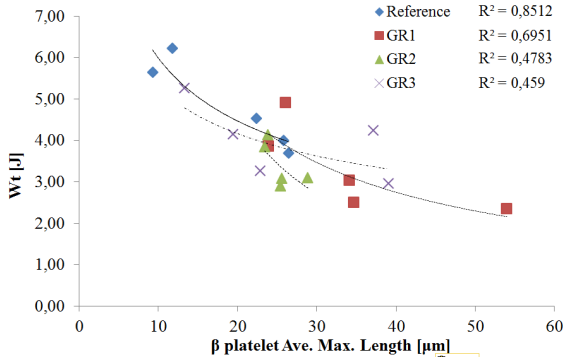

Figure A.17 – *Total impact energy of the studied alloys as a function of β-platelet average maximum length.*

mum load *Wm* and the propagation energy *Wp* as a function of β-platelet average maximum length (mean of the lengths of the three longest β-platelets). As can be seen, the influence of intermetallics size on the energy at maximum load *Wm* is negligible; as a matter of fact, microstructural features affect the propagation of fracture, while crack initiation is primary due to the presence of the notch. Concerning *Wp*, the power correlation is established only for the Reference alloy, whereas the grain refined ones show very low correlation coefficients. The same observation also applies to the total absorbed energy *Wt* (Figure A.17). Nevertheless, it can be stated that the increase in β-platelets average maximum length leads to a decrease in total impact energy.

Low correlation coefficients can be explained as follows. When grain refiners are added to the melt, the grain refinement causes not only a positive effect linked to the decrease in grain size, but also a negative one related to the increase in SDAS, which consequently leads to a mainly transgranular fracture mode. Moreover, even if the improved nucleation distributes the intermetallics in the interdendritic regions more homogeneously, the increase in size caused by the grain refinement is detrimental for impact properties.

The concurrent effects of SDAS and β-platelets average maximum length on total impact energy can be taken into account using the multiple regression analysis technique, under the

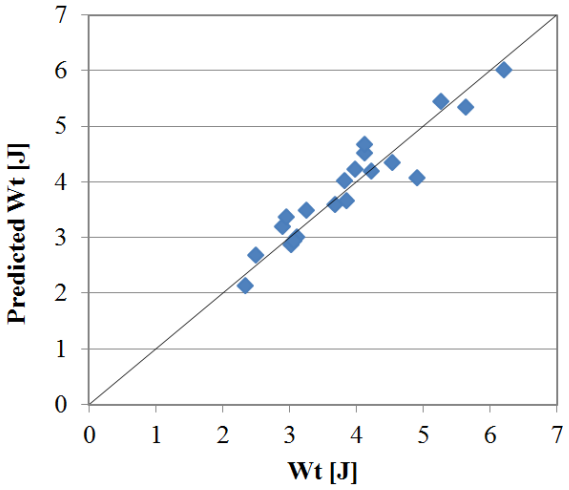

Figure A.18 – *Multiple regression model predictions vs. measured data of total impact energy.*

proved assumptions of constant solidification rate, negligible effects of grain size on impact properties and aspect ratio of silicon eutectic particles not influenced by the grain refiners addition. Therefore, the equation which links total impact energy to SDAS and β-platelets average maximum length (AML) can be written as:

$$Wt = 9.840 - 0.136 \cdot SDAS - 0.022 \cdot AML \tag{A.1}$$

Figure A.18 plots the experimental data against the multiple regression analysis predictions for total impact energy *Wt*. The validity of the approach is proven by means of the determination of the correlation coefficient (R^2 = 0.897). This justifies the hypothesis that total impact energy does not depend on SDAS and β-platelets size taken individually, but has a more complex dependence which generally involves many microstructural parameters.

A.5 Conclusions

When grain refiners are added to the melt, the effects on microstructural features are complex, involving changes in shape and size of grains, SDAS and intermetallic compounds. These changes in size and shape of microstructural features strongly affect the impact toughness of the alloys. From the present investigation on the influence of three commercial Ti-B based grain refiners on impact properties of the A356 cast aluminium alloy, the following conclusions can be drawn:

1. All grain refiners cause a decrease in terms of maximum load (*Fmax*) and total absorbed energy (*Wt*). However, because of its lower deviation from the total absorbed energy of the Reference, the powder (GR3) appears to have a less detrimental effect than GR1 and GR2.

2. Both the Reference and the refined alloys show a mixed transgranular-intergranular fracture mode. Fracture profile follows a preferential path through the eutectic phase, and in many cases it separates a secondary dendrite arm from the following one.

3. The decrease in grain size does not influence the two contributions to total absorbed energy (*Wm* and *Wp*), so that no direct correlation between grain size and impact properties is found.

4. The addition of grain refiners increases the secondary dendrite arm spacing and leads to a more severe transgranular fracture, which requires a smaller energy amount with respect to the more irregular grain boundary zone. Maximum load (*Fmax*) and total impact energy (*Wt*) have a nearly linear dependence on SDAS.

5. The propagation energy (*Wp*) decreases for the alloys refined with GR1 and GR2. This is caused by the complementary effects of bad refinement, large dendrite cell size (i.e. transgranular fracture) and increase in β-platelets average maximum length. Conversely, GR3 shows an energy propagation value nearer to that of the Reference.

6. The influence of β-iron intermetallics size on the energy to maximum load *Wm* is negligible. As regards to propagation energy and total impact energy, the power correlation is established only for the Reference alloy, whereas the grain refined ones show very low correlation coefficients.

7. Total impact energy does not depend on SDAS and β-platelets size taken individually. The concurrent effects of SDAS and β-platelets average maximum length on total impact energy can be taken into account using the multiple regression analysis technique. The validity of the approach is proven by means of the determination of the correlation coefficient ($R^2 = 0.897$).

Acknowledgements

The authors wish to thank the foundry "Fonderia Scacchetti Leghe Leggere s.r.l"of S. Felice sul Panaro (Modena - Italy) for the use of its installations and equipments. The authors also acknowledge Mr. Lorenzo Pivetti for his helpful contributions during foundry activities.

References

[1] I. Maxwell and A. Hellawell, "A simple model for grain refinement during solidification," *Acta Metall.*, vol. 23, pp. 229–237, 1975.

[2] D. G. McCartney, "Grain refining of aluminium and its alloys using inoculants," *Int. Mater. Rev.*, vol. 34, pp. 247–260, 1989.

[3] P. Schumacher, A. L. Greer, J. Worth, P. V. Evans, M. A. Kearns, P. Fisher, and A. H. Green, "New studies of nucleation mechanisms in aluminium alloys: implications for grain refinement practice," *Mater. Sci. Technol.*, vol. 14, pp. 394–404, 1998.

[4] A. L. Greer, A. M. Bunn, A. Tronche, P. V. Evans, and D. J. Bristow, "Modelling of inoculation of metallic melts: application to grain refinement of aluminium by Al-Ti-B," *Acta Mater.*, vol. 48, pp. 2823–2835, 2000.

[5] Y. Birol, "A novel Al-Ti-B alloy for grain refining Al-Si foundry alloys," *J. Alloy Compd.*, vol. 486, pp. 219–222, 2000.

[6] C. Lee and S. Chen, "Quantities of grains of aluminium and those of TiB2 and Al3Ti particles added in the grain-refining process," *Mater. Sci. Eng. A*, vol. 325, pp. 242–248, 2002.

[7] C. Limmaneevichitr and W. Eidhed, "Novel technique for grain refinement in aluminium casting by Al-Ti-B powder injection," *Mater. Sci. Eng. A*, vol. 355, pp. 174–179, 2003.

[8] C. Wang, M. Wang, B. Yu, D. Chen, P. Qin, M. Feng, and Q. Dai, "The grain refinement behavior of TiB2 particles prepared with in situ technology," *Mater. Sci. Eng. A*, vol. 459, pp. 238–243, 2007.

[9] Z. Zhang, X. Bian, Y. Wang, and X. Liu, "Microstructure and grain refining performance of melt-spun Al-5Ti-1B master alloy," *Mater. Sci. Eng. A*, vol. 352, pp. 8–15, 2003.

[10] A. Cibula, "The Mechanism of Grain Refinement of Sand Castings in Aluminium Alloys," *J. Inst. Met.*, vol. 76, pp. 321–360, 1949.

[11] P. S. Mohanty and J. E. Gruzleski, "Mechanism of grain refinement in aluminium," *Acta Metall. Mater.*, vol. 43, pp. 2001–2012, 1995.

[12] G. P. Jones and J. Pearson, "Factors affecting the grain refinement of aluminium using titanium and boron additives," *Metall. Trans. B*, vol. 7, pp. 223–234, 1976.

[13] G. K. Sigworth, "The Grain Refining of Aluminum and Phase Relationships in the Al-Ti-B System," *Metall. Trans. A*, vol. 15, pp. 277–282, 1984.

[14] ——, "Author's reply," *Metall. Trans. A*, vol. 17, pp. 349–351, 1986.

[15] M. Johnsson, "The influence of composition on equiaxed crystal-growth mechanisms and grain-size in Al-alloys," *Z. Metallkd*, vol. 87, pp. 216–220, 1996.

[16] P. A. Tøndel, "Grain refinement of hypoeutectic Al-Si foundry alloys," Ph.D. dissertation, University of Trondheim, 1994.

[17] J. A. Spittle and S. Sadli, "Effect of alloy variables on grain-refinement of binary aluminum-alloys with Al-Ti-B," *Mater. Sci. Technol.*, vol. 11, pp. 533–537, 1995.

[18] M. Easton and D. StJohn, "Grain Refinement of Aluminum Alloys: Part II. Confirmation of, and a Mechanism for, the Solute Paradigm," *Metall. Mater. Trans. A*, vol. 30, pp. 1625–1633, 1999.

[19] T. E. Quested and A. L. Greer, "The effect of the size distribution of inoculant particles on as-cast grain size in aluminium alloys," *Acta Mater.*, vol. 52, pp. 3859–3868, 2004.

[20] B. T. Sofyan, D. J. Kharistal, L. Trijati, K. Purba, and R. E. Susanto, "Grain refinement of AA333 aluminium cast alloy by Al-Ti granulated flux," *Mater. Design*, vol. 31, pp. 536–543, 2010.

[21] S. Murali, K. S. Raman, and K. S. S. Murthy, "Effect of magnesium, iron (impurity) and solidification rates on the fracture toughness of Al-7Si-0.3Mg casting alloy," *Mater. Sci. Eng. A*, vol. 151, pp. 1–10, 1992.

[22] Z. Ma, A. M. Samuel, F. H. Samuel, H. W. Doty, and S. Valtierra, "Effect of Fe Content and Cooling Rate on the Impact Toughness of Cast 319 and 356 Aluminum Alloys," *AFS Trans.*, vol. 3, pp. 255–265, 2003.

[23] S. Shivkumar, L. Wang, and C. Keller, "Impact properties of A356-T6 Alloys," *J. Mater. Eng. Perform.*, vol. 3, pp. 83–90, 1994.

[24] D. L. Zhang, L. H. Zheng, and D. H. S. John, "Effect of a short solution treatment time on microstructure and mechanical properties of modified Al-7wt.%Si-0.3wt.%Mg alloy," *J. Light Met.*, vol. 2, pp. 27–36, 2002.

[25] M. Merlin, G. Timelli, F. Bonollo, and G. L. Garagnani, "Impact behaviour of A356 alloy for low-pressure die casting automotive wheels," *J. Mater. Process. Tech.*, vol. 209, pp. 1060–1073, 2009.

[26] Y. Birol, "Influence of grain refinement and modification on microstructure and mechanical properties of Al-7Si and Al-7Si-2.5Cu cast alloys," *Mater. Charact.*, vol. 59, pp. 283–289, 2008.

[27] J. Campbell, *Castings - Second Edition*. Butterworth-Heinemann, Oxford (2003).

[28] S. G. Shabestari and M. Malekan, "Thermal analysis study of the effect of cooling rate on the microstructure and solidification parameters of 319 aluminum alloy," *Can. Metall. Q.*, vol. 44, pp. 305–312, 2005.

[29] ——, "Assessment of the effect of grain refinement on the solidification characteristics of 319 aluminum alloy using thermal analysis," *J. Alloy Compd.*, vol. 44, pp. 134–142, 2010.

[30] M. Wang, S. Wang, Z. Liu, Z. Liu, T. Song, and X. Zuo, "Effect of B/Ti ratio on grain refining of low-titanium aluminum produced by electrolysis," *Mater. Sci. Eng. A*, vol. 416, pp. 312–316, 2006.

[31] S. Haro-Rodríguez and R. E. Goytia-Reyes and D. K. Dwivedi and V. H. Baltazar-Hernández and H. Flores-Zúniga and M. J. Pérez-López, "On influence of Ti and Sr on microstructure, mechanical properties and quality index of cast eutectic Al-Si-Mg alloy," *Mater. Design*, vol. 32, pp. 1865–1871, 2011.

[32] A. M. A. Mohamed, A. M. Samuel, F. H. Samuel, and H. W. Doty, "Influence of additives on the microstructure and tensile properties of near eutectic Al-10.8%Si cast alloy," *Mater. Design*, vol. 30, pp. 3943–3957, 2009.

[33] C. H. Cáceres and B. I. Selling, "The deformation and fracture behaviour of an Al-Si-Mg casting alloy," *Mater. Sci. Eng. A*, vol. 197, pp. 171–179, 1995.

[34] Q. G. Wang, "Microstructural Effects on the Tensile and Fracture Behavior of Aluminum Casting Alloys A356/357," *Metall. Mater. Trans. A*, vol. 34, pp. 2887–2899, 2003.

[35] C. H. Cáceres and J. R. Griffiths, "Damage by the cracking of Silicon particles in an Al-7Si-0.3Mg casting alloy," *Acta Mater.*, vol. 44, pp. 25–33, 1996.

[36] F. Berto, P. Lazzarin, and C. H. Wang, "Three-dimensional linear elastic distributions of stress and strain energy density ahead of V-shaped notches in plates of arbitrary thickness," *Int. J. Fract.*, vol. 127, pp. 265–282, 2004.

[37] P. Meyer, D. Massinon, P. Guerin, and L. Wong, "Influence of Microstructure on the Static and Thermal Fatigue Properties of 319 Alloys," *SAE International*, vol. 106, pp. 627–634, 1997.

[38] Z. Li, A. M. Samuel, F. H. Samuel, C. Ravindran, H. W. Doty, and S. Valtierra, "Influence of Microstructure on the Static and Thermal Fatigue Properties of 319 Alloys," *Mater. Sci Eng. A*, vol. 26, pp. 2359–2372, 2004.

[39] S. A. Kori, B. S. Murty, and M. Chakraborty, "Development of an efficient grain refiner for Al-7Si alloy and its modification with strontium," *Mater. Sci. Eng. A*, vol. 283, pp. 94–104, 2000.

[40] F. Paray, B. Kulunk, and J. E. Gruzleski, "Impact properties of Al-Si foundry alloys," *Int. J. Cast Metals Res.*, vol. 13, pp. 17–37, 2000.

[41] E. N. Pan and M. W. Hsieh and S. S. Jang and C. R Loper Jr, "Study of the Influence of Processing Parameters on the Microstructure and Properties of A356 Aluminum Alloy," Defense Technical Information Center OAI-PMH Repository, 1998.

Article B

The effect of Ni and V trace elements on the mechanical properties of A356 aluminium foundry alloy in as-cast and T6 heat treated conditions

Authors: D. Casari[1], T.H. Ludwig[2], L. Arnberg[3], M. Merlin[1] and G.L. Garagnani[1]
Submitted to: Materials Science and Engineering A

Abstract

In this study, the tensile properties of unmodified A356 alloys with trace additions of Ni or V were investigated by analysing specimens obtained from sand and permanent mould casting in as-cast and T6 heat treated conditions. The nominal concentration of the trace elements Ni and V was 600 and 1000 ppm, respectively. It was found that the precipitation of Ni-rich intermetallics strongly influences the tensile properties of the sand cast A356 alloy in as-cast condition, leading to a reduction of both the yield strength ($Rp_{0.2}$) and ultimate tensile strength (UTS) by 87% and 37%, respectively. Conversely, V addition increased $Rp_{0.2}$ and UTS by 42% and 25% most likely due to a solid solution strengthening effect. After T6 heat treatment, the sand cast A356 alloys containing V exhibited slightly higher mechanical properties as compared to an A356 reference alloy ($\approx$ 18%), whereas the detrimental effect of Ni was eliminated. The cooling rate became the main parameter influencing the mechanical properties of permanent mould cast alloys: no significant difference in mechanical properties was observed between the reference alloy and Ni- or V-containing alloys in both as-cast and T6 conditions.

[1]Engineering Department - ENDIF, University of Ferrara, Via Saragat 1, I-44122 Ferrara, Italy
[2]Hydro Aluminium AS, Verksvegen 1, N-6882 Øvre Årdal, Norway
[3]Department of Materials Science and Engineering, NTNU, Alfred Getz vei 2, N-7491 Trondheim, Norway

B.1 Introduction

Al-Si foundry alloys are widely used in the automotive industry owing to their good castability, high strength-to-weight ratio, corrosion resistance and ease of recycling. Good mechanical properties at room temperature can be obtained in these alloys by a heat treatment involving solutionising and subsequent age hardening. Depending on the chemical composition of the alloy, several phases, such as Mg_2Si, precipitate in the α-Al matrix, thus significantly increasing its strength by preventing the motion of dislocations [1].

Aluminium producers that are currently focusing primarily on the control of dissolved hydrogen, Na content and inclusion removal, are now facing increasing Ni and V concentrations originating from the petroleum coke used for manufacturing of anodes for the Al electrolysis. In the upcoming years, the levels of Ni and V in the coke are expected to rise to 420 and 1080 ppm, respectively [2]. Since there is yet no cost efficient method available for removal of these elements, the concentration of V and Ni will also increase in the metal [3]. Estimates show that approximately 50% of these elements partition into the primary aluminium during the electrolytic reduction of alumina affecting the final quality of the downstream products such as aluminium foundry alloys. Thus it is important to establish whether these concentrations can have a beneficial or detrimental effect on the microstructural features, and consequently on mechanical, corrosion and manufacturing properties.

Recent literature focuses primarily on Ni and V as alloying elements. It was shown that Ni serves as an iron neutralisers, since it transforms the brittle plate-like β-Al_5FeSi intermetallics into the Al_9FeNi phase through a peritectic reaction [4, 5]. However, the Al_9FeNi phase is also brittle and can contribute to the nucleation of fatigue cracks [6]. Furthermore, it has been recently observed that Ni stabilises the mechanical properties of aluminium alloys for high temperature applications. Since it is well-established that Al-Si alloys possess a fairly low thermal and metallurgical stability [7,8], several authors have investigated complex hypoeutectic and near-eutectic Al-Si based alloys, in order to make these alloys suitable for high temperature applications (i.e. up to 250 °C) [9–13]. Improved mechanical properties at high temperature were obtained by Heusler *et al.* [9], which presented a new alloy for engine applications based on the Al-Si-Mg-Cu-Fe-Ni system with increased fatigue properties (+ 20%) and tensile strength. This increase was attributed to the presence of Ni-bearing intermetallic compounds. Ashgar *et al.* [10] reported significant elevated-temperature strength in an Al-12SiNi alloy, where the addition of 1.2 wt% Ni led to the formation of an interconnected hybrid reinforcement consisting of eutectic Si and Ni and Fe aluminides. In another investigation on the elevated-temperature properties of different Ni- and Cu-added Al-Si piston alloys, Li *et al.* [11] found that the stable δ-Al_3CuNi phase possesses the most efficient contribution to high temperature strength compared to the other Ni-containing phases due to its strip-like interconnected morphology. Farkoosh *et al.* [12] also observed that this phase produces the most significant contribution to the T7 hardness of an Al-7Si-0.5Cu-0.35Mg-

0.1Fe-*X*Ni alloy, its amount being maximised at Ni:Cu $\approx$ 1.5. Thermally stable Ni intermetallics are also credited for the increase of the yield strength of this alloy at 300 °C [13]. However, the Al_9FeNi phase is very brittle even at this temperature and its cracking at the early stage of creep deformation can reduce the creep resistance of the alloy.

The addition of peritectic forming solutes such as V has been reported to be an effective approach to introduce active heterogeneous nucleant particles through in-situ formation in the melt, thus promoting the grain refinement of the alloy [14]. Recently, Kasprzak *et al.* [15] developed a high temperature alloy based on a modified A356 composition. They indicated that stable Al-Si-Zr-Ti nanoprecipitates in the α-Al matrix are the cause of superior mechanical properties at high temperature for this modified alloy, compared to the reference alloy (+34% yield strength, +37% UTS). In addition, also the V concentration was increased to 0.2 wt%. However, V-based intermetallic compounds were not observed in the microstructure of their alloys.

Only few investigations deal with the effects of Ni and V as trace impurity elements in hypoeutectic Al-Si alloys such as the commercial A356 foundry alloy, which currently contains low levels of Ni and V, in the range of 20 - 30 ppm and 100 - 110 ppm each [3,16]. In a recent publication Zhu *et al.* showed that the addition of trace element Ni up to 0.02 wt% does not influence the as-cast microstructure of A356 alloy, whereas an unidentified phase with high Ni content is formed when the Ni concentration is increased to 0.05 wt% [17]. Microstructural observations reported by Ludwig *et al.* [18] on both high purity and commercial purity Al-7wt pct Si foundry alloys revealed that Ni concentrations exceeding 300 ppm forms the Al_3Ni phase in the high purity alloy, and both Al_3Ni and Al_9FeNi intermetallic phases were found to precipitate in the commercial purity alloy. This study also indicated that V in concentrations up to 0.06 wt%, remains in solid solution or is dissolved in ternary Al-Fe-Si phases. Since it is well-known that the solid solubility of V in Al is approximately 0.1 wt% [19], most of the V will remain in the α-Al matrix. Beyond this concentration, V and Si will precipitate as pre-eutectic Si_2V crystals with a distinct polyhedral morphology [16,20].

At present, only the EN 1676-2010 specification defines an upper concentration limit for V of 0.03 wt% for EN-AB 42100 aluminium foundry alloys, which corresponds to A356 alloys, whereas there exist no information about the maximal tolerable Ni concentration in this alloy system. Therefore, the aim of the present work is to investigate the effect of trace elements Ni and V on the mechanical properties of as-cast and T6 heat-treated A356 aluminium foundry alloys in two commercially important casting processes: (i) sand and (ii) permanent mould casting. Microstructural and fractographic analyses were performed to investigate the microstructural features involved in the fracture process. This study also intends to give an indication of the tolerable levels of Ni and V for this widely used alloy, in order to establish if current alloy specifications can be adjusted to accommodate higher Ni and V concentrations while the alloy maintains similar mechanical properties as the uncontaminated reference alloy.

B.2 Materials and Methods

A commercial A356 aluminium alloy was used as base alloy in the present study. The as-received alloy ingots were melted in charges of 16 kg each in a boron-nitride coated clay-graphite crucible. Trace elements were added in the form of Al-10 wt% Ni and Al-10 wt% V master alloys according to the targeted nominal concentrations of 600 and 1000 ppm of Ni and V, respectively. In order to avoid any masking effects or interactions with additional elements, neither Sr nor Na were added as modifier agents. The melting temperature was monitored with the Alspek-H probe and was kept constant at 740 °C ± 5 °C. Samples from the three different melts were taken throughout the casting trials and were analysed by optical emission spectroscopy (OES). The chemical composition of the reference and the Ni- or V- containing alloys is given in Table B.1.

Alloy	Addition (ppm)	Si	Fe	Mg	Ni	V	Al
A356	-	7.054	0.092	0.355	0.003	0.007	bal.
A356 + Ni	600	6.902	0.087	0.344	0.061	0.007	bal.
A356 + V	1000	6.992	0.094	0.349	0.003	0.108	bal.

Table B.1 – *Chemical composition (wt%) of A356 reference alloy and Ni/V-contaminated alloys as measured by OES.*

The hydrogen content in the melts was measured in-situ with the Alspek-H probe. Melts were degassed with argon gas in order to reach a hydrogen concentration of 0.08 mlH_2/100 gAl. The alloys were then poured in both sand and steel moulds. Sand castings were produced using an upgraded version of the tensile test bar design proposed by Dispinar and Campbell [21]. In this new casting design, the shape of the bars varied from cylindrical to tapered, with diameters increasing gradually from 15 mm (bottom) to 20 mm (top). Permanent mould castings were obtained by pouring the molten alloys into a L-shaped preheated steel mould, manufactured according to UNI 3039 specification. The temperature of the die was kept at a temperature of 300 °C during the casting trials. This setup yields cooling rates of 1.3 K/s and 4.2 K/s in the middle of sand cast and permanent mould cast tensile specimens, respectively. Tensile specimens with a round cross section were machined according to the EN ISO 6892-1 specification (Figure B.1, 40 mm gauge length and 8.5 mm diameter).

In order to compare the effect of Ni and V in as-cast and heat treated condition, samples originating from the same casting were subject to a T6 heat treatment including solutionising at 540 °C for 4 h followed by quenching in a water bath at 20 °C. Subsequently, the samples were aged at 160 °C for 6 h. As a result, twelve different experimental conditions were investigated (Table B.2), and at least 5 samples were tested in each condition.

Tensile tests were performed at room temperature, using a MTS 810 Material Testing System. The crosshead speed was 0.05 mm/s and the applied load was restricted to 40 kN. Stress-strain curves were obtained by attaching a knife-edge extensometer to the specimens'

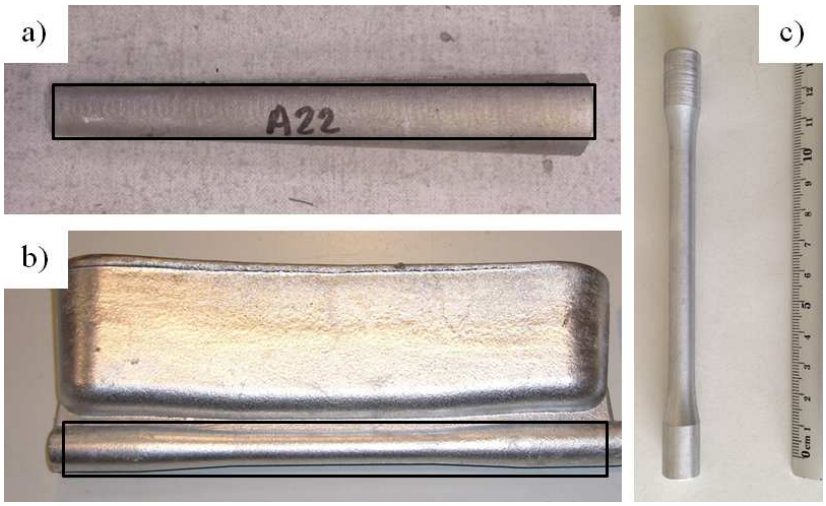

Figure B.1 – *Castings obtained from: a) sand mould; b) permanent mould. The black rectangles mark the areas where the tensile specimens c) were machined.*

Alloy	Mould	Condition	Alloy Code
A356	Sand	as-cast	A356 - AC
		T6	A356 - T6
A356 + 600 ppm Ni	Sand	as-cast	Ni - AC
		T6	Ni - T6
A356 + 1000 ppm V	Sand	as-cast	V - AC
		T6	V - T6
A356	Permanent Mould	as-cast	A356 PM - AC
		T6	A356 PM - T6
A356 + 600 ppm Ni	Permanent Mould	as-cast	Ni PM - AC
		T6	Ni PM - T6
A356 + 1000 ppm Ni	Permanent Mould	as-cast	V PM - AC
		T6	V PM - T6

Table B.2 – *Experimental plan.*

gauge length and the tensile properties, such as yield strength, ultimate tensile strength and percentage elongation ($Rp_{0.2}$, UTS and A%, respectively) were determined.

Samples for metallographic investigation were sectioned parallel to the fracture surface. They were then embedded in phenolic resin and prepared according to standard grinding and polishing procedures. Microstructures and fracture surfaces of the specimens after tensile testing were analysed with a ZEISS ULTRA 55 field emission scanning electron microscope (FE-SEM) equipped with energy dispersive X-ray spectroscopy (EDS). SDAS measurements were performed using the line intercept method. The distribution of the alloying elements Al, Mg, V and Ni in the primary α-Al matrix and within secondary phase particles was measured using a JEOL JXA-8500F electron probe micro-analyser (EPMA).

B.3 Results

B.3.1 Mechanical Properties

The average values of the tensile properties of sand cast and permanent mould cast alloys are summarized in Table B.3 and Table B.4. It was observed that the addition of Ni strongly influences the tensile properties of the sand cast samples in the as-cast condition (*A356 - AC*, *Ni - AC* and *V - AC* in Figure B.2), compared to the reference alloy, leading to a reduction of both the yield strength ($Rp_{0.2}$) and ultimate tensile strength (UTS) by 87% and 37%, respectively. Conversely, the V addition increases $Rp_{0.2}$ and UTS by 42% and 25%. After T6 heat treatment (- *T6*), the sand cast A356 alloys with Ni and V show slightly higher mechanical properties than the reference alloy ($\approx$ 18%). However, the increase related to Ni addition appears not to be of statistical significance because of the larger scatter in tensile properties compared to the V-containing alloy, indicating that V may produce a further strengthening effect on the base alloy in T6 condition. In addition, minor differences in elongation (A%) are found between as-cast and T6 treated samples, the latter possessing slightly lower average values.

No statistically significant difference in mechanical properties is observed between the base and Ni- or V-containing alloys in both as-cast and T6 conditions with respect to permanent mould cast alloys (Table B.4 and Figure B.3). This indicates that Ni and V additions have no influence on the mechanical properties at higher solidification rates.

Alloy Code	**$Rp_{0.2}$ [MPa]**	**UTS [MPa]**	**A%**
A356 - AC	80.7 ± 10.4	128.4 ± 8.0	1.46 ± 0.53
A356 - T6	183.2 ± 14.0	212.0 ± 30.1	0.99 ± 0.67
Ni - AC	43.2 ± 6.0	93.8 ± 9.1	1.73 ± 0.28
Ni - T6	212.7 ± 31.3	244.6 ± 30.6	0.90 ± 0.36
V - AC	114.5 ± 4.7	160.5 ± 10.0	1.33 ± 0.45
V - T6	216.9 ± 7.9	250.4 ± 8.8	1.14 ± 0.59

Table B.3 – *Mechanical properties of the sand cast reference and Ni/V-contaminated alloys.*

Alloy Code	**$Rp_{0.2}$ [MPa]**	**UTS [MPa]**	**A%**
A356 PM - AC	93.4 ± 4.8	172.8 ± 7.0	4.00 ± 0.75
A356 PM - T6	224.3 ± 2.0	282.0 ± 6.9	3.22 ± 0.84
Ni PM - AC	93.4 ± 5.5	169.1 ± 9.9	3.44 ± 1.32
Ni PM - T6	228.7 ± 3.1	284.8 ± 7.4	3.25 ± 1.21
V PM - AC	91.6 ± 4.0	171.1 ± 10.4	3.54 ± 1.12
V PM - T6	224.2 ± 1.5	289.5 ± 8.6	3.60 ± 1.50

Table B.4 – *Mechanical properties of the permanent mould cast reference and Ni/V-contaminated alloys.*

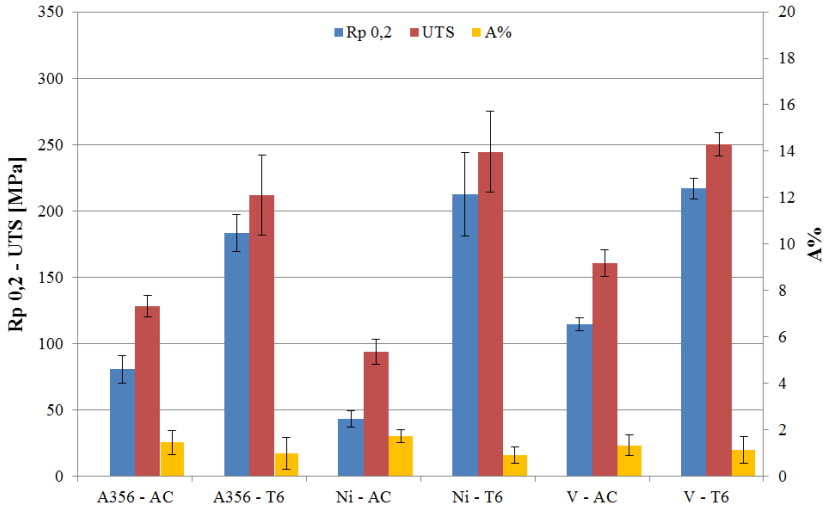

Figure B.2 – *Mechanical properties of the sand cast reference and Ni/V-contaminated alloys in as-cast and T6 conditions.*

B.3.2 Microstructural and Fractographic Observations

Representative microstructures of the sand cast reference alloy and alloys containing Ni and V in as-cast and T6 heat treated condition are shown in Figure B.4. The general features in the alloys are α-Al dendrites (dark grey) and needle-like Si particles (light grey). Similar microstructures were obtained for the permanent mould cast alloys. For the sake of simplicity, however, only the as-cast microstructures are shown in Figure B.5. The average size of eutectic Si particles is reduced in permanent mould cast alloys due to the increased cooling rate.

Depending on the alloy composition and the thermal history, various intermetallic phases such as π-$Al_8FeMg_3Si_6$, β-Al_5FeSi, Mg_2Si and Ni-bearing compounds can be detected in the interdendritic regions. The representative chemical composition of some of the investigated phases determined by EDS is given in Table B.5. In sand cast alloys in as-cast condition (- *AC*), the morphology of β-Al_5FeSi is acicular and occasionally polygonal, whereas π-$Al_8FeMg_3Si_6$ and Mg_2Si exhibit a "Chinese-script"morphology (Figure B.4a,e). Ni-based intermetallic phases are found as discrete polygonal particles or with "Chinese-script"morphology (Figure B.4c). According to the EDS measurements, these particles were identified as Al_3Ni (Figure B.6) and Al_9FeNi, which is in good agreement with the data determined by Ludwig *et al.* [18]. Microstructural observations also reveal an increased amount of π-$Al_8FeMg_3Si_6$ and Mg_2Si phases in the V-containing alloy, as can be noted from the comparison of Figure B.4a and Figure B.4e. Additionally, a minor V accumulation in β-Al_5FeSi intermetallics can sometimes be observed.

EPMA line scans (Figure B.7) along the longitudinal direction of secondary dendrite arms indicate that V remains in solid solution, which is to be expected since its maximum solubility in α-Al matrix is approximately 0.1 wt% [19]. Additionally, it appears that Mg and V follow two complementary trends within the α-Al matrix (Figure B.7c). The EPMA analysis

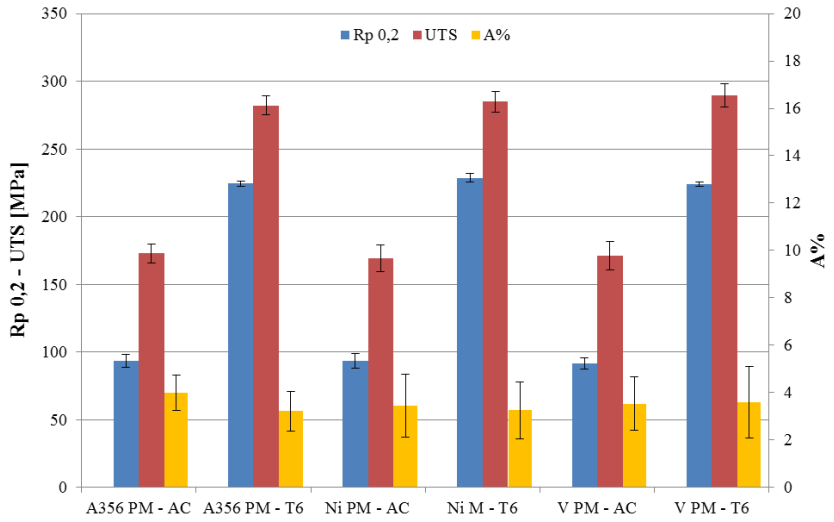

Figure B.3 – *Mechanical properties of the permanent mould cast reference and Ni/V-contaminated alloys in as-cast and T6 conditions.*

	Composition in (at%)					
Phase	**Al**	**Si**	**Fe**	**Ni**	**V**	**Mg**
Al_3Ni	67.1 - 83.1	1.0 - 2.4	0.3 - 2.7	12.9 - 28.1	-	-
Al_9FeNi	81.7 - 84.8	3.0 - 5.7	3.5 - 6.0	6.8 - 11.1	-	-
π-$Al_8FeMg_3Si_6$	63.4 - 75.8	12.6 - 17.0	2.1 - 4.6	0.4 - 1.6	-	9.3 - 14.9
β-Al_5FeSi	81.7 - 86.6	6.9 - 9.1	6.4 - 10.3	-	0.1 - 0.2	-
Mg_2Si	1.6 - 2.3	30.4 - 35.6	-	-	-	68.0 - 70.4

Table B.5 – *Composition ranges of some intermetallic phases measured by semi-quantitative EDS.*

also shows that Ni mainly segregates into the eutectic regions and to the Al grain boundaries (Figure B.7b). Similarly to eutectic Si particles, the average size of intermetallic phases is reduced in permanent mould cast alloys in as-cast condition (*PM - AC*) due to the increased cooling rate (Figure B.5).

The application of a solution heat treatment yields some changes in the intermetallic phases. Mg_2Si dissolves completely in the α-Al matrix in both sand cast and permanent mould cast alloys (- *T6*, *PM - T6*), whereas the π-$Al_8FeMg_3Si_6$ intermetallics undergo necking and are partially replaced by the β-Al_5FeSi phase through the progressive dissolution of Mg and Si into the α-Al matrix (Figures B.4b and B.4f) [22–24]. Conversely, the π-phase is replaced by the Al_9FeNi intermetallic compound in the alloys containing Ni (Figure B.4d and EDS element mapping in Figure B.8). Acicular β-Al_5FeSi intermetallic phases formed during solidification are generally not affected by solution heat treatment [22]. Similarly, Al_9FeNi intermetallics that precipitated during solidification remain unchanged after solution heat treatment, whereas Al_3Ni undergoes spheroidisation. The subsequent ageing process of the alloys at 160 °C results in the precipitation of the Mg_2Si second phase particles in the α-Al matrix without inducing any additional changes in the morphology of eutectic Si and intermetallic compounds.

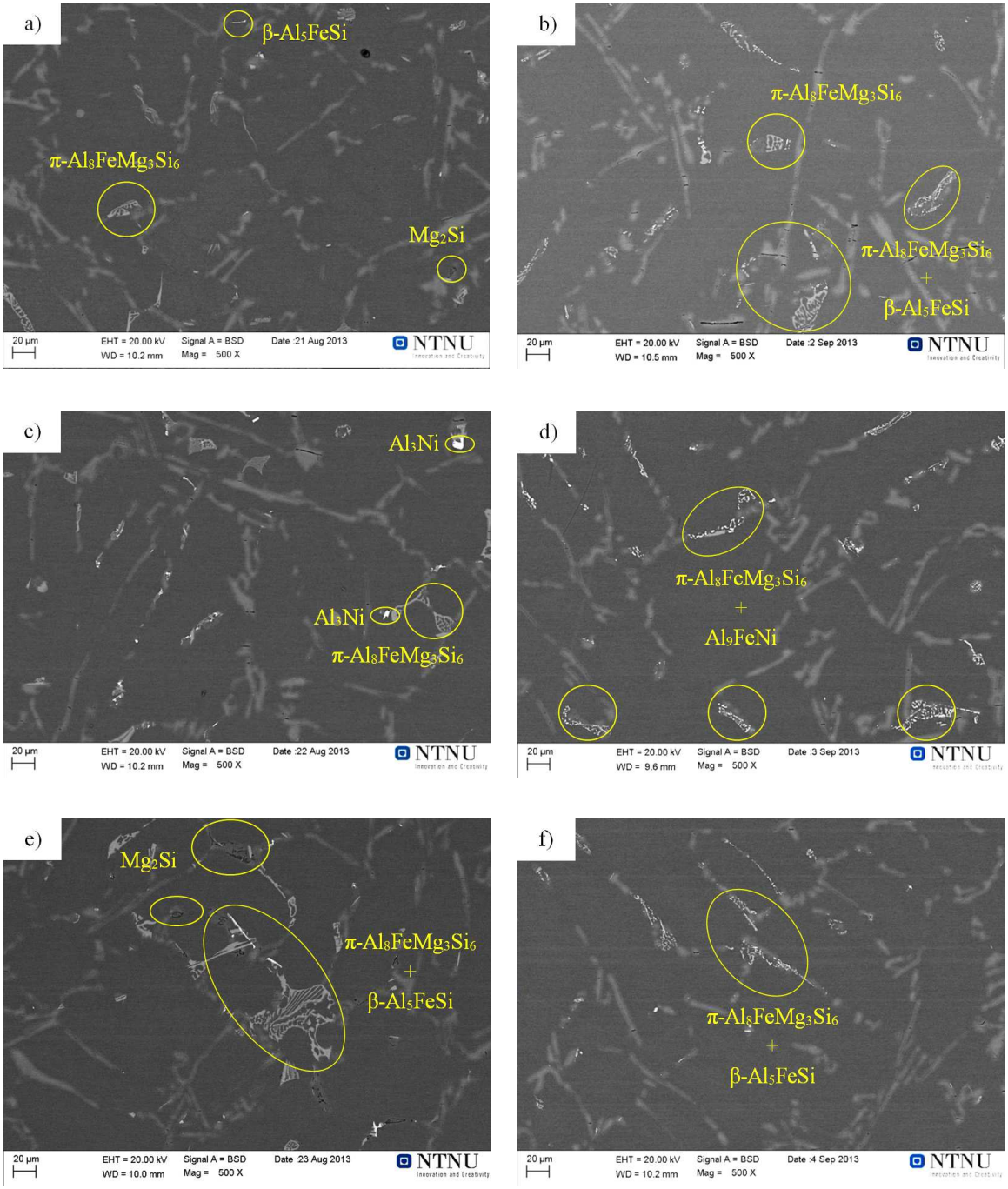

Figure B.4 – *BSE micrographs of sand cast reference alloy and alloys with Ni and V in as-cast and T6 conditions: a)* A356 - AC, *b)* A356 - T6, *c)* Ni - AC, *d)* Ni - T6, *e)* V - AC, *f)* V - T6. *Aluminium dendrites are in dark grey, whereas Si particles in the interdendritic regions appear in light grey.*

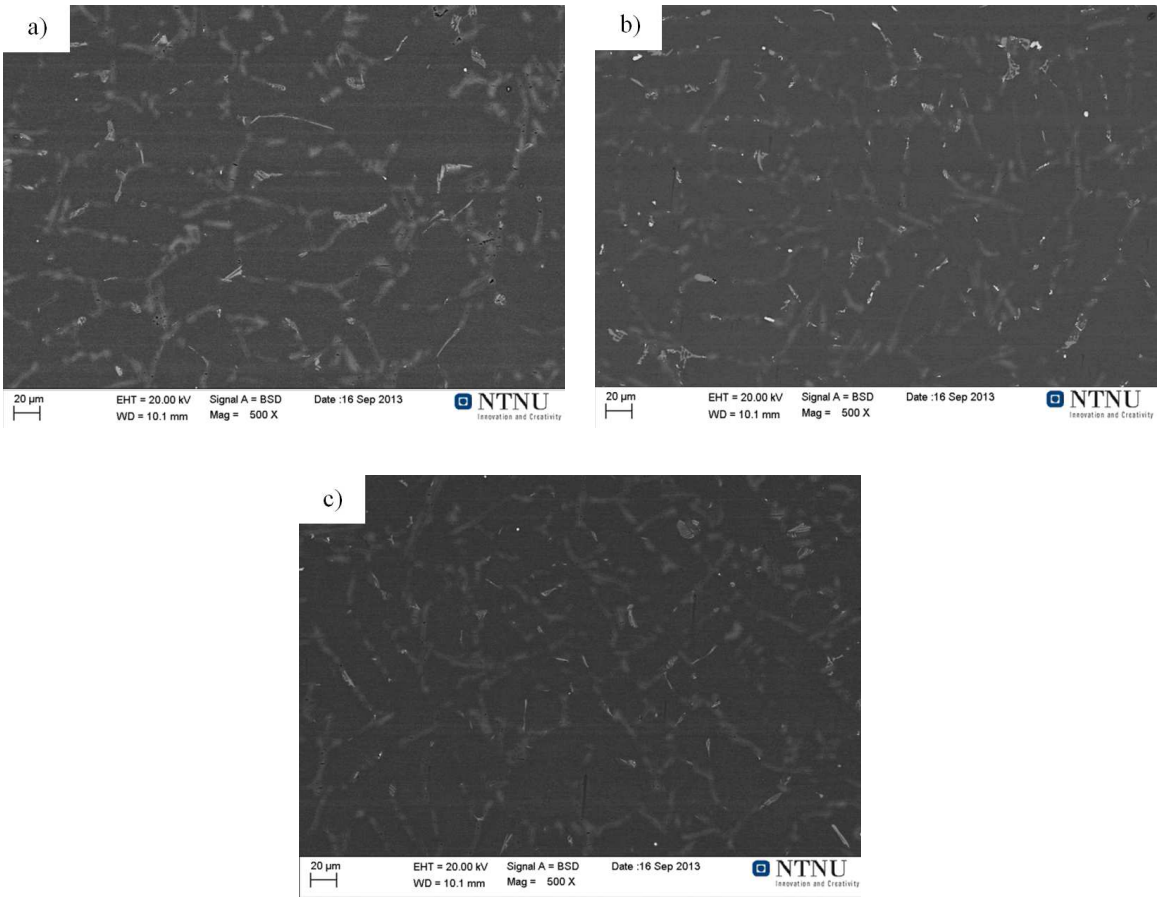

Figure B.5 – *BSE micrographs of permanent mould cast reference and Ni- or V-containing alloys in as-cast condition: a)* A356 PM - AC, *b)* Ni PM - AC, *c)* V PM - AC. *Aluminium dendrites (dark grey), Si particles (light opaque grey), π-$Al_8FeMg_3Si_6$ (light clear grey) and Ni-rich intermetallics (white spots) are observed.*

Figures B.9a, B.9c and B.9e show details of the fracture profiles of the sand cast reference alloy and alloys with added Ni and V in as-cast condition (- *AC*). As already observed by others [25, 26], fracture initiates because of both debonding and intercrystalline cracking of rod-like eutectic Si particles and brittle intermetallics. Once a critical number of fractured particles is reached, the principal crack is formed by the local linkage of adjacent microcracks, and subsequent propagation of these. As can be also observed, the crack follows a preferential path through the eutectic Si particles in the interdendritic regions, thus showing a transgranular fracture mode. Since the microstructural analyses indicate larger SDAS for the sand cast alloys ($60 \pm 7\ \mu m$, regardless of Ni or V contamination), this behaviour appears to be in good agreement with previous findings [25, 27, 28], which provides evidence that, in coarser structures, the fraction of eutectic Si particles located between the secondary dendrite arms constitute an easier path for crack propagation rather than those located at or in the vicinity of Al grain boundaries. Cracks in sand cast base and V-contaminated samples (*A356 - AC*, *V - AC*) mainly originate and propagate along eutectic Si particles, fol-

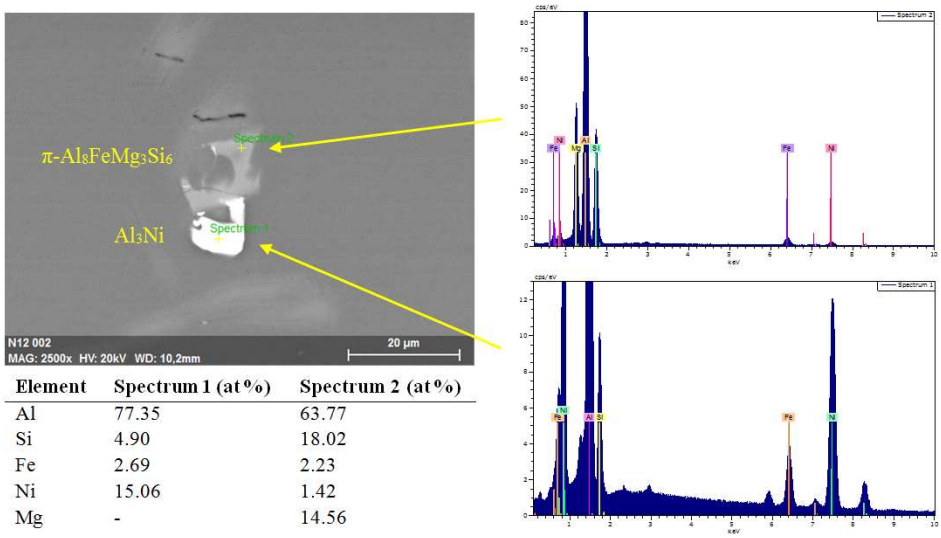

Element	Spectrum 1 (at %)	Spectrum 2 (at %)
Al	77.35	63.77
Si	4.90	18.02
Fe	2.69	2.23
Ni	15.06	1.42
Mg	-	14.56

Figure B.6 – *BSE image of some intermetallic phases detected in the interdendritic regions of sand cast alloy with 600 ppm Ni (as-cast condition). EDS measurements indicate the nature of the intermetallic compounds as Al_3Ni and π-$Al_8FeMg_3Si_6$.*

lowing a fragile quasi-cleavage fracture path with a minor amount of plastic deformation (i.e. few dimples). Conversely, many intermetallic particles can be observed on the fracture profile of sand cast Ni-containing alloy (*Ni - AC*). Analysis of these precipitates with semi-quantitative EDS and the comparison of the at% ratios with published data identify them as π-$Al_8FeMg_3Si_6$, Al_9FeNi and Al_3Ni. Since Al_3Ni phase precipitates later in the Al-Si eutectic reaction, as already indicated by other authors [18, 19, 29], this phase is frequently observed to be coupled to either eutectic Si or π-$Al_8FeMg_3Si_6$, appearing as coarse polygonal particles and in interconnected "Chinese-script"morphology. However, due to the low level of Ni into the alloy, it is unlikely that these Ni aluminides have the same high degree of interconnectivity as in the alloys where Ni is intentionally added to improve high temperature properties [10].

Typical fracture profiles of the sand cast reference alloy and alloys with Ni and V in T6 heat treated condition (- *T6*) exhibit features similar to those of the as-cast ones. The majority of eutectic Si particles still show an elongated acicular morphology even after the solution treatment step (Figures B.9b, B.9d and B.9f). Microcracks that originate from these micro-constituents will subsequently connect to produce the main crack. Therefore, in the absence of modifier elements e.g. Sr or Na, the selected solution heat treatment holding time appears to be insufficient to obtain complete necking and spheroidisation of the eutectic phase. Hence several areas with high stress concentration (acicular particles) are retained in the castings leading to premature failure.

SEM observations of the fracture surfaces of sand cast alloys confirm the Si-driven quasi-cleavage nature of fracture (Figure B.10): no significant differences in fracture paths are observed between the as-cast and T6 heat treated alloys. Additionally, a large number of Ni-rich intermetallics are observed on the fracture surfaces of the alloys with 600 ppm Ni

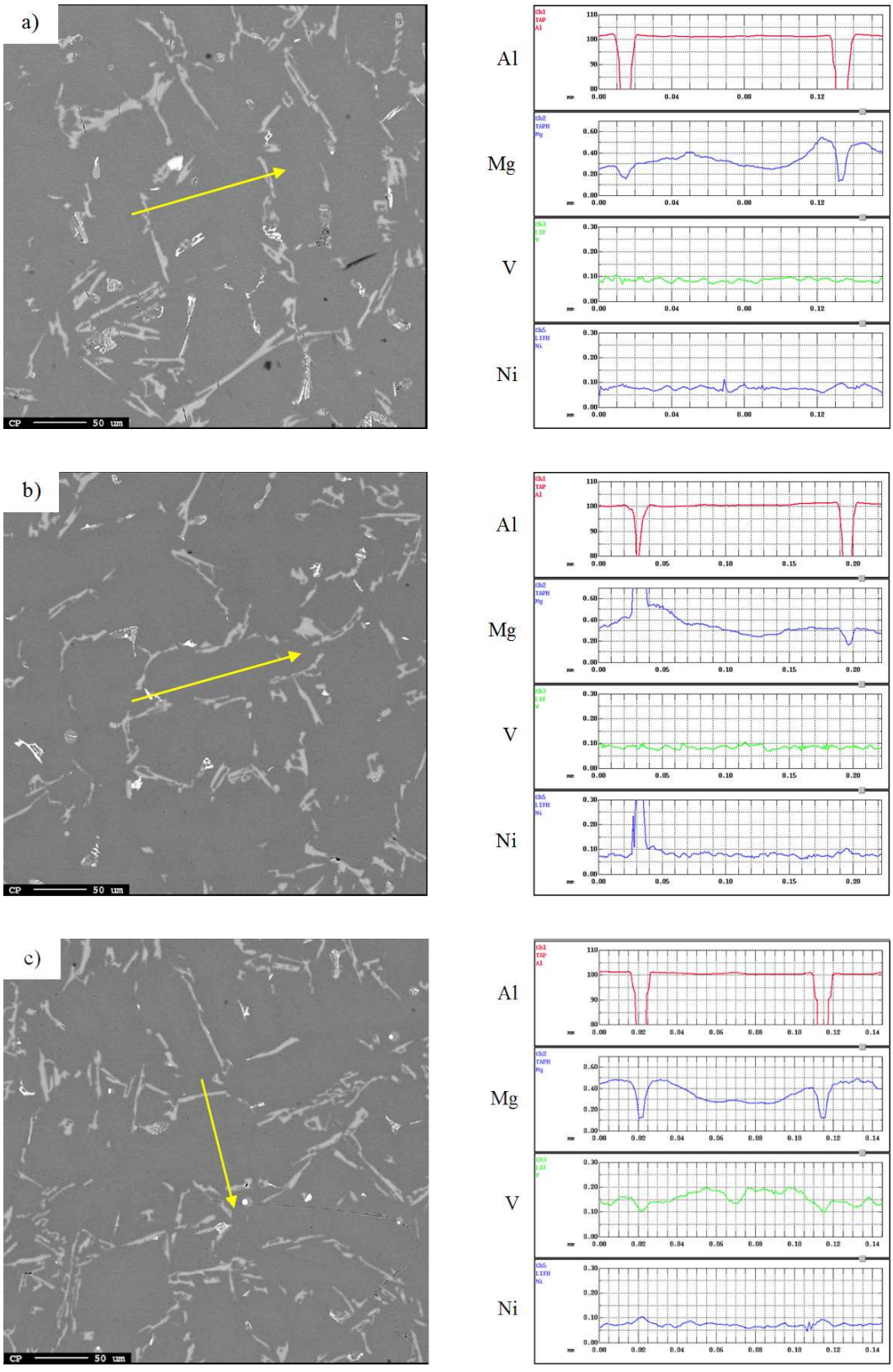

Figure B.7 – *Semi-quantitative EMPA profiles of the Al, Mg, V and Ni concentrations within α-Al dendrites and secondary phases for a)* A356 - AC, *b)* Ni - AC *and c)* V - AC *alloys. The scanning direction is indicated by arrows.*

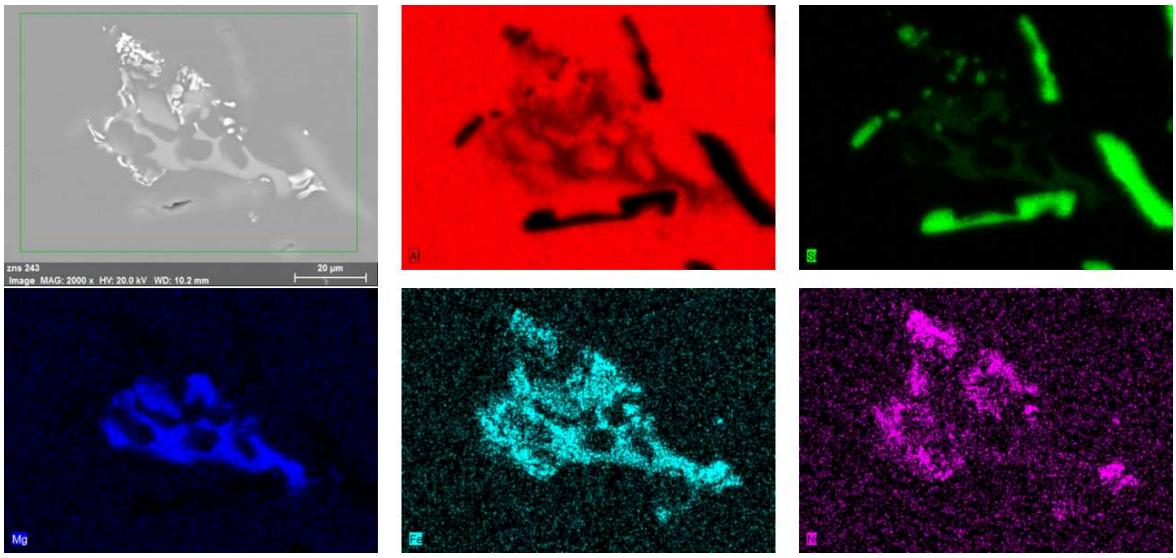

Figure B.8 – *EDS element mapping of some intermetallic phases (π-$Al_8FeMg_3Si_6$ in light grey, Al_9FeNi in white) detected in the interdendritic regions of sand cast alloy with 600 ppm Ni (T6 condition).*

(Figure B.11a and B.11b). These particles have a polygonal and flake-like morphology in the *Ni - AC* alloy (Al_9FeNi and Al_3Ni compounds, Figure B.11c), whereas in the *Ni - T6* alloy the intermetallic compounds are mostly identified as Al_9FeNi, which also originate from π-$Al_8FeMg_3Si_6$ phase due to Mg and Si diffusion to the α-Al matrix (Figure B.6). They subsequently spheroidise, which makes them less harmful in terms of fracture initiation and propagation (Figure B.11d).

With respect to permanent mould cast reference and Ni/V-contaminated alloys (*A356 PM - AC*, *A356 PM - T6*, *Ni PM - AC*, *Ni PM - T6*, *V PM - AC*, *V PM - T6*), the fracture profiles and surfaces possess a more irregular fracture path (Figure 12). This crack behaviour is related to the lower SDAS measured for these alloys ($34 \pm 4\ \mu m$) and, as a direct consequence, can be attributed to the reduction of the amount of particles (eutectic Si or intermetallics) located at the boundaries of secondary dendrite arms. In consequence, fracture is forced to partially propagate via the grain boundaries, which offer an alternative continuous path. This transition from transgranular to mixed transgranular-intergranular fracture mode is generally accompanied by an increase in the ductility of the alloys [25,27,30]. Additionally, finer micro-constituents require larger strains to crack. Therefore, the contribution of plastic deformation of the α-Al matrix to the final crack must increase, leading to a more ductile fracture behaviour, as shown by the large number of dimples in Figure B.12b compared to Figures B.10a and B.10b.

B.4 Discussion

Generally, strength of sand cast alloys in as-cast condition (- *AC*) is lower than in T6 heat treated alloys (or Sr or Na modified alloys) due to the coarse flake-like or acicular eutectic

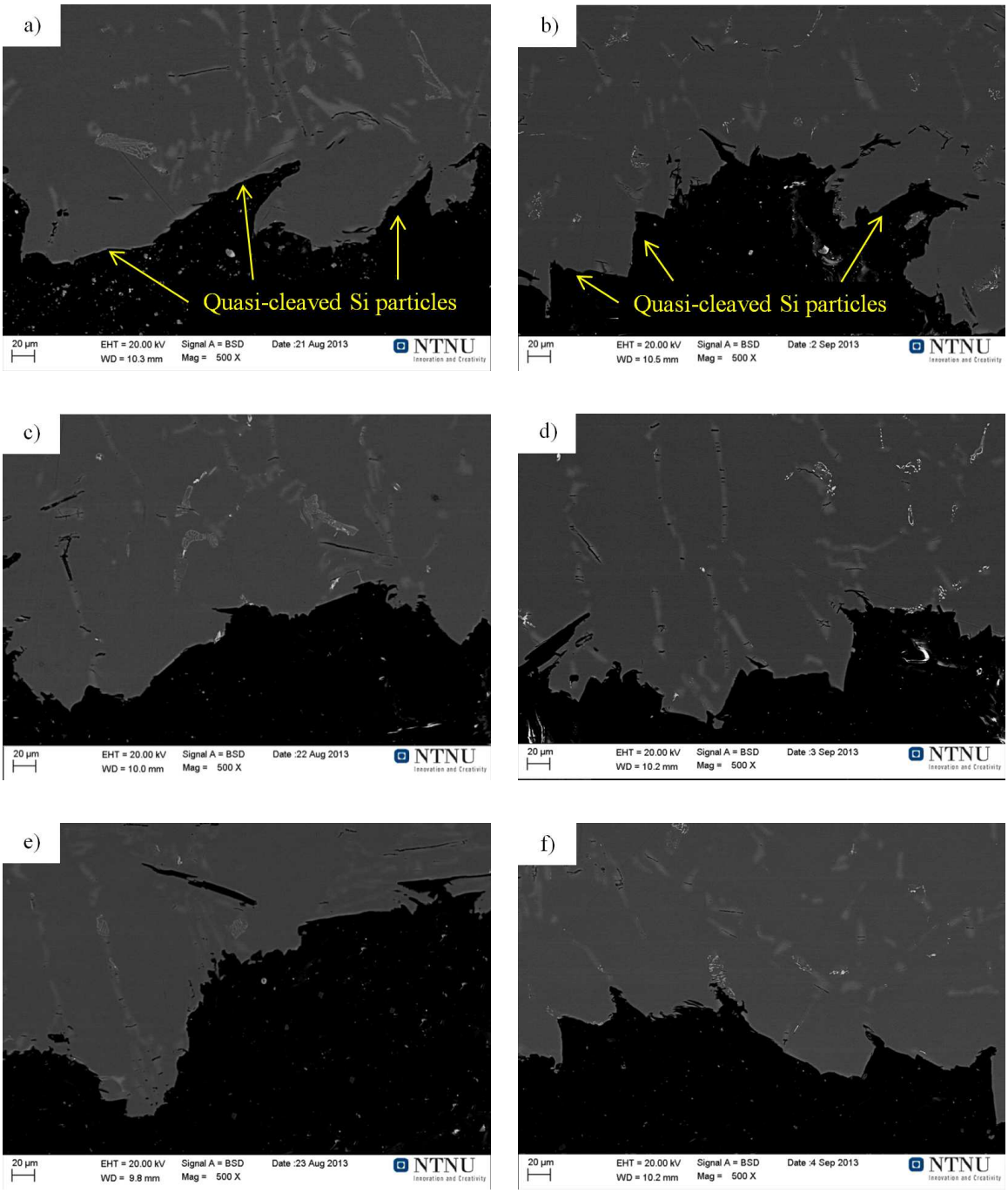

Figure B.9 – *Fracture profiles of the sand cast reference alloy and alloys with Ni and V in as-cast and T6 conditions: a)* A356 - AC, *b)* A356 - T6, *c)* Ni - AC, *d)* Ni - T6, *e)* V - AC, *f)* V - T6. *A Si-driven quasi-cleavage nature of fracture can easily be observed. No significant differences in crack paths are observed between as-cast and T6 heat treated alloys.*

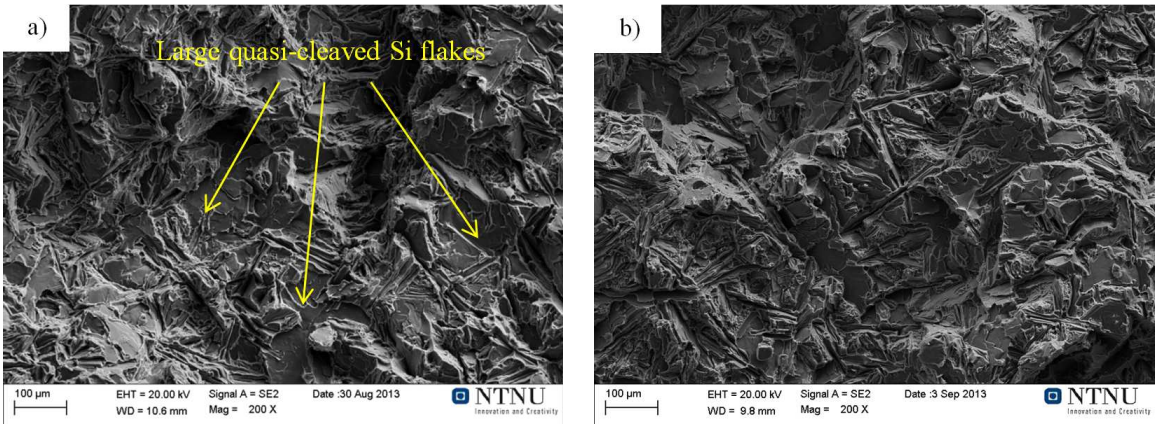

Figure B.10 – *SEM fractographs of the sand cast reference alloys in a) as-cast and b) T6 conditions. Note that the typical characteristics of fragile fracture still remain in T6 heat treated sample, thus indicating that the solution heat treatment holding time was insufficient to obtain a complete necking and spheroidisation of eutectic Si particles.*

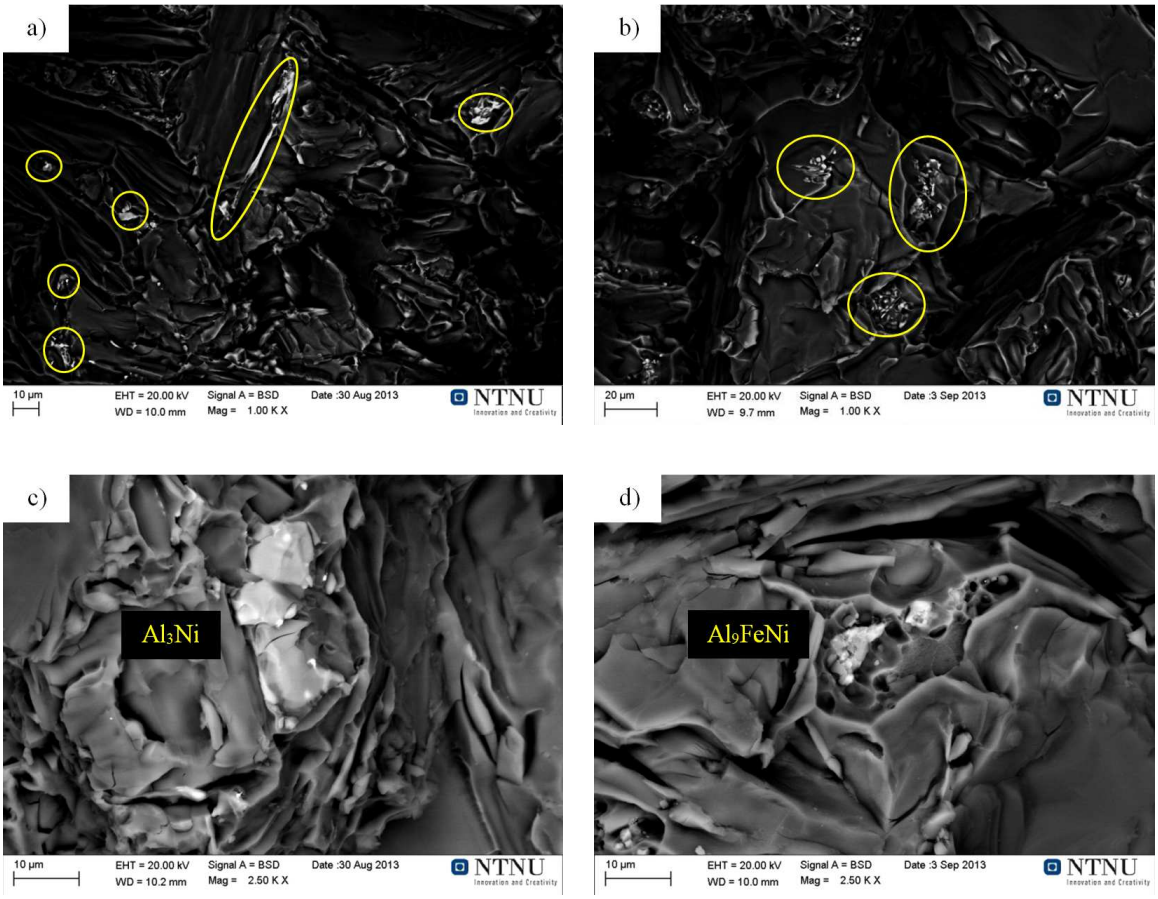

Figure B.11 – *Distribution (a,b) and morphology (c,d) of Ni-rich intermetallic compounds in sand cast alloys with 600 ppm Ni in as-cast (a,c) and T6 (b,d) conditions.*

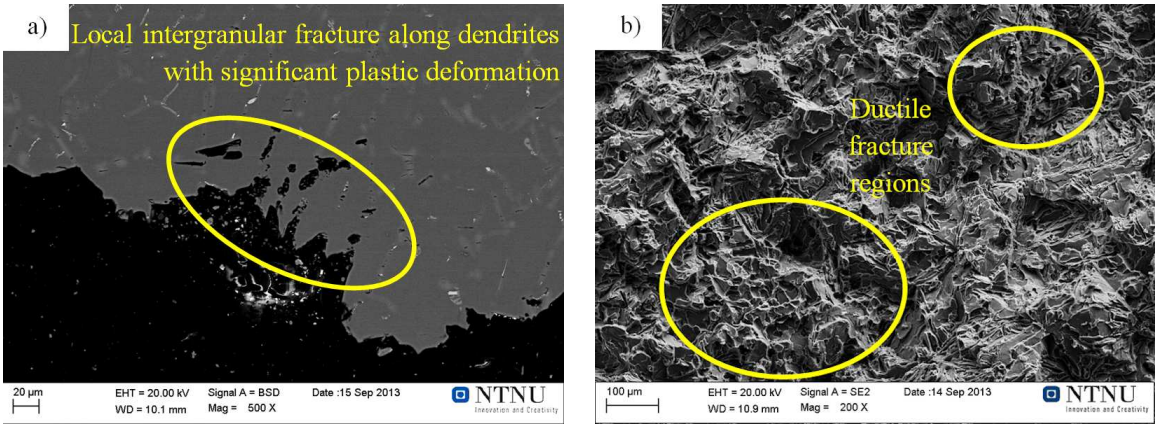

Figure B.12 – *SEM images of a) fracture profile and b) surface of the permanent mould cast reference alloy in as-cast condition (*A356 PM - AC*) showing mixed transgranular-intergranular fracture mode and typical features of ductile fracture (dimples).*

Si, which is the most prominent phase precipitating in hypoeutectic Al-Si alloys. However, the addition of Ni to these alloys in as-cast condition (*Ni - AC*) leads to a further drastic drop in yield strength and ultimate tensile strength, whereas the percentage elongation remains largely unaffected. Ni-rich intermetallic compounds were usually found along the fracture profiles and in the fracture surfaces of these samples. Therefore, it is suggested that they have an active role in fracture initiation and propagation.

This fracture behaviour can be explained using the approach proposed by Moffat [6], which takes the hardness and Young's Modulus parameters of the intermetallic compounds obtained by nanoindentation tests into account. It also considers the mechanism of load transfer. In the present work, existing data obtained by means of reliable techniques, such as nanoindentation tests, Vickers microhardness and compression tests were carefully revised and summarized in Table B.6. The alloys studied in this work consist of a soft, low E matrix and hard, high E intermetallics and eutectic Si particles. When these alloys are subject to external loads, an inhomogeneity in stress distribution results from the discrepancy in the elastic properties of the different phases. Similar to a composite material, the stiffer particles generally reinforce the matrix by bearing a larger proportion of the applied load. However, if the stress induced at the reinforcing particles or at the matrix-particle interface exceeds a critical value, then fracture of the particles or decohesion occurs [31, 32]. The pile-up of dislocations at the particles can also cause particle cracking because of the increased local stress even if the average applied stress that the tensile sample experiences is lower than the fracture strength of the particles.

It is well-established that hardness H can be related to UTS by simple empirical relationships:

$$H = f(UTS) \tag{B.1}$$

Phase	Hardness [GPa]	UTS [GPa]	f(ϵ_{fr})
Eutectic Si	11.13 [33]	147.6 [33]	0.0754
β-Al_5FeSi	11.5 [34]	196 [34]	0.0587
π-$Al_8FeMg_3Si_6$	5.85 [19]	-	-
Mg_2Si	4.1 [35]	76 [35]	0.0539
Al_9FeNi	7.71 [33]	161.5 [33]	0.0477
Al_3Ni	7.73 [36]	141 [36]	0.0548

Table B.6 – *Hardness, Young's modulus and relative fracture strain for eutectic Si and a number of intermetallic phases. The corresponding references are in square brackets.*

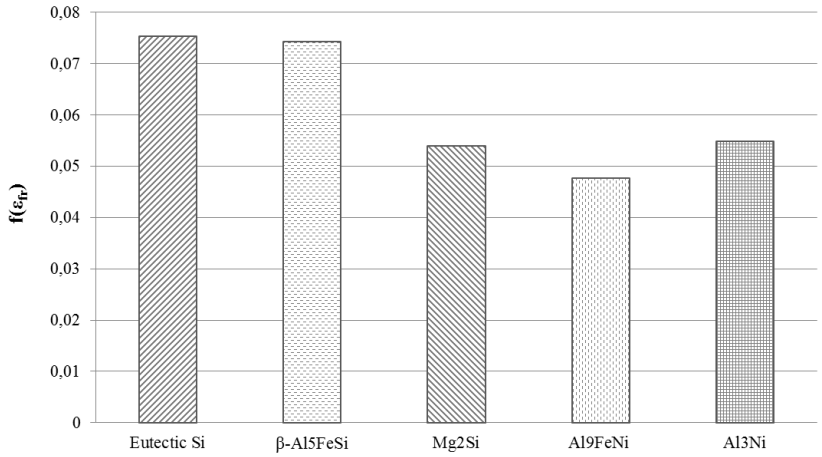

Figure B.13 – *Comparison of the relative fracture strain for eutectic Si and a number of intermetallic phases.*

Furthermore, assuming that eutectic Si and intermetallic particles have a linear elastic behaviour, the deformation to fracture ϵ_{fr} can be expressed as:

$$\epsilon_{fr} = \frac{f(UTS)}{E} \tag{B.2}$$

where *E* is the elastic modulus obtained by means of the above-mentioned techniques. Since absolute relationships are not required, relative differences in ϵ_{fr} between phases are sufficient to determine which phase is likely to fail preferentially. As a consequence equations (B.1) and (B.2) can be combined to yield:

$$f(\epsilon_{fr}) = \frac{H}{E} \tag{B.3}$$

Assuming homogeneity of the strain distribution for each phase, the values of *H* and *E* can be used in equation (B.3) to determine the relative fracture strain *f(ϵ_{fr})*, and results are shown in Figure B.13.

No Young's Modulus data for the π-$Al_8FeMg_3Si_6$ phase were found in literature, so *f(ϵ_{fr})* cannot be calculated. It can be seen that all intermetallic phases are likely to fracture at a lower strain than the eutectic Si particles. In particular, the Ni-rich phases and Mg_2Si have the lowest values of *f(ϵ_{fr})*. The brittle nature of Al_9FeNi intermetallics has already been

mentioned in the literature [6, 13, 33]. By taking the low $f(\epsilon_{fr})$ value found for the Al_3Ni phase and the microstructural observations of fracture profiles and surfaces into account, the following fracture mechanism for the sand cast alloy with 600 ppm Ni in as-cast condition (*Ni - AC*) is proposed. Once the tensile load is applied, the increase of local stresses around coarse polygonal Al_3Ni and Al_9FeNi compounds first leads to rupture of these intermetallics or to cracks forming at the matrix/particle interface. Moreover, since the Al_3Ni phase is often observed to be coupled to either eutectic Si or π-$Al_8FeMg_3Si_6$, further intercrystalline cracks can be created within these brittle phases or at the interface with α-Al matrix. This creates very large decohesion areas since the early stage of tensile deformation. In order to bear the applied load on a smaller cross section, the residual material is subject to severe plastic deformation. Consequently, the samples reach yield strength ($Rp_{0.2}$) at a lower stress compared to the base alloy (*A356 - AC*). For the same reason, the subsequent steep increase in local stress around eutectic Si particles and intermetallics in the remaining eutectic areas leads to fracture at lower UTS in samples with added Ni. However, this does not affect the elongation of the alloy (i.e. the tensile ductility), which is known to be dominated by the SDAS and the size of eutectic Si particles [25, 37]. Therefore the values for the Ni-containing alloys must be similar to the ones of the reference alloy. It can also be noted in Figure B.13, that Mg_2Si intermetallics show a tendency to fracture comparable to that of the Al_3Ni phase. However, since no cracked Mg_2Si particles were found on fracture profiles and surfaces of the investigated alloys, it is suggested that their "Chinese-script"morphology increase their resistance to crack to a some extent.

The higher mechanical properties of sand cast alloys with 1000 ppm V in as-cast condition (*V - AC*) can be explained by a strengthening effect caused by the solid solution of this element in the α-Al matrix (Figure B.7c). Dislocation movement and pile-up around eutectic Si and intermetallics is decelerated by their interactions with both Mg and V atoms in solution. Therefore, intermetallic phases crack at higher stresses and eventually both yield strength and UTS increase.

After T6 heat treatment (- *T6*), the precipitation of fine coherent Mg_2Si dispersoids in the α-Al matrix exerts a strong effect on the tensile properties of the sand cast reference and Ni- or V-containing alloys. The coherent Mg_2Si precipitates with their needle-like morphology prevent the motion of dislocations, which accumulate and contribute significantly to the increased strength of the α-Al matrix [38]. Despite this improvement, the α-Al matrix is prone to crack more easily due to the hardening particles, so that when the fracture of brittle particles begins, the following microcrack linking process is faster and leads to a slightly lower ductility compared to the corresponding as-cast alloys. It is also important to note that the detrimental effect of Ni-rich intermetallics becomes negligible compared to the increase in strength related to the precipitation of Mg_2Si dispersoids. A slight increase in yield strength and ultimate tensile strength, probably due to the spheroidisation of Ni-rich intermetallics during solution heat treatment, is also observed for the Ni-contaminated alloy (*Ni - T6*). However, Ni additions seem not to produce a statistically relevant increase in me-

chanical properties because of the large scatter in both tensile parameters. For the case of the V-containing alloy, the higher yield strength and ultimate tensile strength values compared to the reference alloy and the smaller scatter of experimental data are consistent with an actual increase caused by solid solution strengthening. This increase may also be partly related to the acceleration of precipitation kinetics of hardening coherent Mg_2Si particles. As observed by Camero *et al.* [39], the addition of 0.1 wt% V seems to promote the formation of the Mg_2Si hardening phase, thus shifting its maximum density into α-Al dendrites, i.e. maximum strengthening effect, to shorter ageing treatment times.
Data from tensile tests and microstructural analysis reveal significant differences between sand cast and permanent mould cast alloys in both mechanical properties and cracking behaviour. In accordance with previous findings [25–27], this is due to the higher cooling rates during die casting. As a direct consequence, this changes microstructural features leading to (i) decreased SDAS and (ii) decreased size and altered shape of eutectic Si particles and intermetallic compounds. This results in a shift from an entirely transgranular to a mixed transgranular-intergranular fracture mode. It is also evident from the similarity in yield strength, ultimate tensile strength and percentage elongation between permanent mould cast reference alloy and alloys with Ni and V in both as-cast and T6 conditions, that the cooling rate becomes the main parameter influencing the mechanical properties. The overall finer microstructure neutralises both the detrimental effects induced by Ni-containing intermetallics and the improvement related to V solid solution strengthening. Additionally, starting from smaller sizes, eutectic Si particles and intermetallic compounds are easier to fragment and spheroidise during solution heat treatment than the large particles in sand cast alloys [30, 40]. Therefore, after T6 heat treatment, the increase in mechanical properties of the reference alloy and the alloys with Ni and V is consistent with both the formation of fine coherent Mg_2Si particles strengthening the primary α-Al matrix and the reduced size and aspect ratio of eutectic Si particles and intermetallic phases.

B.5 Conclusions

The effect of Ni and V trace elements on the mechanical properties of A356 aluminium foundry alloy in as-cast and T6 heat treated conditions was investigated by analysing tensile specimens obtained from both sand and permanent mould castings. The following conclusions can be drawn from this work:

1. Ni strongly influences the tensile properties of the sand cast A356 alloy in as-cast condition, leading to a reduction of both the yield strength ($Rp_{0.2}$) and ultimate tensile strength (UTS) by 87% and 37%, respectively. Conversely, V addition increases $Rp_{0.2}$ and UTS by 42% and 25%. After T6 heat treatment, the sand cast A356 alloys with Ni and V show slightly higher mechanical properties than the reference alloy ($\approx$ 18%). However, the increase related to Ni is not statistically significant.

2. With respect to permanent mould cast alloys, no statistically significant difference in mechanical properties is observed between the reference and Ni- or V-containing alloys in both as-cast and T6 conditions, indicating that neither Ni nor V have any influence on the mechanical properties at higher solidification rates.

3. Fracture initiates because of debonding and intercrystalline cracking of rod-like eutectic Si particles and brittle intermetallics. While the sand cast alloys show a transgranular fracture due to their large SDAS and eutectic Si particles, a more ductile mixed transgranular-intergranular fracture was detected in the permanent mould cast alloy.

4. A large number of Ni-rich intermetallics are observed on the fracture surfaces of the Ni-containing sand cast alloys (*Ni - AC*). These particles, identified as Al_9FeNi and Al_3Ni, have a polygonal and flake-like morphology. The approach based on the relative fracture strain $f(\epsilon_{fr})$ of eutectic Si particles and intermetallic phases demonstrates that Ni-rich intermetallics are prone to fracture more easily than the other secondary phases. Moreover, since the Al_3Ni phase is often observed to be coupled to either eutectic Si or π-$Al_8FeMg_3Si_6$, further intercrystalline cracks can be created in these brittle phases or at the interface with α-Al matrix, thus creating very large decohesion areas since the early stage of tensile deformation. This leads to lower yield strength ($Rp_{0.2}$) and ultimate tensile strength (UTS).

5. The higher mechanical strength of sand cast V-containing alloys in as-cast condition (*V - AC*) is due to the solid solution strengthening effect produced by this element in the α-Al matrix. As a consequence, intermetallic phases crack at higher stresses and eventually both yield strength and UTS increase.

6. After T6 heat treatment (- *T6*), the precipitation of fine coherent Mg_2Si dispersoids in the α-Al matrix exerts a strong effect on the tensile properties of sand cast alloys. The detrimental effect of Ni-rich intermetallics becomes negligible, whereas the V-containing alloy shows even higher yield strength and ultimate tensile strength values compared to the reference alloy. Solid solution strengthening and acceleration of precipitation kinetics of Mg_2Si particles are credited for these increased tensile properties.

7. The cooling rate becomes the main parameter influencing the mechanical properties in permanent mould cast alloys. The finer microstructure neutralise both the detrimental effects of Ni-containing intermetallic phases and the improvement related to V solid solution strengthening.

Therefore, the experimental findings suggest that the application of a T6 heat treatment is sufficient to counteract the detrimental effects induced by the precipitation of additional intermetallic phases in the presence of Ni as a trace element in the A356 alloy. This is particularly recommended for low cooling rate casting methods, such as sand casting, whereas in high cooling rate techniques (i.e. permanent mould casting), its presence can be tolerated.

Conversely, V addition appears to always be beneficial for the tensile properties of the A356 alloy. In conclusion, provided that aluminium castings in A356 alloy (EN-AB 42100) are subject to T6 heat treatment, the maximum tolerable concentration for Ni and V as listed in current alloy specification charts e.g. EN 1676-2010 may be increased without impairing the alloys mechanical properties.

Acknowledgements

This research project was supported by the "Bando Giovani Ricercatori - Fondi 5x1000 anno 2010 e Fondi Unicredit 2013"of the University of Ferrara. In addition, the authors gratefully acknowledge Hydro Aluminium AS (Norway) for financial support. Thanks are also due to Hermann Hovland from Sør-Norge Aluminium AS (Norway) for the generous supply of master alloys and to Arne Nordmark and Kurt Sandaunet for the help during the manufacture of castings.

References

[1] R. X. Li, R. D. Li, Y. H. Zhao, L. Z. He, C. X. Li, H. R. Guan, and Z. Q. Hu, "Age-hardening behavior of cast Al-Si base alloy," *Mater. Lett.*, vol. 58, pp. 2096–2101, 2004.

[2] G. Jha, S. Ningileri, X. Li, and R. Bowers, "The Challenge of Effectively Utilizing Trace Elements/Impurities in a Varying Raw Materials Market," in *LIGHT METALS 2013*, B. Sadler, Ed. TMS, 2013, pp. 929–934.

[3] J. Grandfield, L. Sweet, C. Davidson, J. Mitchell, A. Beer, S. Zhu, X. Chen, and M. Easton, "An initial assessment of the effects of increased Ni and V content in A356 and AA6063 alloys," in *LIGHT METALS 2013*, B. Sadler, Ed. TMS, 2013, pp. 39–44.

[4] L. F. Mondolfo, *Aluminum Alloys: structure and properties*. Butterworths, London (1976).

[5] T. O. Mbuya, B. O. Odera, and S. P. Ng'ang'a, "Influence of iron on castability and properties of aluminium silicon alloys: literature review," *Int. J. Cast. Metal. Res.*, vol. 16, pp. 451–465, 2003.

[6] A. J. Moffat, "Micromechanistic analysis of fatigue in aluminium silicon casting alloys," Ph.D. dissertation, School of Engineering Sciences - University of Southampton, 2007.

[7] E. Sjölander and S. Seifeddine, "Artificial ageing of Al-Si-Cu-Mg casting alloys," *Mater. Sci. Eng. A*, vol. 528, pp. 7402–7409, 2011.

[8] M. Zeren, "Effect of copper and silicon content on mechanical properties in Al-Cu-Si-Mg alloys," *J. Mater. Process. Tech.*, vol. 169, pp. 292–298, 2005.

[9] L. Heusler, F. J. Feikus, and M. O. Otte, "Alloy and Casting Process Optimization for Engine Block Application," *AFS Trans.*, vol. 109, pp. 215–223, 2001.

[10] Z. Asghar, G. Requena, and F. Kubel, "The role of Ni and Fe aluminides on the elevated temperature strength of an AlSi12 alloy," *Mater. Sci. Eng. A*, vol. 527, pp. 5691–5698, 2010.

[11] Y. Li, Y. Yang, Y. Wu, L. Wang, and X. Liu, "Quantitative comparison of three Ni-containing phases to the elevated-temperature properties of Al-Si piston alloys," *Mater. Sci. Eng. A*, vol. 527, pp. 7132–7137, 2010.

[12] A. R. Farkoosh, M. Javidani, M. H. D. Larouche, and M. Pekguleryuz, "Phase formation in as-solidified and heat-treated Al-Si-Cu-Mg-Ni alloys: Thermodynamic assessment and experimental investigation for alloy design," *J. Alloy Compd.*, vol. 551, pp. 596–606, 2013.

[13] A. R. Farkoosh and M. Pekguleryuz, "The effects of manganese on the T-phase and creep resistance in Al-Si-Cu-Mg-Ni alloys," *Mater. Sci. Eng. A*, vol. 582, pp. 248–256, 2013.

[14] F. Wang, Z. Liu, D. Qiu, J. A. Taylor, M. A. Easton, and M. Zhang, "Revisiting the role of peritectics in grain refinement of Al alloys," *Acta Mater.*, vol. 61, pp. 360–370, 2013.

[15] W. Kasprzak, D. Emadi, M. Sahoo, and M. Aniolek, "Development of Aluminium Alloys for High Temperature Applications in Diesel Engines," *Mater. Sci. Forum*, vol. 618–619, pp. 595–600, 2009.

[16] T. H. Ludwig, P. L. Schaffer, and L. Arnberg, "Influence of Vanadium on the Microstructure of A356 Foundry Alloy," in *LIGHT METALS 2013*, B. Sadler, Ed. TMS, 2013, pp. 1023–1028.

[17] S. Zhu, J. Yao, L. Sweet, M. Easton, J. Taylor, P. Robinson, and N. Parson, "Influences of Nickel and Vanadium Impurities on Microstructure of Aluminum Alloys," *JOM - J. Min. Met. Mat. S.*, vol. 65, pp. 584–592, 2013.

[18] T. H. Ludwig, P. L. Schaffer, and L. Arnberg, "Influence of Some Trace Elements on Solidification Path and Microstructure of Al-Si Foundry Alloys," *Metall. Mater. Trans. A*, vol. 44, pp. 3783–3796, 2013.

[19] N. A. Belov, D. G. Eskin, and A. A. Aksenov, *Multicomponent phase diagrams: applications for commercial aluminum alloys*. Elsevier Science (2005).

[20] B. Huber, H. S. Effenberger, and K. W. Richter, "Phase equilibria in the Al-Si-V system," *Intermetallics*, vol. 18, pp. 606–615, 2010.

[21] D. Dispinar and J. Campbell, "Porosity, hydrogen and bifilm content in Al alloy castings," *Mater. Sci. Eng. A*, vol. 528, pp. 3860–3865, 2011.

[22] J. A. Taylor, D. H. StJohn, L. H. Zheng, G. A. Edwards, J. Barresi, and M. J. Couper, "Solution Treatment Effects in Al-Si-Mg Casting Alloys: Part I. Intermetallic Phases," *Alum. Trans.*, vol. 4–5, pp. 95–110, 2001.

[23] J. A. Taylor, D. H. StJohn, J. Barresi, and M. J. Couper, "Influence of Mg Content on th Microstructure and Solid Solution Chemistry of Al-7%Si-Mg Casting Alloys During Solution Treatment," *Mater. Sci. Forum*, vol. 331–337, pp. 277–282, 2000.

[24] E. Sjölander and S. Seifeddine, "The heat treatment of Al-Si-Cu-Mg casting alloys," *J. Mater. Process. Tech.*, vol. 210, pp. 1249–1259, 2010.

[25] Q. G. Wang, "Microstructural Effects on the Tensile and Fracture Behavior of Aluminum Casting Alloys A356/357," *Metall. Mater. Trans. A*, vol. 34, pp. 2887–2899, 2003.

[26] M. Zhu, Z. Jian, G. Yang, and Y. Zhou, "Effects of T6 heat treatment on the microstructure, tensile properties, and fracture behavior of the modified A356 alloys," *Mater. Design*, vol. 36, pp. 243–249, 2012.

[27] C. H. Cáceres, C. J. Davidson, and J. R. Griffiths, "The deformation and fracture behaviour of an Al-Si-Mg casting alloy," *Mater. Sci. Eng. A*, vol. 197, pp. 171–179, 1995.

[28] D. Casari and A. Fortini and M. Merlin, "Fracture behaviour of grain refined A356 cast aluminium alloy: tensile and Charpy impact specimens." Proceedings of the Convegno Nazionale IGF XXII, Rome, 2013.

[29] V. S. Zolotorevsky, N. A. Belov, and M. V. Glazoff, *Casting Aluminum Alloys*. Elsevier (2007).

[30] Q. G. Wang and C. H. Cáceres, "The fracture mode in Al-Si-Mg casting alloys," *Mater. Sci. Eng. A*, vol. 241, pp. 72–82, 1998.

[31] I. Sinclair and P. J. Gregson, "Structural performance of discontinuous metal matrix composites," *Mater. Sci. Technol.*, vol. 13, pp. 709–726, 1997.

[32] M. Huang and Z. Li, "Influences of particle size and interface energy on the stress concentration induced by the oblate spheroidal particle and the void nucleation mechanism," *Int. J. Solids Struct.*, vol. 43, pp. 4097–4115, 2006.

[33] C. L. Chen, A. Richter, and R. C. Thomson, "Mechanical properties of intermetallic phases in multi-component Al-Si alloys using nanoindentation," *Intermetallics*, vol. 17, pp. 634–641, 2009.

[34] S. Seifeddine, S. Johansson, and I. L. Svensson, "The influence of cooling rate and manganese content on the β-Al_5FeSi phase formation and mechanical properties of Al-Si-based alloys," *Mater. Sci. Eng. A*, vol. 490, pp. 385–390, 2008.

[35] V. Milekhine, M. I. Onsøien, J. K. Solberg, and T. Skaland, "Mechanical properties of FeSi (ϵ), $FeSi_2$(ζ_α) and Mg_2Si," *Intermetallics*, vol. 10, pp. 743–750, 2002.

[36] J. M. Song, T. Y. Lin, and H. Y. Chuang, "Microstructural Characteristics and Vibration Fracture Properties of Al-Mg-Si Alloys with Excess Cu and Ni," *Mater. Trans.*, vol. 48, pp. 854–859, 2007.

[37] Q. G. Wang, "Plastic Deformation Behavior of Aluminum Casting Alloys A356/357," *Metall. Mater. Trans. A*, vol. 35, pp. 2707–2718, 2004.

[38] G. E. Dieter, *Mechanical Metallurgy*. Wiley-WHC Verlag (1988).

[39] S. Camero, E. S. Puchi, and G. Gonzales, "Effect of 0.1% vanadium addition on precipitation behavior and mechanical properties of Al-6063 commercial alloy," *J. Mater. Sci.*, vol. 41, pp. 7361–7373, 2006.

[40] E. Ogris, A. Wahlen, H. Luchinger, and P. J. Uggowitzer, "On the silicon spheroidization in Al-Si alloys," *J. Light. Met.*, vol. 2, pp. 263–269, 2002.

Article C

Impact behaviour of A356 foundry alloys in the presence of trace elements Ni and V

Authors: D. Casari[1], T.H. Ludwig[2], L. Arnberg[3], M. Merlin[1] and G.L. Garagnani[1]
Submitted to: Journal of Materials Engineering and Performance

Abstract

In the present work, the impact behaviour of unmodified A356 alloys with the addition of Ni or V in as-cast and T6 heat treated conditions was assessed by investigating notched specimens obtained from sand and permanent mould casting. Low total absorbed energy average values ($Wt < 2$ J) were measured for the investigated range of alloys. SEM investigations of fracture profiles and surfaces indicated a Si-driven crack propagation with a predominant transgranular fracture mode. Occasionally, intergranular contributions to fracture were detected in the permanent mould cast alloys, most likely because of the locally finer microstructure. Complex and interconnected mechanisms related to the chemical composition (V solid solution strengthening within α-Al matrix), solidification conditions (SDAS and eutectic Si particle size) and heat treatment (precipitation of coherent Mg_2Si particles) were found to interact during the fracture process, thus governing the impact properties of sand cast and permanent mould cast alloys in both as-cast and T6 heat treated conditions. According to the experimental results and microstructural analyses, the trace element Ni exerted only minor effects on the impact toughness of the A356 alloy. On the other hand, V had a strong influence on the impact properties: (i) V-containing sand cast alloys generally absorbed slightly higher impact energies compared to the corresponding A356 base alloys;

[1]Engineering Department - ENDIF, University of Ferrara, Via Saragat 1, I-44122 Ferrara, Italy
[2]Hydro Aluminium AS, Verksvegen 1, N-6882 Øvre Årdal, Norway
[3]Department of Materials Science and Engineering, NTNU, Alfred Getz vei 2, N-7491 Trondheim, Norway

(ii) in the permanent mould cast alloys, V in solid solution led to a considerable loss of ductility and, as a result, to a significant reduction in the propagation energy, which in turn decreased the total absorbed energy.

C.1 Introduction

The hypoeutectic A356 aluminium foundry alloy (Al-7%Si-0.3%Mg) bases on the quaternary Al-Si-Fe-Mg system and is commonly used in a wide range of automotive, aerospace and other structural applications due to its good castability, high strength to weight ratio, corrosion and wear resistance and ease of recycling. The mechanical performance of A356 castings depends on their microstructure, which in turn is governed by several parameters such as the alloy chemistry, melt treatment processes (e.g. Sr or Na modification of the Al-Si eutectic and/or grain refinement), cooling rate and heat treatment. The application of a T6 heat treatment is usually performed in the manufacturing process and is a well-established method to increase the strength and ductility of the A356 alloy. In order to obtain an increase in strength, all steps of a T6 heat treatment are required to occur, i.e. solution treatment, quenching and artificial ageing. The main contribution is obtained from the precipitation of a large amount of fine Mg_2Si particles, which harden the soft α-Al matrix after ageing. On the other hand, a benefit in ductility is generally achieved after the solution treatment stage and is related to necking, fragmentation and subsequent spheroidisation of eutectic Si crystals [1–6]. Eventually, a further optimisation of A356 tensile properties by solution treatment involves a change of the volume fraction of Fe-bearing intermetallic phases, which leads to a replacement of the π-$Al_8FeMg_3Si_6$ with a "Chinese-script"morphology by fine clusters of β-Al_5FeSi needles [7].

Today, the Charpy impact test has become a standard method to evaluate the effect of different process parameters on dynamic fracture toughness of engineering materials. The latter is particularly critical as the demand for high ductility alloys that have to meet specific service conditions, e.g. automotive structural parts, has risen in the last decade. Murali *et al.* [8] investigated the influence of Mg and Fe on the impact toughness of the AlSi7Mg0.3 alloy. They demonstrated that either the increase of Mg content from 0.32 to 0.65 wt% or the increase of Fe concentration from 0.2 to 0.8 wt% at 0.32 wt% Mg leads to a decrease of the total absorbed energy. Ma *et al.* [9] also studied the effect of varying Fe concentrations from 0.1 to 0.8 wt% in an A356.2 alloy, showing that a significant reduction in impact toughness occurs when Fe levels are above 0.2 wt% or, in terms of β-intermetallics' size, when the length of β-needles lies within the range of 10 - 50 μm. Shivkumar *et al.* [10] showed that Sr modification and an increase of the cooling rate improve the impact properties of an A356-T6 alloy. Typical impact energies for unmodified and Sr-modified sand cast impact specimens were reported on the order of 1.5 and 3.0 J. In contrast, permanent mould castings exhibited higher total absorbed energies, on the order of 7 and 13 J in unmodified and Sr-modified alloys, respectively. Merlin *et al.* [11] applied instrumented Charpy impact test to measure

the total absorbed energy of subsize specimens. They stated that casting defects close to the V-notch have a strong detrimental effect on impact toughness. Hence the appearance of casting defects became the predominant parameter masking the influence of the actual microstructural features. Finally, in the authors previous work [12] it was found that the impact properties of a Sr-modified A356 alloy are not directly affected by Ti-B based grain refiners. However, all the grain refiners were reported to produce secondary changes in the microstructural features, increasing both SDAS and β-intermetallics' size. As a direct consequence, a reduction in the total absorbed energies of the grain refined alloys was observed.

Some authors [6, 10] have noticed that there exists a region where the impact energy of a T6 heat treated A356 alloy decreases to a minimum before it increases again. It has been suggested that this behaviour is caused by a compromise between the negative contribution to ductility due to the precipitation of Mg_2Si particles in the α-Al matrix, and the positive contribution associated with the fragmentation and spheroidisation of eutectic Si particles. Solution and homogenisation kinetics that lead to the precipitation of fine Mg_2Si particles during ageing, and consequently to the increase in strength, are faster compared to Si spheroidisation, which usually occurs after prolonged solution heat treatments. Zhang *et al.* [6] have reported that short solution treatment times in the range of 1.5 - 10 min produce a significant reduction in the impact energy of a low pressure die cast A356 alloy (approximately 3 J and 4 J after 5 min and 20 min, respectively). Even though the alloy is modified with Sr, eutectic Si particles have only begun to spheroidise during these short times, so that the positive contribution to ductility is poor and is completely counteracted by the precipitation of the Mg_2Si strengthening phase. The results of Shivkumar *et al.* [10] have shown that the previously described scenario is not observed when longer solution times are applied, e.g. an impact energy of 2.0 J has been measured for an unmodified permanent mould cast A356 alloy in the as-cast condition, whereas an impact energy of 5.6 J has been reported for the same alloy subjected to 2 h solution treatment, natural ageing for 24 h and artificial ageing at 171 °C for 4 h. Conversely, low impact energy values are maintained over longer solution times in sand cast alloys (i.e. low cooling rates, and hence coarse microstructures), with noticeable differences between Sr-modified and unmodified alloys: the latter usually require further time for the fragmentation and subsequent spheroidisation of eutectic Si particles, so that the corresponding increase in impact energy is postponed.

Finally, Elsebaie *et al.* [13] have recently investigated the effect of artificial ageing on the impact properties of unmodified and Sr-modified 356 alloys subjected to the same solution heat treatment at 540 °C for 8 h. It has been observed that the ageing at 180 °C for ageing time varying from 2 h to 8 h exerts a negative effect on the impact behaviour of the alloys due to the progressive precipitation of coherent and semi-coherent Mg_2Si particles. Increasing the ageing time to 12 h, however, results in a slight recovery in the impact energies of these alloys. This effect has been attributed to the coarsening and coherency loosening of stable Mg_2Si precipitates, which lead to easy motion of dislocation into α-Al matrix. As a direct consequence, the ductility of the alloy is increased.

Even if many different aspects of A356 impact behaviour have been investigated so far, no data are available in the literature concerning the impact properties of A356 alloy in the presence of Ni and V trace elements. Increasing concentrations of Ni and V impurity elements coming from the manufacturing process of primary aluminium, particularly from the petroleum coke used for the production of anodes for the aluminium electrolysis, have recently arisen as a major issue for the final quality of foundry alloy products [14, 15]. Since currently there are no cost efficient techniques for removal, these elements may constitute a problem for the static and dynamic properties of this widely used alloy.
The aim of the present work is to study the influence of Ni and V trace additions on the impact properties of as-cast and T6 heat treated A356 aluminium foundry alloys in two commercially important casting processes, i.e. sand and permanent mould casting. Instrumented Charpy impact tests have been performed and the acquired data have been analysed in terms of maximum load and total absorbed energy. The latter parameter has then been divided into its two main contributions, namely the crack initiation energy, also indicated as energy at maximum load, and the propagation energy, in order to better correlate the experimental findings to the microstructural features of the alloys and to separate the net effects of trace element additions and T6 heat treatment. Moreover, a fractographic analysis has been carried out to investigate the fracture mechanisms and the microstructural features involved in the fracture process.

C.2 Materials and Methods

A commercial A356 aluminium alloy was used as the base alloy. The as-received alloy ingots were melted in charges of 16 kg each in a boron-nitride coated clay-graphite crucible. Trace elements were added in the form of Al-10 wt% Ni and Al-10 wt% V master alloys according to the targeted nominal concentrations of 600 and 1000 ppm of Ni and V, respectively. In order to avoid any further interactions, neither Sr nor Na were added as modifier agents. The melting temperature was monitored with the Alspek-H probe and kept constant at 740 °C $\pm$ 5 °C. Samples from the three different melts were taken throughout the casting trials and were analysed by optical emission spectroscopy (OES). The chemical composition of the investigated alloys is given in Table C.1.

Alloy	Addition (ppm)	Si	Fe	Mg	Ni	V	Al
A356	-	7.054	0.092	0.355	0.003	0.007	bal.
A356 + Ni	600	6.902	0.087	0.344	0.061	0.007	bal.
A356 + V	1000	6.992	0.094	0.349	0.003	0.108	bal.

Table C.1 – *Chemical composition (wt%) of the A356 reference alloy and Ni/V-containing alloys as measured by OES.*

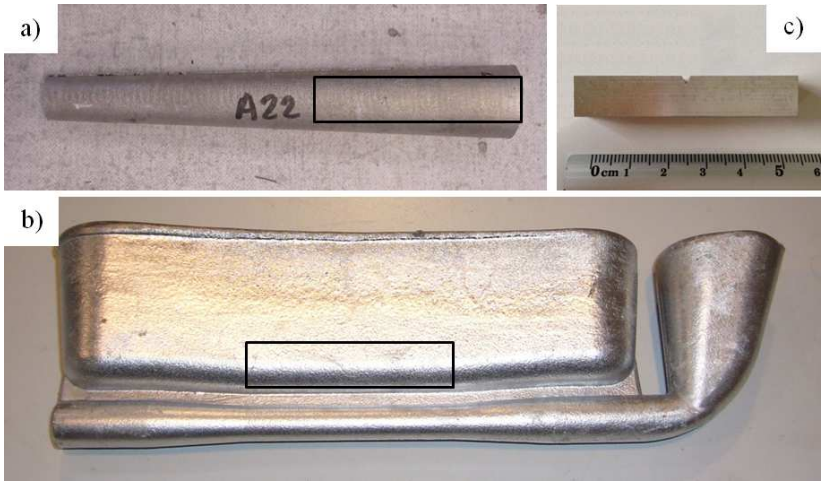

Figure C.1 – *Castings obtained from: a) sand mould; b) permanent mould. The black rectangles mark the areas where the Charpy specimens c) were machined.*

The hydrogen content in the melts was measured in-situ with the Alspek-H probe. Melts were degassed with argon gas in order to reach a hydrogen concentration of 0.08 mlH_2/100 gAl. The alloys were then poured in both sand and steel moulds. Sand castings were produced using an improved version of the tensile test bar design proposed by Dispinar and Campbell [16]. In this new casting design, the shape of the bars varied from cylindrical to tapered, with diameters increasing gradually from 15 mm (bottom) to 20 mm (top). Permanent mould castings were obtained by pouring the molten alloys into a L-shaped preheated steel die, manufactured according to the UNI 3039 specification. The steel die was kept at a constant temperature of 300 °C during the casting trials. This setup yields a cooling rate of 1.2 K/s and 2.5 K/s in the centre of sand cast and permanent mould cast Charpy impact specimens, respectively. Charpy impact specimens were machined according to the UNI EN ISO 148-1 specification (10x10x55 mm). The sand cast impact samples were machined from the upper part of the tapered bars, whereas the permanent mould samples were obtained along the centreline of the feeders (Figure C.1).

In order to evaluate the effect of Ni and V in both as-cast and heat treated conditions, specimens from the same casting were subjected to a T6 heat treatment including solutionising at 540 °C for 4 h, followed by quenching in a water bath at 20 °C. Subsequently, the samples were aged at 160 °C for 6 h. As a result, twelve different experimental conditions could be examined (Table C.2), and at least 5 samples were tested in each condition.

The impact tests were carried out on a CEAST instrumented Charpy pendulum according to the ASTM E-23 specification. Data were acquired using a DAS 8000 analyser. During impact testing, the total absorbed energy (*Wt*) was determined, along with a number of specific parameters such as crack initiation (*Wm*) and propagation (*Wp*) energies and the maximum load required to break the specimens (*Fmax*). *Wm* was calculated as the integral of load-deflection curve from the beginning of the test (i.e. when the pendulum hits the specimen) to the maximum load. This was also defined as the energy at maximum load, whereas the

Alloy	Mould	Condition	Alloy Code
A356	Sand	as-cast	A356 - AC
		T6	A356 - T6
A356 + 600 ppm Ni	Sand	as-cast	Ni - AC
		T6	Ni - T6
A356 + 1000 ppm V	Sand	as-cast	V - AC
		T6	V - T6
A356	Permanent Mould	as-cast	A356 PM - AC
		T6	A356 PM - T6
A356 + 600 ppm Ni	Permanent Mould	as-cast	Ni PM - AC
		T6	Ni PM - T6
A356 + 1000 ppm Ni	Permanent Mould	as-cast	V PM - AC
		T6	V PM - T6

Table C.2 – *Experiment matrix.*

energy absorbed from the maximum load to 2% of the peak value was designated as the propagation energy *Wp*.

After the impact tests, each specimen was sectioned perpendicular to the fracture surface, embedded and prepared with standard metallographic procedures. Microstructures and fracture profiles were then studied with an optical microscope (OM) and scanning electron microscopes (SEM). A detailed investigation of fracture surfaces was performed using a ZEISS EVO MA 15 and a ZEISS ULTRA 55 SEM equipped with EDS microprobe. Leica Application Suite 3.6 was used to measure the SDAS, applying the line intercept method, and the maximum Feret diameter of eutectic Si particles. As far as SDAS is concerned, between 350 and 500 measurements were performed near the fracture profiles for each sample in order to achieve statistically meaningful results. Regarding eutectic Si, a number of 25 micrographs were observed and more than 5000 particles were measured for each specimen.

C.3 Results

C.3.1 Impact Properties

It is well-established that the shape of both the load-time and the load-deflection curves can give information about the deformation and the fracture history of the impact specimens [17–19]. Qualitative observations of average load-deflection curves (Figure C.2a-d) clearly indicate that T6 heat treated alloys exhibit a less ductile fracture behaviour than the as-cast ones. Even if the maximum load increases in both sand cast and permanent mould cast T6 heat treated specimens, the following sharp decrease after the peak load is indicative of unstable crack propagation. The analysis of the corresponding average energy-deflection curves also reveals that generally a smaller amount of energy is absorbed by heat treated specimens.

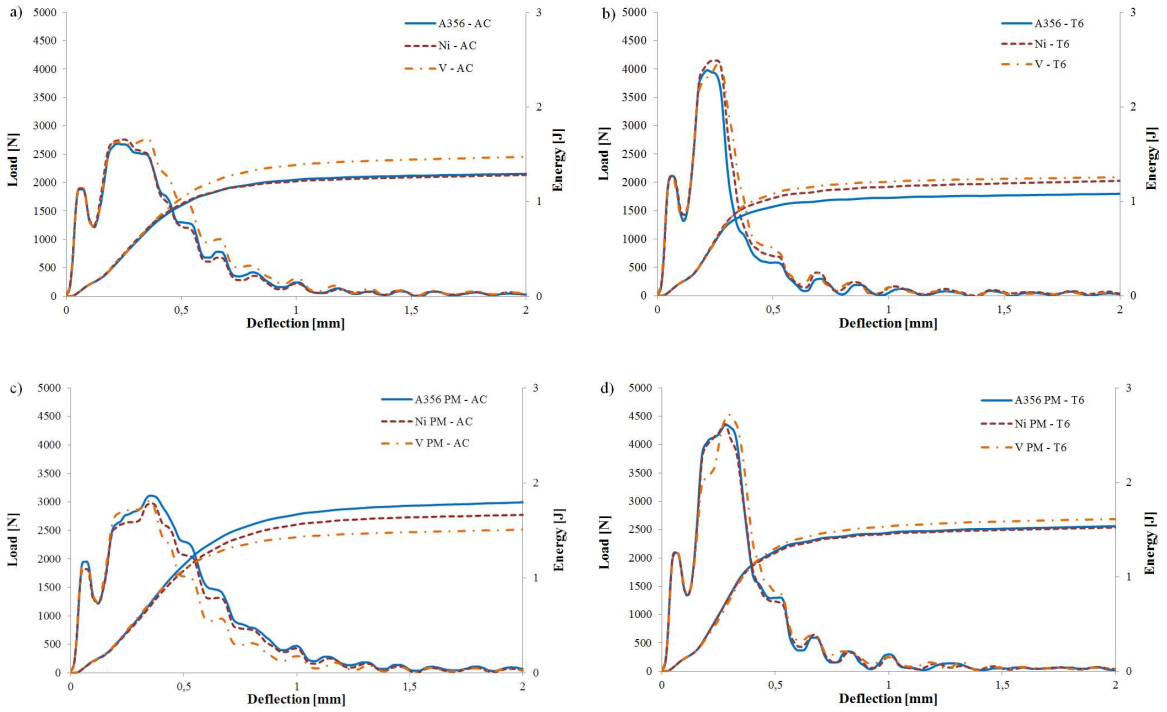

Figure C.2 – *Load-deflection and energy-deflection average curves for the different experimental conditions: a) sand mould, as-cast; b) sand mould, T6; c) permanent mould, as-cast; d) permanent mould, T6.*

The average values of the impact properties of sand cast and permanent mould cast alloys, as well as their standard deviations, are summarized in Table C.3 and Table C.4 and shown in Figure C.3. It is obvious that the heat treatment has a key influence on the impact properties of the alloys. Firstly, it leads to an increase of the maximum loads required to break the specimens *Fmax* (Figure C.3a); secondly, it leads to a general decrease in propagation energies *Wp* (Figure C.3c). However, considering the plots of the energy at maximum load *Wm* (Figure C.3b) and the total absorbed energy *Wt* (Figure C.3d), it is evident that the T6 heat treatment alone is not sufficient to affect the impact properties. Other parameters such as the SDAS and eutectic Si particles size must be considered as well.

The addition of the trace element Ni to an A356 base alloy exerts a very small effect on the total absorbed energy (*Wt*) of as-cast samples (- *AC*). On the other hand, V has a strong influence. It increases the average total absorbed energy of the sand cast specimens, whereas the same parameter is reduced up to 20% in permanent mould cast samples. Considering the deconvolution of total absorbed energy into its two main contributions, namely *Wm* and *Wp*, it is observed that Ni does not lead to any significant change in any of the impact parameters compared to the average values of the corresponding sand and permanent mould cast base alloys. In particular, since the scatter of *Wp* values for the *Ni PM - AC* alloy is large and includes the *A356 PM - AC Wp* average value, it is not possible to determine a clear influence of Ni addition on the propagation energy. The effect of V addition is less ambiguous. Although the scatter of *Wm* values for the sand cast alloy is large, a sharp increase in

Alloy Code	Fmax [N]	Wt [J]	Wm [J]	Wp [J]
A356 - AC	2704 ± 86	1.32 ± 0.05	0.45 ± 0.04	0.87 ± 0.05
A356 - T6	3987 ± 93	1.05 ± 0.08	0.52 ± 0.08	0.53 ± 0.08
Ni - AC	2818 ± 62	1.31 ± 0.06	0.45 ± 0.09	0.86 ± 0.06
Ni - T6	4186 ± 76	1.22 ± 0.06	0.67 ± 0.05	0.55 ± 0.03
V - AC	2810 ± 62	1.51 ± 0.06	0.71 ± 0.17	0.80 ± 0.14
V - T6	4133 ± 100	1.25 ± 0.08	0.68 ± 0.05	0.57 ± 0.04

Table C.3 – *Impact properties of the sand cast base and Ni/V-containing alloys.* Fmax *is the maximum load required to break the specimens;* Wt *is the total absorbed energy;* Wm *is the energy at maximum load;* Wp *is the propagation energy.*

Alloy Code	Fmax [N]	Wt [J]	Wm [J]	Wp [J]
A356 PM - AC	3122 ± 132	1.84 ± 0.20	0.79 ± 0.07	1.05 ± 0.13
A356 PM - T6	4362 ± 184	1.52 ± 0.13	0.81 ± 0.09	0.71 ± 0.06
Ni PM - AC	2971 ± 63	1.68 ± 0.17	0.78 ± 0.02	0.91 ± 0.16
Ni PM - T6	4401 ± 318	1.51 ± 0.22	0.78 ± 0.10	0.73 ± 0.14
V PM - AC	3012 ± 143	1.54 ± 0.15	0.82 ± 0.15	0.72 ± 0.12
V PM - T6	4598 ± 148	1.60 ± 0.11	0.88 ± 0.08	0.72 ± 0.13

Table C.4 – *Impact properties of the permanent mould cast base and Ni/V-containing alloys.* Fmax *is the maximum load required to break the specimens;* Wt *is the total absorbed energy;* Wm *is the energy at maximum load;* Wp *is the propagation energy.*

energy at maximum load is detected (Figure C.3b, *V - AC vs. A356 - AC*). However, the trace element V has a detrimental effect on the propagation energy of permanent mould impact specimens (Figure C.3c, *V PM - AC vs. A356 PM - AC*). It yields a decrease of Wp from 1.05 to 0.72 J.

For the case of the T6 heat treated alloys (- *T6*), the net influence of the trace elements Ni and V on the total absorbed energy was only observed in the sand cast specimens. The partition of this parameter into its two main contributions showed that both Ni and V increased the energy at maximum load, whereas propagation energy remained unaffected. Conversely, the alloys poured into the permanent mould did not show any significant variation of the average *Wt* values, compared to the corresponding T6 base alloy.

It is worth noting that an inversion in the relative contributions of *Wm* and *Wp* to *Wt* generally occurs between as-cast and T6 heat treated sand cast and permanent mould cast alloys (Figure C.4). As shown, the contribution of the propagation energy to the total absorbed energy is higher than *%Wm* for the reference alloys, the Ni-containing alloys and the sand cast V added alloy in as-cast condition (*A356 - AC*, *Ni - AC*, *V - AC*, *A356 PM - AC*, *Ni PM - AC*), whereas the remaining alloys generally show an opposite tendency. Hence, it is evident that several parameters need to be considered to completely describe the impact behaviour of sand cast and permanent mould cast alloys in both as-cast and T6 heat treated conditions.

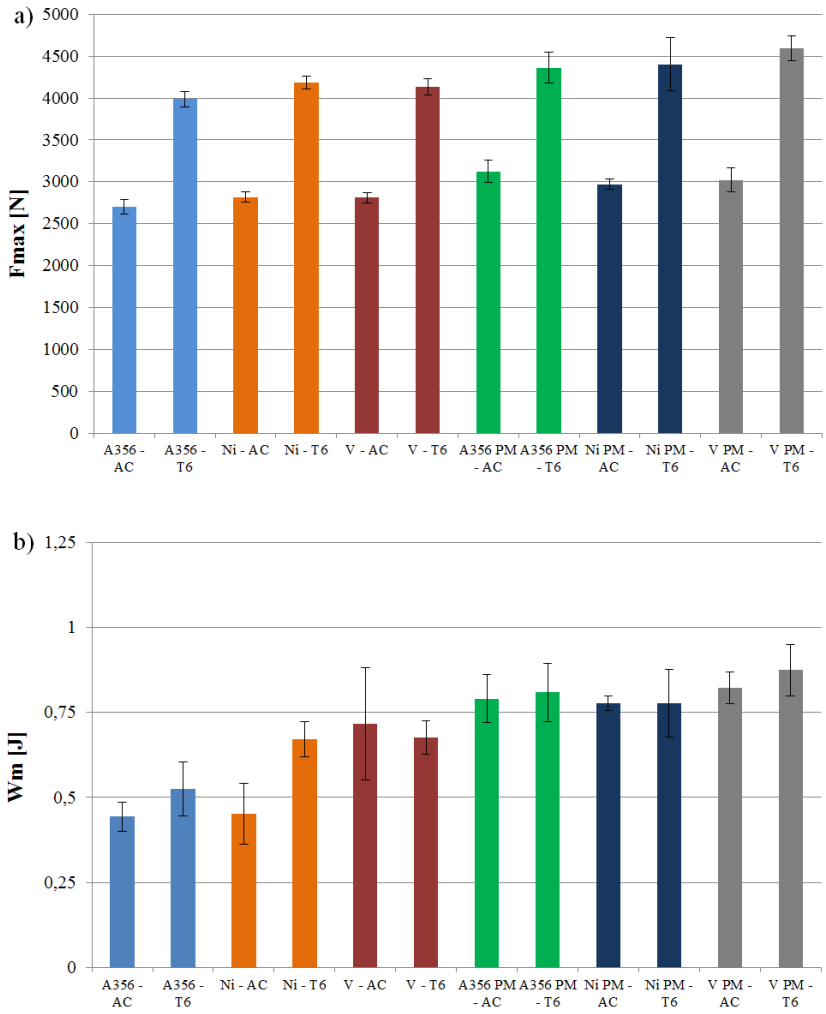

Figure C.3 – *Impact properties of the sand cast and permanent mould cast reference and Ni/V-containing alloys in as-cast and T6 conditions: a) maximum load* Fmax*; b) energy at maximum load* Wm*, c) propagation energy* Wp*; d) total absorbed energy* Wt*. The standard deviation is given as error bars.*

C.3.2 Microstructural and Fractographic Observations

The as-cast microstructures of reference alloys and alloys with Ni and V additions comprise soft α-Al dendrites and acicular eutectic Si particles (Figure C.5). During heat treatment some of the unmodified Si particles undergo necking, separate into segments, and then spheroidise and coarsen. However most of them still show an elongated acicular shape in both sand cast and permanent mould cast alloys (Figures C.5b and C.5d).

Various intermetallic phases such as π-$Al_8FeMg_3Si_6$, β-Al_5FeSi, Mg_2Si and Ni-bearing compounds can be observed in the interdendritic regions depending on the composition of the as-cast alloy (Figure C.6). The β-Al_5FeSi phase appears in the form of randomly distributed needles, whereas the π-$Al_8FeMg_3Si_6$ and Mg_2Si intermetallics have a "Chinese-script"morphology. Microstructural observations also reveal an increased amount of the latter two phases in the V-containing alloy, as can be noted from the comparison of Figure

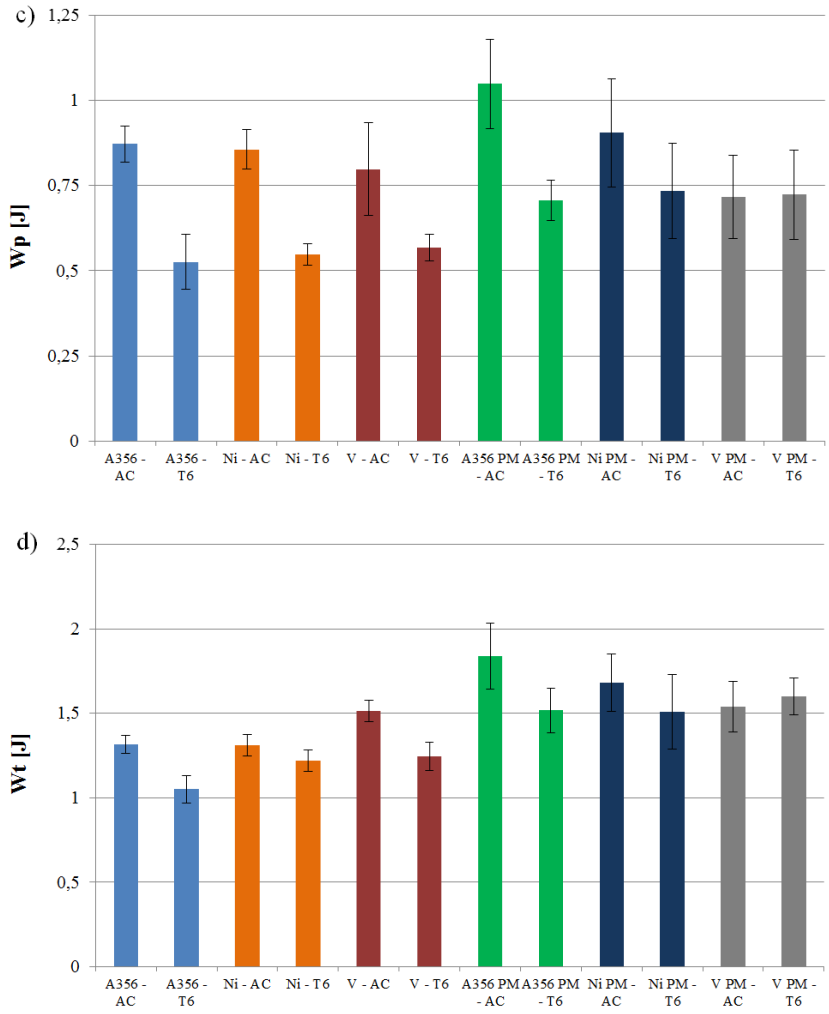

Figure C.3 – *(continued)*

C.6a and Figure C.6c. As shown in Figure C.6b, Ni-based intermetallic compounds precipitate as discrete particles or with a "Chinese-script"morphology. EDS spot measurements identify these phases as Al_3Ni and Al_9FeNi (Figure C.7). This is consistent with the microstructural investigations carried out by Ludwig *et al.* [20] in a commercial purity A356 alloy with Ni concentration ranging between 300 and 600 ppm. The average size of the intermetallics decreases in permanent mould cast alloys due to the higher cooling rate that was obtained with this casting technique.

Fine scale "Chinese-script"Mg_2Si intermetallics are not observed after solution heat treatment as reported in a number of previous studies [2, 7, 13, 21]. This provides evidence that they completely dissolve in the α-Al matrix for the given solution time and temperature of 4 h and 540 °C, respectively. Additionally, the fraction of the π-$Al_8FeMg_3Si_6$ phase diminishes by gradual dissolution of Mg and Si into the matrix and is to a some extent replaced by a Mg-free phase similar in composition to the β-Al_5FeSi phase (Figure C.8a) in the base and V-containing alloys, and to the Al_9FeNi phase (Figure C.8b) in the alloys added with

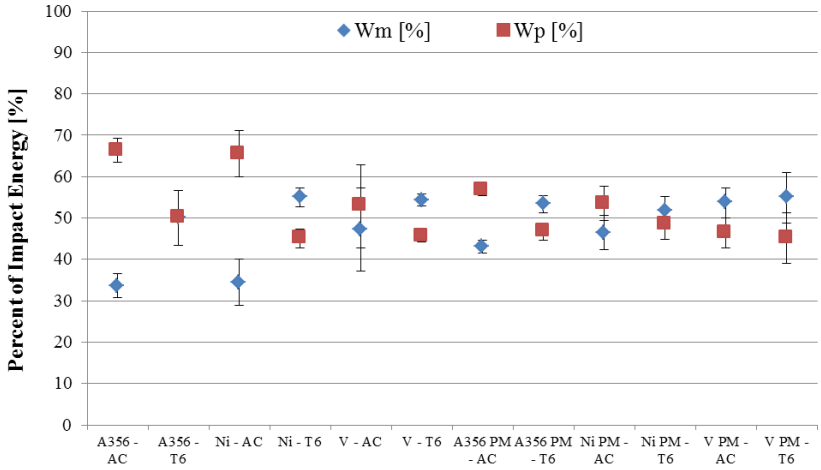

Figure C.4 – *Relative contribution of* Wm *and* Wp *to the total absorbed energy during crack nucleation and propagation for the different experimental conditions. The standard deviation is given as* error bars.

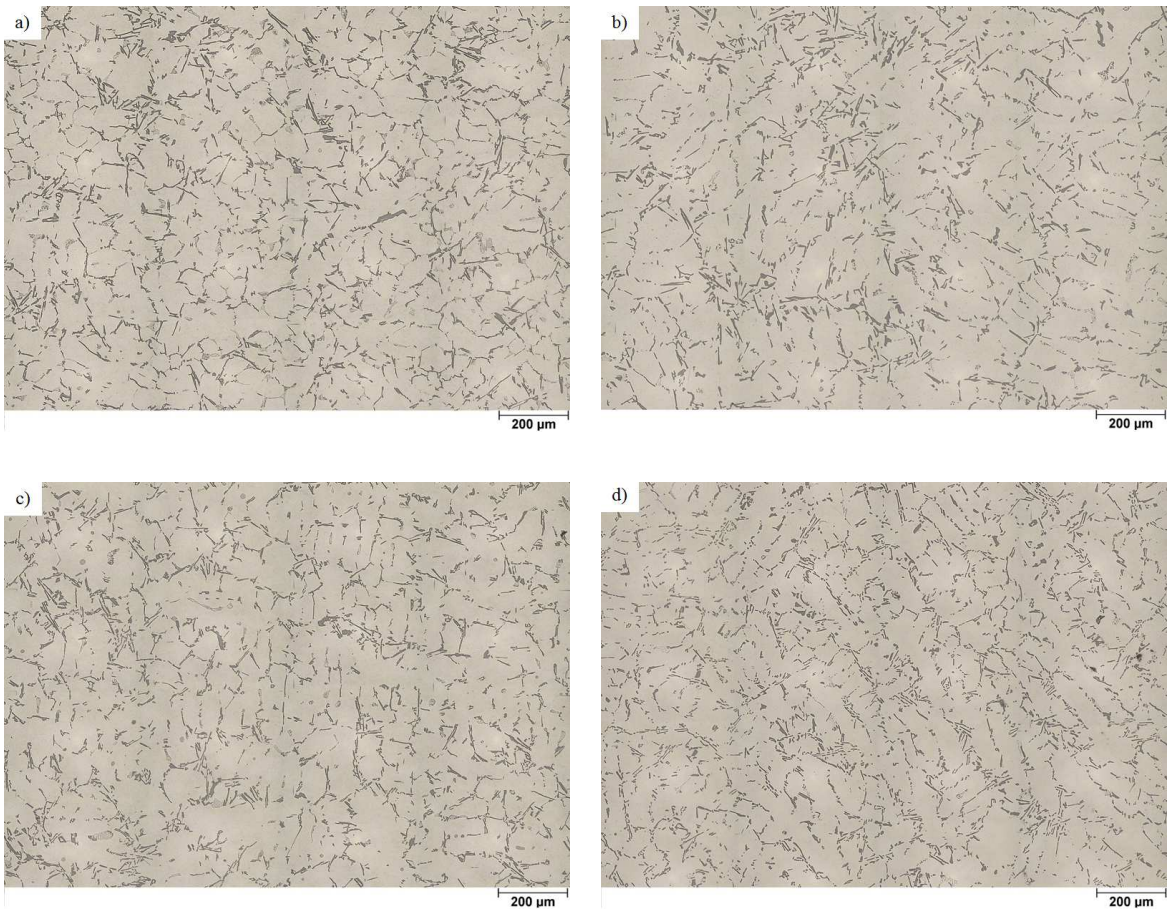

Figure C.5 – *Microstructures of the investigated A356 base alloys showing α-Al dendrites and an Al-Si eutectic mixture in the interdendritic regions: a) sand mould, as-cast; b) sand mould, T6; c) permanent mould, as-cast; d) permanent mould, T6. Similar features are observed for the Ni/V-containing alloys.*

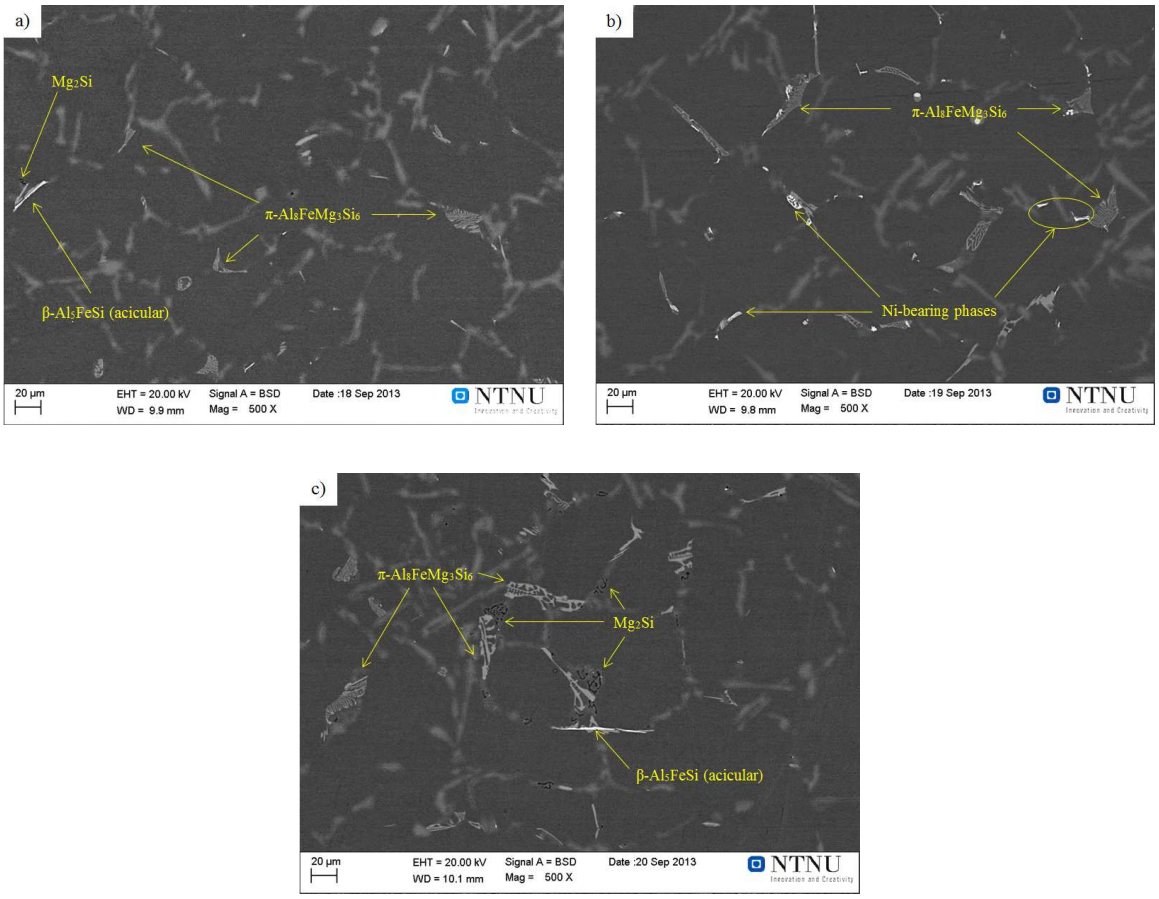

Figure C.6 – *BSE images showing intermetallic phases in the a) A356 reference, b) Ni-containing and c) V-containing alloys. The images are taken from sand cast samples in as-cast condition.*

Ni, as also observed by means of EDS (Figure C.8c). Conversely, acicular β-Al_5FeSi intermetallic phases formed during solidification are generally not affected by solution heat treatment [7], as well as Al_9FeNi intermetallics in the Ni-containing alloys, whereas Al_3Ni undergoes gradual spheroidisation. Apart from the precipitation of hardening Mg_2Si particles into α-Al matrix, the subsequent ageing heat treatment at 160 °C does not produce any further variation in the other microstructural features of the investigated alloys.

Quantitative microstructural analysis of the investigated alloys was only performed by measuring the secondary dendrite arm spacing (SDAS) and the size distribution of eutectic Si particles, since the intermetallic compounds were scarcely found on the fracture profiles and surfaces of the impact specimens. As given in Table C.5, average SDAS values of permanent mould cast alloys are lower than those of the corresponding sand cast alloys. This can be attributed to the higher cooling rate obtained in permanent mould casting as compared to sand casting. Furthermore, it is worthwhile noticing that a T6 heat treatment has no influence on the SDAS within the limits of the experimental scatter. This is in excellent agreement with the observations by other authors [10, 18, 22, 23] concluding that the SDAS is generally independent of the heat treatment even when extended solutionising times were applied to

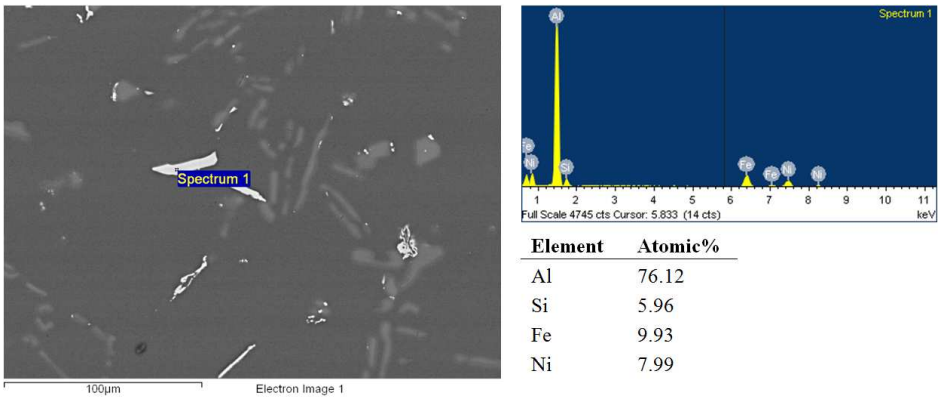

Figure C.7 – *BSE image of Ni-bearing intermetallics with different morphologies detected in the interdendritic regions of the sand cast Ni-containing alloy in as-cast condition. The chemical composition from a coarse flake-like particles as measured by EDS indicates the precipitation of the Al_9FeNi phase.*

the investigated Al-Si-Mg alloys.

In addition to the above-mentioned effects on the intermetallic compounds and on the precipitation behaviour of Mg_2Si hardening particles, the T6 heat treatment mainly affects the size and shape of eutectic Si particles (Figure C.5). Therefore, the size class containing the largest eutectic Si particles in terms of Feret diameter (50) was recorded for each sample and the average values for each experimental condition (i.e. base and Ni/V-containing sand cast and permanent mould cast alloys in both as-cast and T6 heat treated conditions) were calculated and considered as an indirect index of the heat treatment efficiency based on the change of the morphology of the eutectic Si from coarse acicular to fragmented and spheroidised.

It can be observed from the values summarized in Table C.5, that a T6 heat treatment has a larger effect on the permanent mould cast alloys compared to alloys made by sand casting owing to the higher cooling rate. This led to the precipitation of finer micro-constituents, and in consequence these particles were easier to fragment and spheroidise during solution heat treatment, i.e. the Si crystals were moderately refined due to the higher velocity of the advancing eutectic solid-liquid interface. This observation further substantiates the observations of Wang *et al.* [24] and correlates well with the model proposed by Ogris *et al.* [25]. Corresponding size distributions of eutectic Si particles shown in Figures C.9a and C.9b clearly indicate a higher tendency to necking and fragmentation of eutectic Si crystals for the T6 heat treated permanent mould cast base alloy (*A356 PM - T6*) compared to the sand cast alloy (*A356 - T6*). Similar observations can be made for alloys containing higher concentrations of Ni or V.

However, as mentioned previously, a large fraction of eutectic Si particles still possess an elongated acicular morphology. This demonstrates that, in the absence of Sr or Na as modifier agents, the selected solution heat treatment holding time is insufficient to obtain complete necking and spheroidisation of the eutectic Si phase. Therefore several areas with high stress concentration in the vicinity of acicular Si crystals maintain in all the T6 heat treated

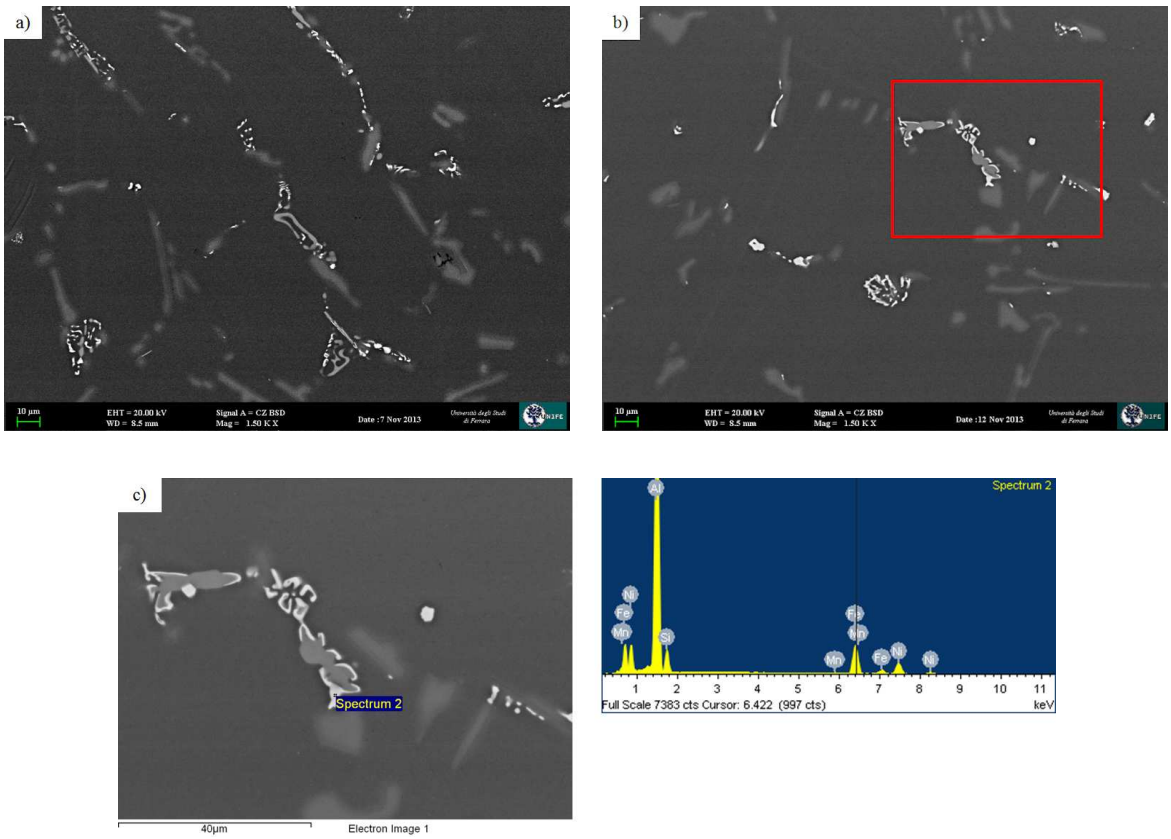

Figure C.8 – *BSE images of the Mg-free intermetallic compounds (in white) precipitated from the π-$Al_8FeMg_3Si_6$ phase after T6 heat treatment: a) β-Al_5FeSi; b) Al_9FeNi, occasionally forming a layered structure on the π-phase; c) Close-up view of the Ni-containing intermetallics with the corresponding EDS spectrum.*

alloys investigated in this study.

Figures C.10a-d show details of fracture profiles for the A356 reference alloy, considering that similar fracture paths can also be detected in the alloys with added Ni and V. Intercrystalline fracture of acicular eutectic Si crystals was the cause for fracture initialisation. Once a critical number of fractured particles is reached, the principal crack is formed by the local linkage of adjacent microcracks. They propagate following a preferential quasi-cleavage path along eutectic Si particles. Note that intermetallics are rarely found along the fracture profiles, thus indicating a Si-driven crack propagation, with a predominantly transgranular fracture mode. Occasionally, small intergranular contributions to fracture were detected in the permanent mould cast alloys (Figure C.10c). This is probably due to the presence of a locally smaller SDAS compared to the total average values measured for the corresponding alloys. This is in good agreement with previous results [22, 24, 26], demonstrating that for coarser microstructures (i.e. large SDAS) a strong interaction occurs during deformation between the slip bands generated in the secondary dendrite arms (also called dendrite cells) and the dense array of Si particles in the surrounding interdendritic regions. The

Alloy Code	SDAS [μm]	Si Feret diameter [μm]
A356 - AC	59.6 ± 5.6	126.0 ± 7.0
A356 - T6	62.6 ± 9.9	119.5 ± 4.8
Ni - AC	60.1 ± 5.5	139.1 ± 9.4
Ni - T6	60.5 ± 6.5	125.0 ± 7.3
V - AC	59.7 ± 6.2	138.1 ± 10.3
V - T6	60.6 ± 6.1	112.9 ± 8.2
A356 PM - AC	50.1 ± 6.8	100.4 ± 11.7
A356 PM - T6	51.7 ± 6.9	73.0 ± 7.4
Ni PM - AC	51.5 ± 5.8	100.7 ± 11.4
Ni PM - T6	53.1 ± 7.4	75.6 ± 17.7
V PM - AC	47.1 ± 7.0	103.5 ± 8.4
V PM - T6	49.0 ± 5.6	74.9 ± 12.5

Table C.5 – *Average values and standard deviations of the measured microstructural features for each experimental condition.*

resulting significant particle cracking and local linkage of microcracks along the interdendritic regions provides an easy path for transgranular crack propagation. On the contrary, smaller SDAS and Si particles make dendrite cell boundaries more discontinuous. As a consequence, transgranular fracture becomes more difficult; fracture then propagates throughout the grain boundaries, which offer an alternative continuous path.

No differences in fracture paths are observed between as-cast and T6 heat treated alloys. As already pointed out, even when some acicular Si particles fragmented and spheroidised during solution heat treatment, most of them still maintained an elongated acicular morphology and imposed a great influence on fracture propagation.

For the sake of simplicity, Figure C.11a-d show only the fracture surfaces of the A356 reference alloys. A careful examination of the surfaces confirms a Si-driven quasi-cleavage fracture mode. As mentioned before, the solution heat treatment decreases the size of Si flakes (Figures C.11b and C.11d). However, the typical characteristics of brittle fracture remain even in alloys where fragmentation and spheroidisation effects seem to be more pronounced (e.g. *A356 PM - T6*, *Ni PM - T6*, *V PM - T6*).

C.4 Discussion

C.4.1 Impact Properties of the base and Ni/V-containing as-cast alloys

It is generally accepted that the fracture process of Al-Si alloys consists of three stages, namely (i) particle cracking, (ii) microcrack formation and growth, and (iii) linkage of microcracks [22]. These stages are controlled by the microstructure in terms of size and shape of eutectic Si particles and intermetallic phases, and their clustering around the secondary arms of α-Al dendrites. When the SDAS is large, the microcrack linking process occurs

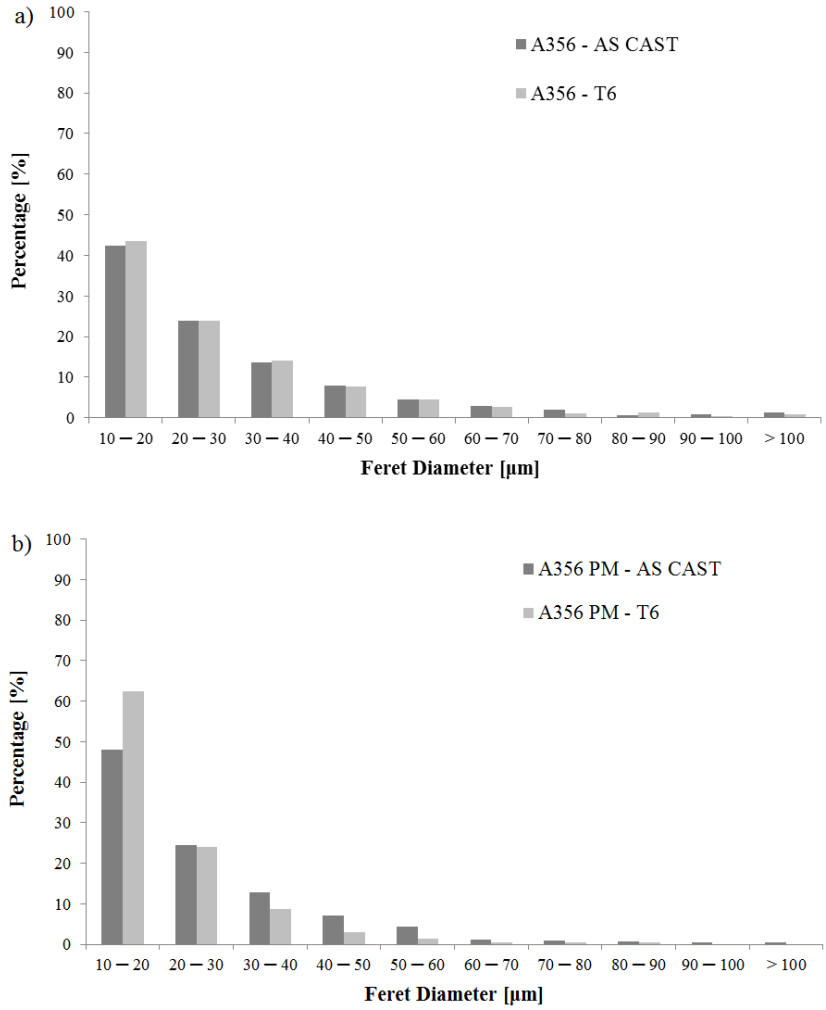

Figure C.9 – *Size distributions of eutectic Si crystals for a) sand cast and b) permanent mould cast base alloys.*

more easily along the cell boundaries leading to a low-energy transgranular fracture mode. In contrast, small SDAS microstructures generally account for higher ductility and impact properties due to a linking process between the microcracks. This involves fracture along the more irregular grain boundary region, i.e. an intergranular fracture mode [12]. It is worth noting that an increase in particle size also increases the probability of fracture, which generally leads to a lower fracture stress [24, 27].

The present results are consistent with these findings. Low total absorbed energy average values ($Wt < 2$ J) are observed for the investigated as-cast alloys (the - *AC* alloys in Tables C.3 and C.4) due to the large SDAS and the resulting significant amount of large acicular eutectic Si particles between secondary arms (Table C.5), which provide an easier path for a low-energy transgranular crack propagation. The slight increase in the total absorbed energies of the reference and Ni-containing permanent mould cast alloys in as-cast condition (*A356 PM - AC*, *Ni PM - AC*) reveals the moderate beneficial effect of a finer microstructure

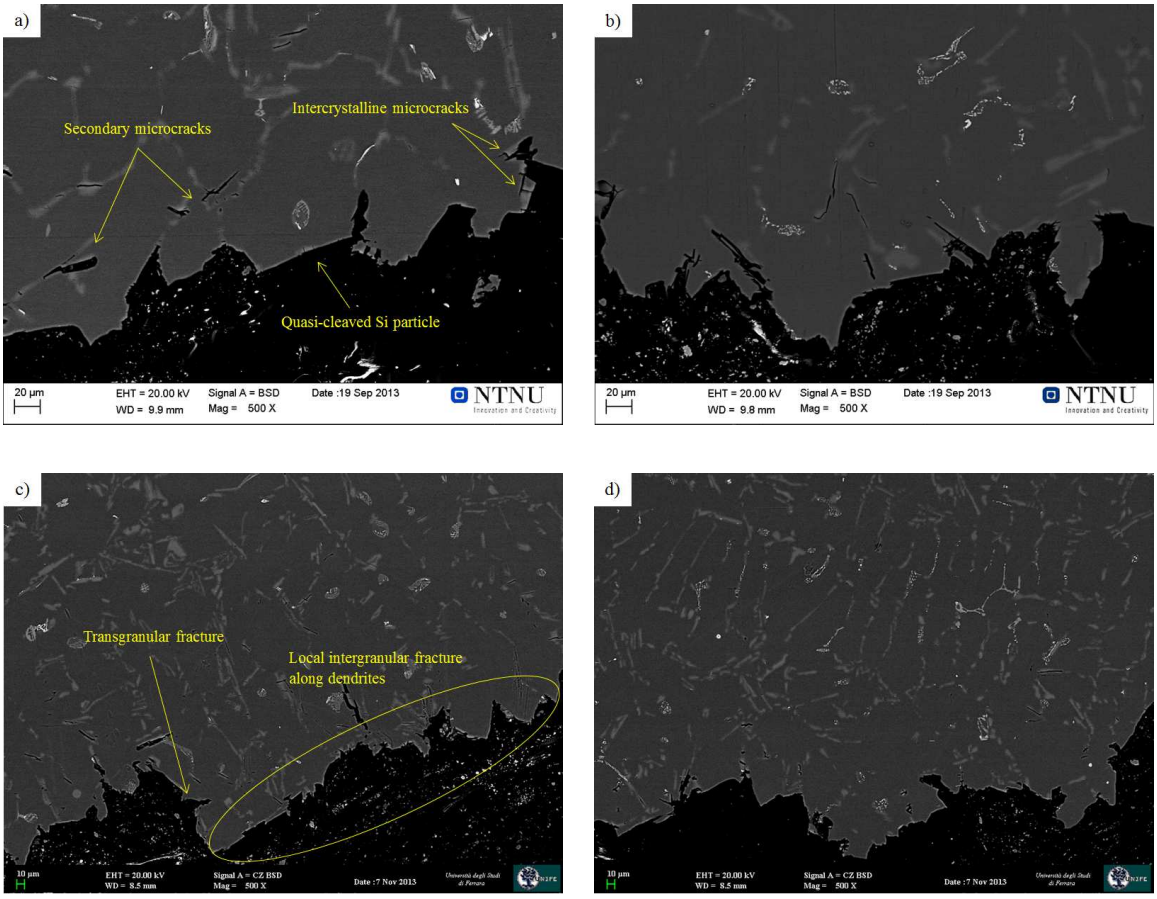

Figure C.10 – *BSE images of the fracture profile of the A356 reference alloy showing the Si-driven nature of impact fracture: a) sand mould, as-cast; b) sand mould, T6; c) permanent mould, as-cast; d) permanent mould, T6. Smaller SDAS are observed in permanent mould cast alloys implying the occurrence of local intergranular fracture c).*

leading to local intergranular contributions to fracture. Since intermetallic compounds are scarcely found on the fracture profiles and surfaces (Figures C.10 and C.11), their influence on impact properties is considered negligible compared to the SDAS and the size and shape of eutectic Si particles, indicating a Si-driven crack propagation. These observations are in excellent agreement with the findings of Kobayashi and Niinomi on the impact toughness of as-cast Al-Si alloys, which was reported to be primarily related to SDAS and eutectic Si rather than other second-phase particles such as intermetallic compounds [28]. According to the microstructural analysis, this also holds for Ni-bearing intermetallic compounds implying that the addition of the trace element Ni exerts no effect on the impact toughness of both sand cast and permanent mould cast A356 aluminium alloys.

Conversely, the comparison between the reference alloys and the corresponding V-containing alloys (*A356 - AC vs. V - AC*, *A356 PM - AC vs. V PM - AC*) in terms of total absorbed energy shows that V has a significant effect on the impact behaviour of the A356 alloy. In particular, the influences of V addition on the total absorbed energies of *V - AC* and *V PM*

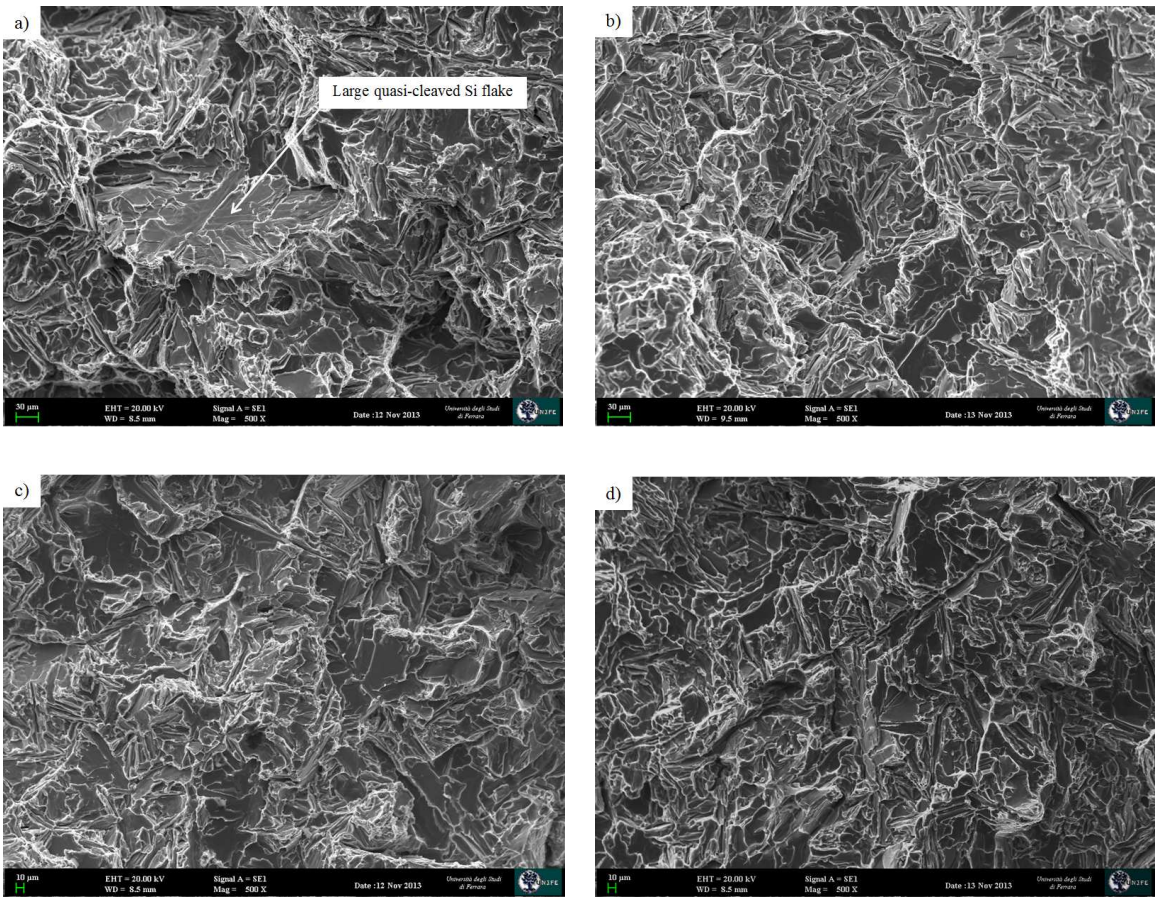

Figure C.11 – *SEM images of fracture surfaces of the A356 reference alloy showing the Si-driven nature of impact fracture: a) sand mould, as-cast; b) sand mould, T6; c) permanent mould, as-cast; d) permanent mould, T6. Note that the typical characteristics of fragile fracture still remain even in alloys where the effect of solution heat treatment appears to be more pronounced d).*

- *AC* alloys need to be analysed. The amount of V added in the present study is close to its maximum solubility in the α-Al matrix ($\approx$ 0.1 wt%) [29]. Hence a solid solution strengthening effect occurs. This enhances the strength of the matrix (*Fmax*, *Wm*), and at the same time reduces its ductility (*Wp*) due to the blockage of dislocation movement and the subsequent dislocation pile-ups. As a result, the microcrack linking process that follows the fracture of eutectic Si particles advances faster, especially in case of coarse microstructures. Therefore, two simultaneous effects occur and interact in V-containing as-cast alloys. In the sand cast alloys (*V - AC vs. A356 - AC*) the higher average value of *Wt* is due to the increase in energy at maximum load linked to solid solution strengthening, whereas the ductility reduction (i.e. the decrease in propagation energy) related to V appears to be moderate and within the experimental scatter. This appears to be reasonable considering the well-established detrimental influence of a coarse microstructure (large SDAS and eutectic Si particles) on the impact properties of A356 alloy [10,13,28,30]. On the contrary, in the permanent mould cast alloys (*V PM - AC vs. A356 PM - AC*), the smaller SDAS and the slightly refined eutectic Si

particles have a prevalent effect on *Fmax* and *Wm* compared to V strengthening: as it can be observed in Table C.4 and Figure C.3b, the alloys show similar values of these parameters (*Fmax* $\approx$ 3100 N, *Wm* $\approx$ 0.80 J). However, it appears that the influence of V on the ductility loss (*Wp*) increases as the microstructure becomes finer, thus contributing to a decrease of the total absorbed energy.

C.4.2 Impact Properties of the base and Ni/V-containing T6 heat treated alloys

It is evident from the average values of total absorbed energies listed in Tables C.3 and C.4 that the selected T6 heat treatment has a negative effect on the impact toughness of all the investigated alloys compared to the as-cast condition. These results are in good agreement with previous investigations, which indicated a noticeable decrease of the impact toughness of unmodified A356 alloys in T6 condition [10, 13]. Although Elsebaie *et al.* [13] studied unnotched impact specimens, it is worth noticing that this reduction was observed in both experiments with alloys with a large SDAS (45 - 48 μm). Additionally, Shivkumar *et al.* [10] reported that increasing solution heat treatment times led to a recovery of the impact toughness.

These findings can be explained as follows. Owing to the fact that the propagation of microcracks in an A356 alloy is governed by the ductility of α-Al matrix, an increase of the relative volume fraction of the matrix is beneficial for the impact properties. This effect can be achieved by the addition of Sr or Na, resulting in the modification of the eutectic Si from a coarse acicular structure to a fine fibrous morphology, and/or the application of a solution treatment [10]. Both treatments produce an increase in inter-particle spacing. However, different to chemical modification, the solutionising locally increases the relative volume fraction of the α-Al matrix due to necking, spheroidisation and coarsening of eutectic Si particles [6, 11, 13, 30, 31]. Without the addition of modifier elements and for insufficient solution treatment holding times and temperatures, the relative volume fraction of the α-Al matrix does not change substantially, and the linkage of microcracks proceeds predominantly along the cell boundaries of alloys with a large SDAS (i.e. low-energy transgranular fracture). Therefore, no significant improvement of the impact toughness is observed [10].

Furthermore, the ageing process that follows the solutionising step may become detrimental for the impact properties, thus causing a decrease in total absorbed energy [13]. A T6 heat treatment is normally applied to increase the strength of Al-Si-Mg alloys by the precipitation of fine coherent Mg_2Si particles. These dispersoids harden the α-Al matrix at the expense of ductility. In fact, they impose an obstacle for dislocation movement leading to a pile up, and consequently contribute significantly to the increase of the strength of the α-Al matrix [32]. Despite this improvement, the matrix is prone to fracture more easily. As a result, when the cracking of acicular Si particles begins, the following microcrack linking process is faster and leads to a lower amount of absorbed energy for fracture propagation. Hence, it is believed that a third parameter, namely the precipitation of coherent Mg_2Si particles, controls the

impact energies of the alloys in T6 condition together with SDAS and eutectic Si particles size and shape.

These two opposing effects of an ageing treatment on strength and ductility of the investigated alloys can clearly be observed in Figure C.3. On the one hand, the T6 heat treatment increases the maximum load required to fracture (*Fmax*); on the other hand, it leads to a general decrease in propagation energies (*Wp*) compared to the as-cast alloys. However, it is worth noticing that two different minimum levels of *Wp* are reached for the T6 heat treated sand cast and permanent mould cast alloys (Figure C.3c). It is suggested that the increase in *Wp* values for the permanent mould cast alloys is related to their finer microstructures in terms of SDAS and eutectic Si particles. In fact, it is already established that the Mg concentration in the α-Al matrix approaches the saturation limit within 30 minutes at 540 °C in alloys with low Mg concentration (0.3, 0.4 wt%), due to the dissolution of the Mg_2Si phase and the transformation of the π-Fe to the β-Fe intermetallic [7, 21, 33]. Since all the investigated alloys were subject to the same T6 heat treatment, which also included an extended solutionising time, i.e. 4 h, the same ductility loss was obtained. Hence, only the smaller SDAS and the slightly refined eutectic Si particles account for the further improvements of the propagation energies. However, these increases remain moderate because of the inadequate solution heat treatment holding time, that did not lead to sufficiently fragmented and spheroidised eutectic Si particles. For the energy at maximum load (Figure C.3b), a small strengthening effect related to Mg_2Si precipitation was observed in the sand cast base alloy (*A356 - T6*). Conversely, as described before for the permanent mould cast alloys in as-cast condition, it is the finer microstructure that appears to control the energy at maximum load of the T6 heat treated permanent mould cast alloys (*A356 PM - T6*, *Ni PM - T6*, *V PM - T6*) rather than the hardening Mg_2Si phase itself. Moreover, no further increases in Wm are observed for these alloys compared to the as-cast ones. This supports the hypothesis of an insufficient fragmentation and spheroidisation of eutectic Si particles.

The large increase in *Wm* for the sand cast Ni-containing alloy (*Ni - T6*) is not completely understood yet and requires further investigations. However, since the decrease in propagation energy is larger than the increase in energy at maximum load, the T6 heat treatment produces an overall reduction in total absorbed energy to fracture.

The presence of V in the α-Al matrix represents another parameter affecting the impact toughness of the T6 heat treated sand cast alloy (*V - T6*). It is noted in Figure C.3b, that the solid solution strengthening effect due to the presence of V produces a significant increase in *Wm*, similar to that observed in the as-cast alloy (*V - AC*). No further improvements of the energy at maximum load originating from the precipitation of Mg_2Si particles are observed. Nevertheless, it is believed that the combination of the ageing treatment and the coarse microstructure decreases the propagation energy of the alloy (Figure C.3c). However, as the beneficial effect of V is predominant, the V-containing alloy in T6 condition absorbs a slightly higher impact energy compared to the corresponding reference alloy (*V - T6 vs. A356 - T6* in Figure C.3d). For the case of permanent mould casting, similarly to the *V PM -*

AC alloy, the presence of trace element V in the α-Al matrix yields a significant decrease in the propagation energy of the corresponding T6 heat treated alloy (*V PM - T6*). In contrast to the T6 heat treated reference and Ni-containing alloys, it appears that the minimum ductility of the α-Al matrix has already been achieved by V solid solution strengthening, so that the additional precipitation of coherent Mg_2Si particles does not reduce the ductility any further. The variations of the percentage contributions to the total absorbed energy (Figure C.4) are due to these complex and interconnected mechanisms, which act simultaneously during the fracture process and govern the impact behaviour of sand cast and permanent mould cast alloys in both as-cast and T6 heat treated conditions.

Conclusions

The impact behaviour of base and Ni- or V-containing A356 alloys in as-cast and T6 heat treated conditions has been studied by testing notched specimens obtained from both sand and permanent mould castings. The main observations can be summarised as follows:

1. Low total absorbed energy average values (*Wt* < 2 J) are observed for all the alloys under investigation. Slightly higher impact energies are reported for the permanent mould cast alloys compared to sand cast specimens.

2. Intermetallic particles are rarely found on the fracture surfaces of the alloys, thus indicating a Si-driven quasi-cleavage crack propagation, with a predominant low-energy transgranular fracture mode. Occasionally, local intergranular contributions to fracture are detected in the permanent mould cast alloys, most likely due to the finer microstructure that forms due to the higher cooling rate. No differences are observed between as-cast and T6 heat treated alloys: even if acicular Si particles undergo fragmentation and spheroidisation during solution heat treatment, most of them still show an elongated acicular shape and maintain a great influence on fracture propagation.

3. With respect to as-cast alloys (- *AC*), the addition of the trace element Ni to an A356 base alloy exerts a minor effect on the total absorbed energy (*Wt*). However, this parameter is affected by the addition of V: while V increases the average total absorbed energy of the sand cast specimens, *Wt* of permanent mould cast samples is decreased up to 20%. This is due to an interaction between V solid solution strengthening and the resultant microstructure, the former being the prevalent parameter when the SDAS and Si particles are large (i.e. in sand cast alloys, *V - AC vs. A356 - AC*). In the permanent mould cast alloys (*V PM - AC vs. A356 PM - AC*), the effect of a smaller SDAS and slightly reduced eutectic Si particles on *Fmax* and *Wm* dominates over the V solid solution strengthening. However, the ductility loss (*Wp*) attributed to V in solid solution leads to a decrease in the total absorbed energy.

4. The T6 heat treatment (- *T6*) has a key influence on the increase of the maximum load required to fracture the specimens, *Fmax*, as well as on the reduction of the propagation energy *Wp*. These opposite effects occur because of the precipitation of fine coherent Mg_2Si particles, which lead to a hardening of the α-Al matrix at the expense of ductility. In addition, the microstructure affects the impact properties of the T6 heat treated alloys to some extent: higher *Wm* and *Wp* average values are reported for the permanent mould cast alloys compared to the corresponding sand cast ones.

5. The overall influence of Ni on the impact properties of the T6 heat treated A356 alloy is negligible. However V exerts a strong effect on the impact toughness of T6 heat treated sand cast and permanent mould cast alloys (*V - T6*, *V PM - T6*): in the former case it yields an increase of the energy at maximum load, whereas in the latter it significantly reduces the propagation energy.

Our investigation suggests that the presence of V, rather than Ni, needs to be taken into account in order to meet the specific service requirements in terms of impact toughness, in particular when structural parts are manufactured with different casting processes and subsequently subjected to a T6 heat treatment. It seems that the same detrimental influence on the impact toughness of a permanent mould cast unmodified A356 alloy is obtained either by adding the trace element V or via the application of T6 heat treatment. However, when these two factors are present simultaneously, their effects do not add up. Conversely, both the hardening of α-Al matrix due to V solid solution strengthening and the ductility loss caused by Mg_2Si precipitation are observed in case of sand cast T6 heat treated alloys (*V - T6*). Therefore, in the light of these results, more investigations are necessary in order to better understand the interactions between these microstructural features, particularly for the case of a Sr-modified A356 alloy, where mechanical properties are further improved by eutectic Si modification.

Acknowledgements

This research project was supported by the “Bando Giovani Ricercatori - Fondi 5x1000 anno 2010 e Fondi Unicredit 2013”of the University of Ferrara. In addition, the authors gratefully acknowledge Hydro Aluminium AS (Norway) for financial support. Thanks are also due to Hermann Hovland from Sør-Norge Aluminium AS (Norway) for the generous supply of master alloys and to Arne Nordmark and Kurt Sandaunet for the help during the manufacture of castings.

References

[1] D. Apelian, S. Shivkumar, and G. Sigworth, "Fundamental aspects of heat treatment of cast Al-Si-Mg alloys," *AFS Trans.*, vol. 97, pp. 727–742, 1989.

[2] E. Sjölander and S. Seifeddine, "The heat treatment of Al-Si-Cu-Mg casting alloys," *J. Mater. Process. Tech.*, vol. 210, pp. 1249–1259, 2010.

[3] K. T. Kashyap, S. Murali, K. S. Raman, and K. S. S. Murty, "Casting and heat treatment variables of Al-7Si-Mg alloy," *Mater. Sci. Technol.*, vol. 9, pp. 189–203, 1993.

[4] L. Pedersen and L. Arnberg, "The Effect of Solution Heat Treatment and Quenching Rates on Mechanical Properties and Microstructures in AlSiMg Foundry Alloys," *Metall. Mater. Trans. A*, vol. 32, pp. 525–532, 2001.

[5] M. Zhu, Z. Jian, G. Yang, and Y. Zhou, "Effects of T6 heat treatment on the microstructure, tensile properties, and fracture behavior of the modified A356 alloys," *Mater. Design*, vol. 36, pp. 243–249, 2012.

[6] D. L. Zhang, L. H. Zheng, and D. H. S. John, "Effect of a short solution treatment time on microstructure and mechanical properties of modified Al-7wt.%Si-0.3wt.%Mg alloy," *J. Light Met.*, vol. 2, pp. 27–36, 2002.

[7] J. A. Taylor, D. H. StJohn, L. H. Zheng, G. A. Edwards, J. Barresi, and M. J. Couper, "Solution Treatment Effects in Al-Si-Mg Casting Alloys: Part I. Intermetallic Phases," *Alum. Trans.*, vol. 4–5, pp. 95–110, 2001.

[8] S. Murali, K. S. Raman, and K. S. S. Murthy, "Effect of magnesium, iron (impurity) and solidification rates on the fracture toughness of Al-7Si-0.3Mg casting alloy," *Mater. Sci. Eng. A*, vol. 151, pp. 1–10, 1992.

[9] Z. Ma, A. M. Samuel, F. H. Samuel, H. W. Doty, and S. Valtierra, "Effect of Fe Content and Cooling Rate on the Impact Toughness of Cast 319 and 356 Aluminum Alloys," *AFS Trans.*, vol. 3, pp. 255–265, 2003.

[10] S. Shivkumar, L. Wang, and C. Keller, "Impact properties of A356-T6 Alloys," *J. Mater. Eng. Perform.*, vol. 3, pp. 83–90, 1994.

[11] M. Merlin, G. Timelli, F. Bonollo, and G. L. Garagnani, "Impact behaviour of A356 alloy for low-pressure die casting automotive wheels," *J. Mater. Process. Tech.*, vol. 209, pp. 1060–1073, 2009.

[12] D. Casari, M. Merlin, and G. L. Garagnani, "A comparative study on the effects of three commercial Ti-B-based grain refiners on the impact properties of A356 cast aluminium alloy," *J. Mater. Sci.*, vol. 48, pp. 4365–4377, 2013.

[13] O. Elsebaie, A. M. Samuel, and F. H. Samuel, "Effects of Sr-modification, iron-based intermetallics and aging treatment on the impact toughness of 356 Al-Si-Mg alloy," *J. Mater. Sci.*, vol. 46, pp. 3027–3045, 2011.

[14] G. Jha, S. Ningileri, X. Li, and R. Bowers, "The Challenge of Effectively Utilizing Trace Elements/Impurities in a Varying Raw Materials Market," in *LIGHT METALS 2013*, B. Sadler, Ed. TMS, 2013, pp. 929–934.

[15] J. Grandfield, L. Sweet, C. Davidson, J. Mitchell, A. Beer, S. Zhu, X. Chen, and M. Easton, "An initial assessment of the effects of increased Ni and V content in A356 and AA6063 alloys," in *LIGHT METALS 2013*, B. Sadler, Ed. TMS, 2013, pp. 39–44.

[16] D. Dispinar and J. Campbell, "Porosity, hydrogen and bifilm content in Al alloy castings," *Mater. Sci. Eng. A*, vol. 528, pp. 3860–3865, 2011.

[17] Z. Li, A. M. Samuel, F. H. Samuel, C. Ravindran, H. W. Doty, and S. Valtierra, "Parameters controlling the performance of AA319-type alloys Part II. Impact properties and fractography," *Mater. Sci. Eng. A*, vol. 367, pp. 111–122, 2004.

[18] N. D. Alexopoulus and A. Stylianos, "Impact mechanical behaviour of Al-7Si-Mg (A357) cast aluminum alloy. The effect of artificial aging," *Mater. Sci. Eng. A*, vol. 528, pp. 6303–6312, 2011.

[19] N. D. Alexopoulus, A. Stylianos, and J. Campbell, "Dynamic fracture toughness of Al-7Si-Mg (A357) aluminum alloy," *Mech. Mater.*, vol. 58, pp. 55–68, 2013.

[20] T. H. Ludwig, P. L. Schaffer, and L. Arnberg, "Influence of Some Trace Elements on Solidification Path and Microstructure of Al-Si Foundry Alloys," *Metall. Mater. Trans. A*, vol. 44, pp. 3783–3796, 2013.

[21] J. A. Taylor, D. H. StJohn, J. Barresi, and M. J. Couper, "Influence of Mg Content on the Microstructure and Solid Solution Chemistry of Al-7%Si-Mg Casting Alloys During Solution Treatment," *Mater. Sci. Forum*, vol. 331–337, pp. 277–282, 2000.

[22] Q. G. Wang, "Microstructural Effects on the Tensile and Fracture Behavior of Aluminum Casting Alloys A356/357," *Metall. Mater. Trans. A*, vol. 34, pp. 2887–2899, 2003.

[23] Y. Harada, S. Tamura, and S. Kumai, "Effects of High-Temperature Solutionizing on Microstructure and Tear Toughness of A356 Cast Aluminum Alloy," *Mater. Trans.*, vol. 52, pp. 848–855, 2011.

[24] Q. G. Wang and C. H. Cáceres, "The fracture mode in Al-Si-Mg casting alloys," *Mater. Sci. Eng. A*, vol. 241, pp. 72–82, 1998.

[25] E. Ogris, A. Wahlen, H. Luchinger, and P. J. Uggowitzer, "On the silicon spheroidization in Al-Si alloys," *J. Light. Met.*, vol. 2, pp. 263–269, 2002.

[26] C. H. Cáceres, C. J. Davidson, and J. R. Griffiths, "The deformation and fracture behaviour of an Al-Si-Mg casting alloy," *Mater. Sci. Eng. A*, vol. 197, pp. 171–179, 1995.

[27] W. H. Hunt, J. R. Brockenbrough, and P. E. Magnusen, "An Al-Si-Mg composite model system: Microstructural effects on deformation and damage evolution," *Scr. Metall. Mater.*, vol. 25, pp. 15–20, 1991.

[28] T. Kobayashi and M. Niinomi, "Fracture Toughness and fatigue characteristics of aluminum casting alloy," *J. JAPAN Inst. Met.*, vol. 41, pp. 398–405, 1991.

[29] N. A. Belov, D. G. Eskin, and A. A. Aksenov, *Multicomponent phase diagrams: applications for commercial aluminum alloys*. Elsevier Science (2005).

[30] F. Paray, B. Kulunk, and J. E. Gruzleski, "Impact properties of Al-Si foundry alloys," *Int. J. Cast Metals Res.*, vol. 13, pp. 17–37, 2000.

[31] S. S. S. Kumari, R. M. Pillai, T. P. D. Rajan, and B. C. Pai, "Effects of individual and combined additions of Be, Mn, Ca and Sr on the solidification behaviour, structure and mechanical properties of Al-7Si-0.3Mg-0.8Fe alloy," *Mater. Sci. Eng. A*, vol. 460–461, pp. 561–573, 2007.

[32] G. E. Dieter, *Mechanical Metallurgy*. Wiley-WHC Verlag (1988).

[33] D. Lados, D. Apelian, and L. Wang, "Solution Treatment Effects on Microstructure and Mechanical Properties of Al-(1 to 13 Pct)Si-Mg Cast Alloys," *Metall. Mater. Trans. B*, vol. 42, pp. 171–180, 2011.

Il tuo indirizzo e-mail
csrdnl@unife.it
Oggetto:
Dichiarazione di conformità della tesi di Dottorato
Io sottoscritto Dott. (Cognome e Nome)
Casari Daniele
Nato a:
Ferrara
Provincia:
Ferrara
Il giorno:
31/03/1986
Avendo frequentato il Dottorato di Ricerca in:
Scienze dell'Ingegneria
Ciclo di Dottorato
26
Titolo della tesi:
The grain refinement and the Ni/V contamination in the A356 aluminium casting alloy: an experimental study on impact and tensile properties
Titolo della tesi (traduzione):
L'affinamento del grano e la contaminazione mediante Ni/V nella lega di alluminio A356 da fonderia: studio sperimentale delle proprietà ad impatto e a trazione
Tutore: Prof. (Cognome e Nome)
Garagnani Gian Luca
Settore Scientifico Disciplinare (S.S.D.)
ING-IND/21
Parole chiave della tesi (max 10):
Alluminio, Affinamento, Nickel, Vanadium, Proprietà Meccaniche, Aluminium, Refinement, Mechanical Properties
Consapevole, dichiara
CONSAPEVOLE: (1) del fatto che in caso di dichiarazioni mendaci, oltre alle sanzioni previste dal codice penale e dalle Leggi speciali per l'ipotesi di falsità in atti ed uso di atti falsi, decade fin dall'inizio e senza necessità di alcuna formalità dai benefici conseguenti al provvedimento emanato sulla base di tali dichiarazioni; (2) dell'obbligo per l'Università di provvedere al deposito di legge delle tesi di dottorato al fine di assicurarne la conservazione e la consultabilità da parte di terzi; (3) della procedura adottata dall'Università di Ferrara ove si richiede che la tesi sia consegnata dal dottorando in 2 copie di cui una in formato cartaceo e una in formato pdf non modificabile su idonei supporti (CD-ROM, DVD) secondo le istruzioni pubblicate sul sito: http://www.unife.it/studenti/dottorato alla voce ESAME FINALE – disposizioni e modulistica; (4) del fatto che l'Università, sulla base dei dati forniti, archivierà e renderà consultabile in rete il testo completo della tesi di dottorato di cui alla presente dichiarazione attraverso l'Archivio istituzionale ad accesso aperto

"EPRINTS.unife.it" oltre che attraverso i Cataloghi delle Biblioteche Nazionali Centrali di Roma e Firenze; DICHIARO SOTTO LA MIA RESPONSABILITA': (1) che la copia della tesi depositata presso l'Università di Ferrara in formato cartaceo è del tutto identica a quella presentata in formato elettronico (CD-ROM, DVD), a quelle da inviare ai Commissari di esame finale e alla copia che produrrò in seduta d'esame finale. Di conseguenza va esclusa qualsiasi responsabilità dell'Ateneo stesso per quanto riguarda eventuali errori, imprecisioni o omissioni nei contenuti della tesi; (2) di prendere atto che la tesi in formato cartaceo è l'unica alla quale farà riferimento l'Università per rilasciare, a mia richiesta, la dichiarazione di conformità di eventuali copie; (3) che il contenuto e l'organizzazione della tesi è opera originale da me realizzata e non compromette in alcun modo i diritti di terzi, ivi compresi quelli relativi alla sicurezza dei dati personali; che pertanto l'Università è in ogni caso esente da responsabilità di qualsivoglia natura civile, amministrativa o penale e sarà da me tenuta indenne da qualsiasi richiesta o rivendicazione da parte di terzi; (4) che la tesi di dottorato non è il risultato di attività rientranti nella normativa sulla proprietà industriale, non è stata prodotta nell'ambito di progetti finanziati da soggetti pubblici o privati con vincoli alla divulgazione dei risultati, non è oggetto di eventuali registrazioni di tipo brevettale o di tutela. PER ACCETTAZIONE DI QUANTO SOPRA RIPORTATO

Firma del dottorando

Ferrara, li 03/02/2014 Firma del Dottorando Daniele Casari

Firma del Tutore

Visto: Il Tutore Si approva Firma del Tutore